Supporting Information

Ambient and Metal-Free C(sp^2)–C(sp^3) Cross-Coupling Polymerization of Dichalcones and Activated Methylenes to Prepare Clusteroluminescent Polyarylacrylonitriles

Tianbai Xiong,[a,b,#] Liguo Xu,[c,#] Yongfu Qiu,[a,d,#] Lingxi Yang,[b] Jia Wang,[b,*] and Xin Wang[b,*]

[a.] *School of Environment and Civil Engineering, Dongguan University of Technology, Dongguan 523808, China.*

[b.] *Songshan Lake Materials Laboratory, Dongguan 523808, China.*

[c.] *College of Light Chemical Industry and Materials Engineering, Shunde Polytechnic University, Foshan, 528333, China.*

[d.] *School of Materials Science and Engineering, Dongguan University of Technology, Guangdong 523808, China.*

[#.] *These authors contributed equally to this work.*

Table of Contents

Materials and instruments

1,4-Phenylenediacetonitrile (**2a**), 1,3-phenylenediacetonitrile (**2b**), terephthalaldehyde, 4,4'-biphenyldicarboxaldehyde, chalcone (**3**), 4-methylbenzyl cyanide (**4**), acetophenone (**6**), *m*-phthalaldehyde (**7**), terephthalaldehyde (**8**), 4,4'-biphenyldicarboxaldehyde (**9**), 4-methoxyacetophenone (**10**), disodium edetate dihydrate (Na_2EDTA), iron(III) chloride hexahydrate, 1,8-diazabicyclo[5.4.0]undecane-7-ene (DBU), dichloromethane (DCM) and *N*,*N*-dimethylformamide (DMF), dimethyl sulfoxide (DMSO), N,N-dimethylacetamide (DMAc), tetrahydrofuran (THF), and acetonitrile (MeCN) were purchased from Energy Chemical. 5-Methyl-1,3-benzenediacetonitrile (**2c**), 1,2-phenylenediacetonitrile (**2d**) were purchased from Macklin reagent. Other solvents were commercially available from Tansoole. All the commercial chemicals were used as received without further purification.

All NMR spectra were measured on a Brucker Avance 400 MHz NMR spectrometer using deuterated chloroform as solvent and tetramethylsilane (TMS, $\delta = 0$) as internal reference. FT-IR spectra were recorded on a PerkinElmer FT-IR spectrometer Spectrum 3. The number- (M_n) and weight- (M_w) average molecular weights and polydispersity indices (PDI = M_w/M_n) of the polymers were estimated by a Waters 1515_2707_2414 gel permeation chromatography system. DMF/LiBr solution (0.05 M LiBr) was used as eluent at a flow rate of 1 mL/min. A set of monodispersed poly(methyl methacrylate) (PMMA), covering the M_w range of 10^3 - 10^7 g/mol, were utilized as standards for molecular weight calibration. Thermogravimetric analysis was carried out on a Mettler Toledo TGA/DSC3+ under nitrogen atmosphere at a heating rate of 20 °C/min. Differential scanning calorimetry was carried out on a MDSC Q100 TA under nitrogen atmosphere at a heating rate of 20 °C/min. UV-vis absorption spectra were recorded on a Thermo Scientific Evolution 201/220. Fluorescence spectra were recorded on a Spectrofluorometer (Edinburgh FS5) fluorescence. PL quantum yields were measured using a Hamamatsu absolute PL quantum yield spectrometer C11347 Quantaurus_QY. High-Resolution Mass Spectrometry (HRMS) was measured by the instrument of waters G2-XS Qtof. Positive mode: voltage 3.5 kv, ion source temperature 110 °C, solvent removal temperature 400 °C, nitrogen flow rate: 800 L/h. Dynamic light scattering was measured on the MICROTRAC MRB Nanotrac wave II.

We conducted a comprehensive study of molecular conformations by integrating the Molclus program [1] with XTB v 6.6.1 [2], employing the precise GFN0-xTB method [3]. For structural optimization, vibrational analysis, and energy calculations, we utilized the Gaussian 16 software package [4], applying the B3LYP functional [5-7] along with the D3BJ dispersion correction [6]. The optimized molecular structures and their corresponding vibrational frequencies were determined using the 6-31G* basis set [8,9]. Excited state energy calculations were carried out using the PBE0 functional [10] and def2-SVP basis sets [11]. Additionally, we conducted an in-depth analysis of excited states with Multiwfn 3.8 [12, 13]. To visualize the structure and weak interactions within the system, we employed VMD [14].

Synthesis of monomers and model compounds

Synthesis of monomer (2E,2'E)-3,3'-(1,3-phenylene)bis(1-phenylprop-2-en-1-one) **1a** (Scheme S1): Magnetic stir bar, *m*-phthalaldehyde (1.34 g, 10 mmol), NaOH (1.00 g, 25 mmol), and 40 mL of methanol were added into a 100 mL double necked flask. Then, 40 mL of methanol solution of

acetophenone (2.40 g, 20 mmol) was dropwise added into the reaction mixture by a pressure-equalizing dropping funnel. After reacting for 12 h, the mixture was filtered to get the filter cake, and purified by silica gel using petroleum ether/CH_2Cl_2 mixture (v/v, 1/1) as eluent. A white solid was obtained in 81.4% yield. IR (KBr disk), v (cm^{-1}): 3035, 1662, 1607, 1446, 1328, 1276, 1211, 1173, 1018, 973, 765, 685. ^{1}H NMR (400 MHz, chloroform-*d*) δ 8.09 – 8.01 (m, 4H), 7.88 (s, 1H), 7.83 (d, J = 15.8 Hz, 2H), 7.68 (s, 2H), 7.65 – 7.41 (m, 9H). ^{13}C NMR (100 MHz, chloroform-*d*) δ 190.30, 143.79, 138.04, 135.75, 132.95, 130.07, 129.61, 128.70, 128.56, 128.26, 123.08.

Scheme S1. The synthetic route to monomer **1a**.

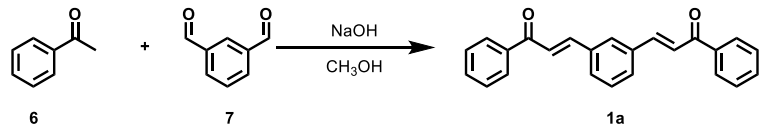

Synthesis of monomer (2E,2'E)-3,3'-(1,4-phenylene)bis(1-phenylprop-2-en-1-one) **1b** (Scheme S2): Magnetic stir bar, terephthalaldehyde (1.34 g, 10 mmol), NaOH (1.00 g, 25 mmol), and 40 mL of methanol were added into a 100 mL double necked flask. Then, 40 mL of methanol solution of acetophenone (2.40 g, 20 mmol) was dropwise added into the reaction mixture by a pressure-equalizing dropping funnel. After reacting for 12 h, the mixture was filtered to get the filter cake, and purified by silica gel using petroleum ether/CH_2Cl_2 mixture (v/v, 1/1) as eluent. A yellow solid was obtained in 66.3% yield. IR (KBr disk), v (cm^{-1}): 3053, 1655, 1606, 1445, 1336, 1292, 1225, 1037, 978, 832, 692. ^{1}H NMR (400 MHz, Chloroform-*d*) δ 8.10 – 7.98 (m, 4H), 7.81 (d, J = 15.7 Hz, 2H), 7.69 (s, 4H), 7.64 – 7.46 (m, 8H). ^{13}C NMR (100 MHz, Chloroform-*d*) δ 190.24, 143.53, 138.08, 136.91, 132.95, 128.96, 128.69, 128.53, 123.10.

Scheme S2. The synthetic route to monomer **1b**.

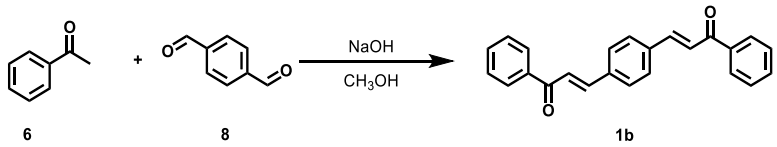

Synthesis of monomer (2E,2'E)-3,3'-([1,1'-biphenyl]-4,4'-diyl)bis(1-phenylprop-2-en-1-one) **1c**: (Scheme S3): Magnetic stir bar, 4,4'-biphenyldicarboxaldehyde (2.10 g, 10 mmol), NaOH (1.00 g, 25 mmol), and 40 mL of methanol were added into a 100 mL double necked flask. Then, 40 mL of methanol solution of acetophenone (2.40 g, 20 mmol) was dropwise added into the reaction mixture by a pressure-equalizing dropping funnel. After reacting for 12 h, the mixture was filtered to get the filter cake, and purified by silica gel using petroleum ether/CH_2Cl_2 mixture (v/v, 1/1) as eluent. A yellow solid was obtained in 76.8% yield. IR (KBr disk), v (cm^{-1}): 3052, 1659, 1634, 1603, 1346, 1218, 1035, 980, 821, 772. ^{1}H NMR (400 MHz, Chloroform-*d*) δ 8.09 – 8.01 (m, 4H), 7.86 (d, J = 15.7 Hz, 2H), 7.78 – 7.65 (m, 8H), 7.64 – 7.45 (m, 8H). ^{13}C NMR (100 MHz, Chloroform-*d*) δ 190.40, 144.08, 142.10, 138.24, 134.50, 132.83, 129.08, 128.66, 128.52, 127.52, 122.29.

Scheme S3. The synthetic route to monomer **1c**.

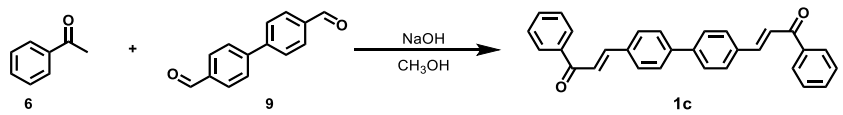

Synthesis of monomer (2E,2'E)-3,3'-(1,3-phenylene)bis(1-(4-methoxyphenyl)prop-2-en-1-one) **1d**: (Scheme S4): Magnetic stir bar, *m*-phthalaldehyde (1.34 g, 10 mmol), NaOH (1.00 g, 25 mmol), and 40 mL of methanol were added into a 100 mL double necked flask. Then, 40 mL of methanol

solution of 4'-methoxyacetophenone (3.0 g, 20 mmol) was dropwise added into the reaction mixture by a pressure-equalizing dropping funnel. After reacting for 12 h, the mixture was filtered to get the filter cake, and purified by silica gel using petroleum ether/CH_2Cl_2 mixture (v/v, 1/1) as eluent. A white solid was obtained in 68.2% yield. IR (KBr disk), ν (cm^{-1}): 3064, 3002, 2936, 2839, 1656, 1606, 1339, 1272, 1214, 1165, 1023, 975, 794. ^{1}H NMR (400 MHz, Chloroform-*d*) δ 8.10 – 8.02 (m, 4H), 7.90 – 7.77 (m, 3H), 7.71 – 7.64 (m, 2H), 7.59 (d, J = 15.7 Hz, 2H), 7.51 – 7.42 (m, 1H), 7.05 – 6.94 (m, 4H), 3.90 (s, 6H). ^{13}C NMR (100 MHz, Chloroform-*d*) δ 188.48, 163.58, 143.01, 135.89, 130.95, 130.89, 129.52, 128.11, 122.83, 113.93, 55.53.

Scheme S4. The synthetic route to monomer **1d**.

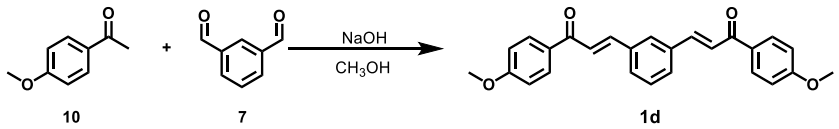

The synthesis of model compound 5-oxo-3,5-diphenyl-2-(p-tolyl)pentanenitrile **5**: Magnetic stir bar, chalcone (208 mg, 1 mmol), 4-methylbenzyl cyanide (157 mg, 1.2 mmol), DBU (30 μL, 0.2 mmol) and 1 mL of DMSO were added into a 10 mL Schlenk tube. After reacting for 24 h, 50 mL of water was added. Dichloromethane was used to extract the solution for three times (3 × 50 mL). The organic layers were combined, and the solvent was removed by vacuum rotary evaporation. Then, the crude product was purified by silica gel column chromatography with petroleum ether/CH_2Cl_2 mixture (v/v, 1/1) as eluent. A transparent liquid was obtained in 94.1% yield. IR (KBr disk), ν (cm^{-1}): 3030, 2923, 2239, 1682, 1597, 1514, 1449, 1211, 987, 816, 749, 689. ^{1}H NMR (400 MHz, Chloroform-*d*) δ 8.03 – 7.82 (m, 2H), 7.65 – 7.38 (m, 3H), 7.33 – 7.19 (m, 4H), 7.15 – 6.95 (m, 5H), 4.52 – 4.08 (m, 1H), 3.98 – 3.63 (m, 2H), 3.57 – 3.21 (m, 1H), 2.44 – 2.17 (m, 3H). ^{13}C NMR (100 MHz, Chloroform-*d*) δ 197.64, 139.70, 138.47, 138.18, 137.87, 136.64, 133.53, 131.09, 129.33, 128.62, 128.32, 127.98, 127.65, 119.56, 45.34, 42.79, 41.70, 21.09.

Synthesis of PAANs

*The typical procedure of synthesis of P**1a2a***. **1a** (203.1 mg, 0.6 mmol), **2a** (93.7 mg, 0.6 mmol), and DBU (17.8 μL, 0.12 mmol) were added into a 25 mL Schlenk tube equipped with a magnetic stir bar. 1 mL of DCM was then injected into the tube and stirred at room temperature for 24 h in air. The polymerization solution was diluted with 4.0 mL of DCM, which was precipitated by adding the mixture dropwise into 100 mL of methanol. The precipitates were filtered and washed with methanol for three times (3 × 20 mL), and dried under vacuum to a constant weight.

*Large scale synthesis of P**1a2a**.* (2E,2'E)-3,3'-(1,3-Phenylene)bis(1-phenylprop-2-en-1-one) **1a** (9.196 g, 27 mmol), 1,4-phenylenediacetonitrile **2a** (4.278 g, 27 mmol) and DBU (806.7 μL, 5.4 mmol) were added into a 250 mL double necked flask equipped with a magnetic stir bar in air. 45 mL of DCM were then injected into the tube and stirred at room temperature for 24 h. The polymerization solution was then precipitated by adding the mixture dropwise into 1000 mL of methanol through a cotton filter. The precipitates were filtered and washed with methanol for three times (3 × 100 mL), and dried under vacuum to a constant weight to afford polymer P**1a2a** as a grayish solid in 99.9 % yield. M_w = 19 600, M_w/M_n = 1.65.

Table S1. Effect of solvents on the polymerization of **1a** and **2a**.

entry [a]	solvent	yield [%]	M_n [b]	M_w [b]	PDI [b]
1	DMSO	64.8	6600	8900	1.35
2	DMAc	63.2	6100	7800	1.29
3	DMF	65.3	6400	8600	1.34
4	MeCN	77.2	7000	10 500	1.49
5	THF	84.5	6700	9500	1.41
6	$CHCl_3$	79.2	6300	8600	1.37
7	DCM	83.4	6900	10 100	1.47

[a] Carried out in different solvents at ambient condition in the presence of DBU for 24 h. [**1a**]: [**2a**]: [DBU] = 1.0: 1.0: 0.4. [**1a**] = 0.2 mmol; [b] Estimated by GPC in DMF based on PMMA standard samples. M_w = weight-average molecular weight; polydispersity index (PDI) = M_w/M_n; M_n = number-average molecular weight.

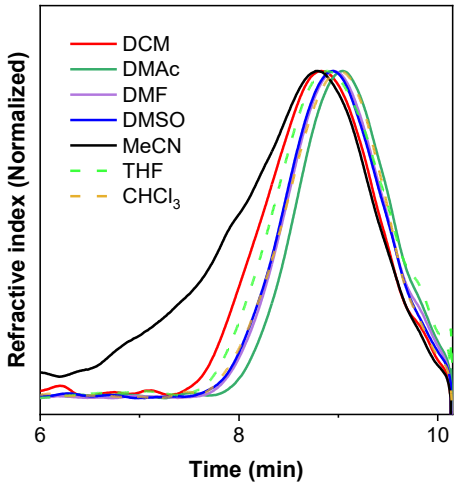

Figure S1. GPC curves of P**1a2a** prepared in different solvents.

Table S2. Effect of different bases on the polymerization of **1a** and **2a**.

entry [a]	base	yield [%]	M_n [b]	M_w [b]	PDI [b]
1	DBU	81.4	6700	9600	1.45
2	TEA				
3	DABCO		No polymer		
4	DMAP				

[a] Carried out in DCM at ambient condition in the presence of different bases for 24 h. [**1a**]: [**2a**]: [catalyst] = 1.0: 1.0: 0.4. [**1a**] = 0.2 mmol; [b] Estimated by GPC in DMF based on PMMA standard samples. M_w = weight-average molecular weight; polydispersity index (PDI) = M_w/M_n; M_n = number-average molecular weight.

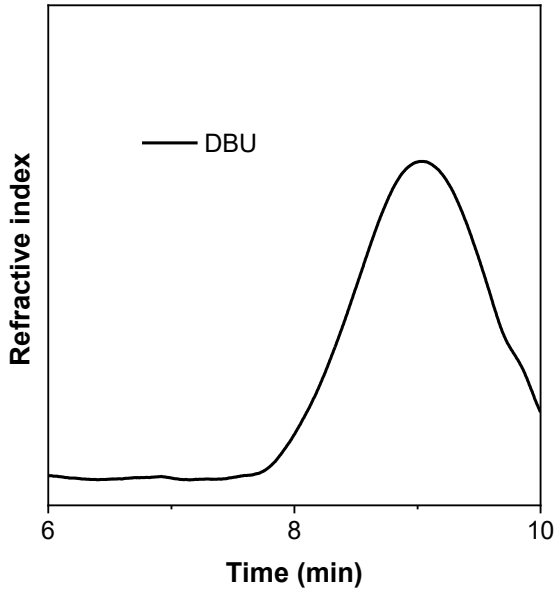

Figure S2. GPC curves of P**1a2a** prepared under the bases of DBU.

Table S3. Effect of concentration on the polymerization of **1a** and **2a**.

entry [a]	[**1a**] [M]	yield [%]	M_n [b]	M_w [b]	PDI [b]
1	0.1	37.5	4400	5000	1.13
2	0.2	82.3	7300	11 000	1.50
3	0.3	86.9	15 800	27 400	1.73
4	0.4	91.6	17 000	28 900	1.72
5	0.5	89.6	19 000	38 200	1.97
6	0.6	91.5	19 000	40 100	2.07
7	0.7	94.0	17 500	39 100	2.23
8	0.8	93.3	17 100	42 100	2.46

[a] Carried out in DCM at ambient condition in the presence of DBU at different monomer concentration for 24 h. [**1a**]: [**2a**]: [DBU] = 1.0: 1.0: 0.4. [**1a**] = 0.1 - 0.8 mmol; [b] Estimated by GPC in DMF based on PMMA standard samples. M_w = weight-average molecular weight; polydispersity index (PDI) = M_w/M_n; M_n = number-average molecular weight.

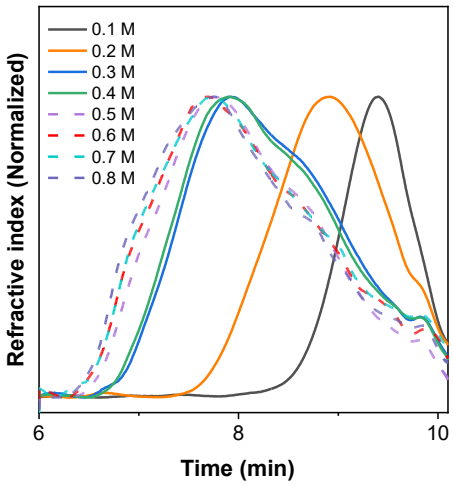

Figure S3. GPC curves of P**1a2a** prepared in different concentration.

Table S4. Effect of catalyst ratio on the polymerization of **1a** and **2a**.

entry [a]	[DBU]/ [**1a**]	yield [%]	M_n [b]	M_w [b]	PDI [b]
1	0.1	96.0	12 800	23 000	1.80
2	0.2	95.8	16 600	33 500	2.02
3	0.3	98.1	15 300	32 100	2.10
4	0.4	94.3	16 200	38 000	2.35

[a] Carried out in DCM at ambient condition in the presence of different DBU ratio for 24 h. [**1a**]: [**2a**] = 1.0: 1.0. [**1a**] = 0.6 mmol; [b] Estimated by GPC in DMF based on PMMA standard samples. M_w = weight-average molecular weight; polydispersity index (PDI) = M_w/M_n; M_n = number-average molecular weight.

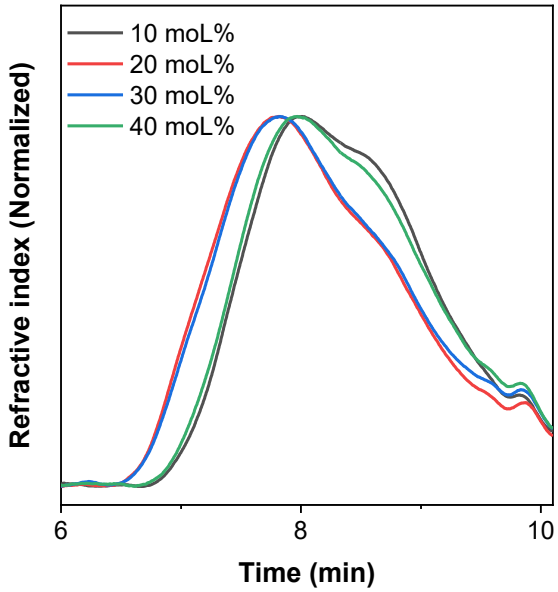

Figure S4. GPC curves of P**1a2a** prepared with different catalyst ratio.

Table S5. Effect of time on the polymerization of **1a** and **2a**.

entry [a]	*t* [h]	yield [%]	M_n [b]	M_w [b]	PDI [b]
1	6	94.7	8500	12 800	1.50
2	12	95.1	12 200	18 000	1.48
3	18	93.3	12 500	22 100	1.77
4	24	92.1	17 300	31 300	1.81

[a] Carried out in DCM at ambient condition in the presence of DBU for different reaction time. [**1a**]: [**2a**]: [DBU] = 1.0: 1.0: 0.2. [**1a**] = 0.6 mmol; [b] Estimated by GPC in DMF based on PMMA standard samples. M_w = weight-average molecular weight; polydispersity index (PDI) = M_w/M_n; M_n = number-average molecular weight.

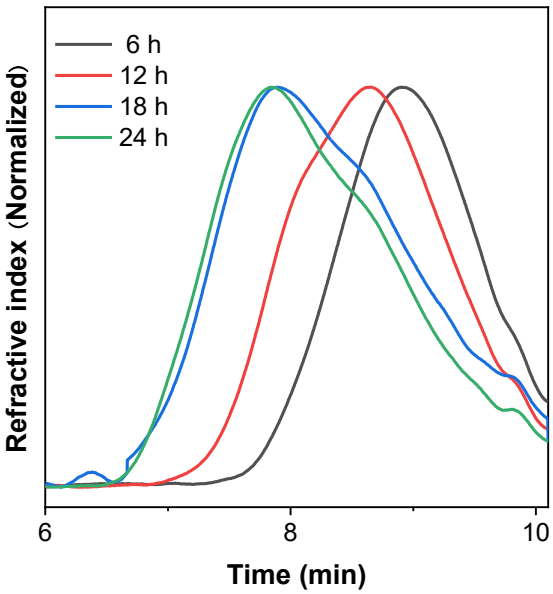

Figure S5. GPC curves of P**1a2a** prepared at different time durations.

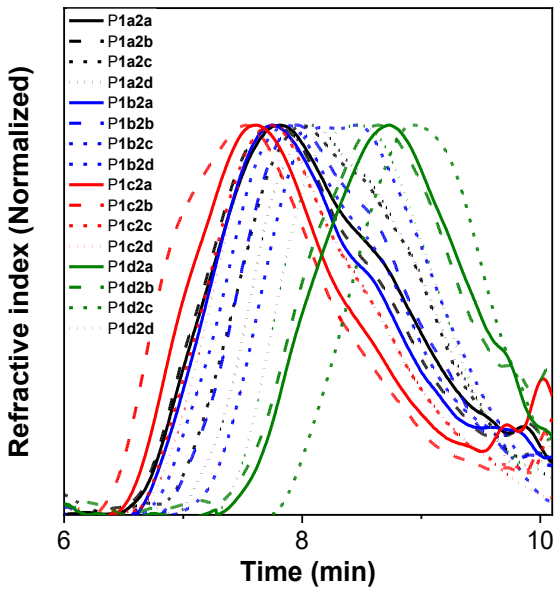

Figure S6. GPC curves of different PAANs.

Characterization data of PAANs

Characterization data for P**1a2a**. A grayish solid was obtained in 95.8% yield. M_w = 33 500, M_w/M_n = 2.02. IR (KBr disk), ν (cm^{-1}): 3058, 2904, 2239 (C≡N), 1684, 1597, 1448, 1213, 1001, 756, 690. ^{1}H NMR (400 MHz, Chloroform-*d*) δ 8.19 – 7.67, 7.67 – 7.30, 7.26 – 6.31, 4.67 – 3.95, 3.94 – 2.98. ^{13}C NMR (100 MHz, Chloroform-*d*) δ 138.66, 138.50, 136.41, 133.44, 128.78, 128.55, 127.99, 119.15.

Characterization data for P**1a2b**. A white solid was obtained in 96.6% yield. M_w = 37 100, M_w/M_n = 1.67. IR (KBr disk), ν (cm^{-1}): 3057, 2926, 2239 (C≡N), 1683, 1596, 1448, 1211, 988, 756, 689. ^{1}H NMR (400 MHz, Chloroform-*d*) δ 8.22 – 7.67, 7.47, 7.26 – 6.60, 4.30, 3.97 – 3.09. ^{13}C NMR (100 MHz, Chloroform-*d*) δ 197.33, 137.74, 136.47, 133.55, 128.76, 128.48, 128.02, 119.03, 44.93, 42.55, 41.37.

Characterization data for P**1a2c**. A white solid was obtained in 95.6% yield. M_w = 47 800, M_w/M_n = 1.64. IR (KBr disk), ν (cm^{-1}): 3028, 2901, 2239 (C≡N), 1683, 1596, 1498, 1447, 1211, 1002, 757, 689. ^{1}H NMR (400 MHz, Chloroform-*d*) δ 8.21 – 7.70, 7.69 – 7.26, 7.22 – 6.74, 4.73 – 4.15, 4.08 – 3.17. ^{13}C NMR (100 MHz, Chloroform-*d*) δ 197.43, 139.58, 137.25, 136.46, 134.57, 133.68, 128.79, 128.72, 128.03, 127.10, 126.75, 119.03, 44.92, 42.55, 41.58.

Characterization data for P**1a2d**. A white solid was obtained in 89.7% yield. M_w = 12 500, M_w/M_n = 1.50. IR (KBr disk), ν (cm^{-1}): 2935, 2840, 2239 (C≡N), 1674, 1600, 1510, 1259, 1170, 1025, 833, 708. ^{1}H NMR (400 MHz, Chloroform-*d*) δ 7.82, 6.89, 4.26, 3.94 – 2.93. ^{13}C NMR (100 MHz, Chloroform-*d*) δ 195.71, 195.13, 163.87, 163.71, 130.86, 130.33, 129.56, 119.26, 113.91, 55.50, 45.28, 42.50.

Characterization data for P**1b2a**. A white solid was obtained in 90.2% yield. M_w = 37 000, M_w/M_n = 1.74. IR (KBr disk), ν (cm^{-1}): 3058, 2927, 2239 (C≡N), 1684, 1596, 1448, 1213, 1001, 755, 690. ^{1}H NMR (400 MHz, Chloroform-*d*) δ 8.22 – 7.68 (m, 4H), 7.62 – 7.31, 7.27 – 6.39, 4.58 – 3.96,

3.93 – 2.90. ^{13}C NMR (100 MHz, Chloroform-*d*) δ 197.12, 136.46, 134.98, 133.48, 128.71, 128.03, 119.32, 45.20, 42.74, 41.35.

Characterization data for P**1b2b**. A white solid was obtained in 88.1% yield. M_w = 25 700, M_w/M_n = 1.67. IR (KBr disk), ν (cm^{-1}): 3058, 2926, 2239 (C≡N), 1683, 1596, 1448, 1212, 1001, 756, 690. ^{1}H NMR (400 MHz, Chloroform-*d*) δ 8.15 – 7.67, 7.58 – 7.17, 7.15 – 6.54, 4.58 – 3.95, 3.92 – 3.13. ^{13}C NMR (100 MHz, Chloroform-*d*) δ 197.31, 196.82, 136.44, 133.47, 128.69, 128.00, 44.84, 42.68, 41.39.

Characterization data for P**1b2c**. A white solid was obtained in 95.5% yield. M_w = 60 200, M_w/M_n = 1.89. IR (KBr disk), ν (cm^{-1}): 3028, 2901, 2238 (C≡N), 1682, 1595, 1497, 1448, 1210, 1002, 755, 689. ^{1}H NMR (400 MHz, Chloroform-*d*) δ 8.14 – 7.68, 7.68 – 7.28, 7.24 – 6.83, 4.60 – 4.01, 4.00 – 3.08. ^{13}C NMR (100 MHz, Chloroform-*d*) δ 197.22, 139.67, 137.21, 136.45, 133.61, 133.43, 128.98, 128.75, 128.51, 128.03, 127.20, 126.91, 119.05, 44.85, 42.75, 41.61.

Characterization data for P**1b2d**. A white solid was obtained in 92.6% yield. M_w = 12 200, M_w/M_n = 1.58. IR (KBr disk), ν (cm^{-1}): 2935, 2840, 2239 (C≡N), 1675, 1600, 1510, 1419, 1260, 1170, 1027, 833, 707. ^{1}H NMR (400 MHz, Chloroform-*d*) δ 8.16 – 7.60, 7.49 – 6.59, 4.53 – 3.97, 3.94 – 2.90. ^{13}C NMR (100 MHz, Chloroform-*d*) δ 195.63, 163.75, 130.84, 130.37, 129.58, 119.43, 113.87, 55.48, 45.32, 42.72, 40.97.

Characterization data for P**1c2a**. A white solid was obtained in 83.1% yield. M_w = 24 000, M_w/M_n = 1.67. IR (KBr disk), ν (cm^{-1}): 3059, 2922, 2239 (C≡N), 1685, 1597, 1448, 1213, 1001, 755, 690. ^{1}H NMR (400 MHz, Chloroform-*d*) δ 8.15 – 7.65, 7.61 – 7.26, 7.10 – 6.44, 4.60 – 3.91, 3.89 – 3.04, 2.31 – 1.82. ^{13}C NMR (100 MHz, Chloroform-*d*) δ 196.67, 136.50, 133.41, 128.68, 128.02, 119.39, 45.27, 42.76, 41.41, 21.06.

Characterization data for P**1c2b**. A white solid was obtained in 86.0% yield. M_w = 18 700, M_w/M_n = 1.56. IR (KBr disk), ν (cm^{-1}): 3058, 2920, 2240 (C≡N), 1684, 1597, 1448, 1213, 1001, 756, 690. ^{1}H NMR (400 MHz, Chloroform-*d*) δ 8.07 – 7.64, 7.62 – 7.25, 7.16 – 6.38, 4.49 – 3.93, 3.92 – 3.06, 2.35 – 1.85. ^{13}C NMR (100 MHz, Chloroform-*d*) δ 197.34, 136.45, 133.46, 128.68, 127.99, 119.09, 44.78, 42.66, 41.44, 21.09.

Characterization data for P**1c2c**. A white solid was obtained in 95.6% yield. M_w = 35 800, M_w/M_n = 1.83. IR (KBr disk), ν (cm^{-1}): 3027, 2919, 2239 (C≡N), 1683, 1596,1498, 1448, 1210, 1002, 755, 689. ^{1}H NMR (400 MHz, Chloroform-*d*) δ 8.19 – 7.68, 7.68 – 7.26, 7.25 – 6.66, 4.56 – 4.00, 4.00 – 3.14, 2.31 – 1.87. ^{13}C NMR (100 MHz, Chloroform-*d*) δ 197.26, 139.80, 138.62, 137.35, 136.48, 134.81, 133.58, 128.75, 128.47, 128.03, 126.92, 119.24, 44.84, 42.76, 42.63, 41.61, 21.15.

Characterization data for P**1c2d**. A white solid was obtained in 85.0% yield. M_w = 9100, M_w/M_n = 1.33. IR (KBr disk), ν (cm^{-1}): 2935, 2841, 2239 (C≡N), 1675, 1600, 1510, 1260, 1170, 1027, 833, 708. ^{1}H NMR (400 MHz, Chloroform-*d*) δ 8.19 – 7.58, 7.53 – 7.15, 7.10 – 6.48, 4.70 – 3.95, 3.95 – 2.98, 2.36 – 1.82. ^{13}C NMR (100 MHz, Chloroform-*d*) δ 195.21, 163.75, 130.84, 130.37, 129.63, 119.52, 113.86, 55.48, 45.38, 42.74, 41.00, 21.09.

Characterization data for P**1d2a**. A pale-pink solid was obtained in 90.3% yield. M_w = 20 800, M_w/M_n = 1.66. IR (KBr disk), ν (cm^{-1}): 3060, 2931, 2238 (C≡N), 1681, 1597, 1448, 1213, 989 754, 689. ^{1}H NMR (400 MHz, Chloroform-*d*) δ 8.15 – 7.70, 7.63 – 7.30, 7.27 – 6.21, 4.63 – 3.98, 3.97 – 3.06. ^{13}C NMR (100 MHz, Chloroform-*d*) δ 197.21, 136.42, 133.62, 128.77, 127.99, 119.19, 45.17, 42.52.

Characterization data for P**1d2b**. A pale-pink solid was obtained in 95.1% yield. M_w = 28 200, M_w/M_n = 1.92. IR (KBr disk), ν (cm^{-1}): 3060, 2928, 2238 (C≡N), 1682, 1596, 1449, 1213, 1001,

754, 689. ^{1}H NMR (400 MHz, Chloroform-*d*) δ 8.31 – 7.68, 7.66 – 7.29, 7.21 – 6.14, 5.39 – 4.18, 4.17 – 3.09. ^{13}C NMR (100 MHz, Chloroform-*d*) δ 197.58, 136.29, 133.60, 131.85, 129.59, 128.74, 128.14, 119.39, 44.51, 41.45, 39.00.

Characterization data for P**1d2c**. A pale-pink solid was obtained in 95.8% yield. M_w = 34 000, M_w/M_n = 1.62. IR (KBr disk), ν (cm^{-1}): 3028, 2930, 2237 (C≡N), 1681, 1596, 1448, 1211, 1002, 754, 689. ^{1}H NMR (400 MHz, Chloroform-*d*) δ 8.17 – 7.76, 7.74 – 7.29, 7.24 – 6.32, 5.47 – 4.21, 4.19 – 3.28. ^{13}C NMR (100 MHz, Chloroform-*d*) δ 197.66, 136.75, 136.34, 133.65, 131.97, 129.40, 128.74, 128.17, 126.87, 120.85, 119.65, 118.22, 44.52, 41.69, 39.22.

Characterization data for P**1d2d**. A pale-pink solid was obtained in 85.5% yield. M_w = 16 600, M_w/M_n = 1.40. IR (KBr disk), ν (cm^{-1}): 2936, 2840, 2238 (C≡N), 1671, 1600, 1510, 1261, 1170, 1028, 833. ^{1}H NMR (400 MHz, Chloroform-*d*) δ 8.33 – 7.29, 7.22 – 6.13, 5.55 – 4.20, 4.29 – 2.85. ^{13}C NMR (100 MHz, Chloroform-*d*) δ 195.82, 163.78, 132.28, 130.50, 128.16, 120.10, 113.78, 55.48, 44.60, 41.08, 39.22.

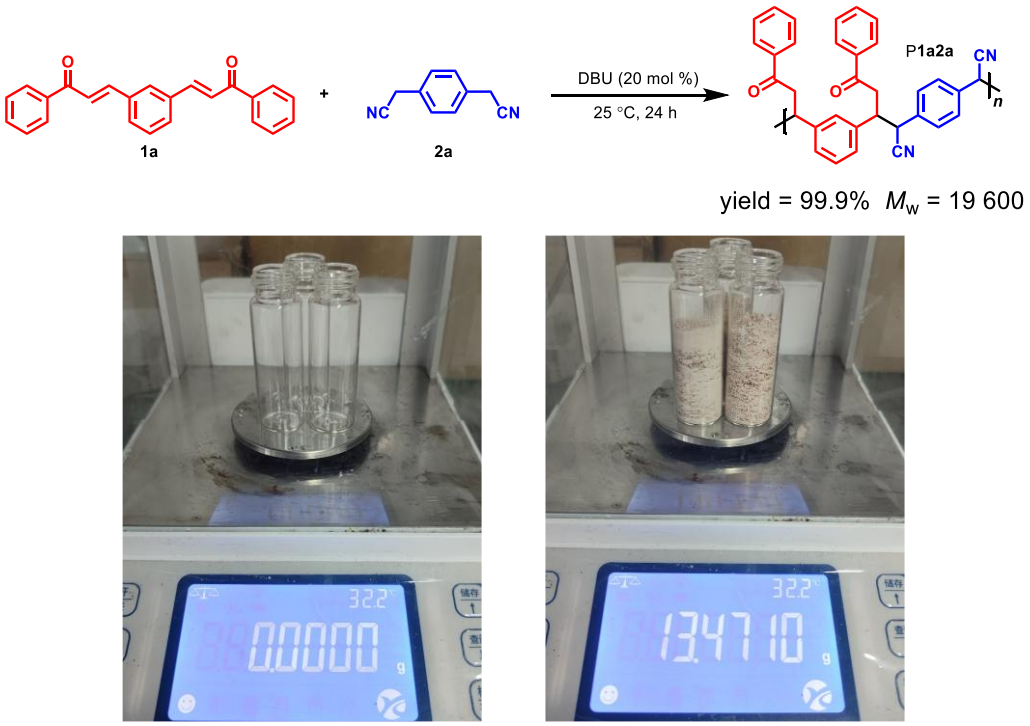

Figure S7. Large-scale preparation of P**1a2a**.

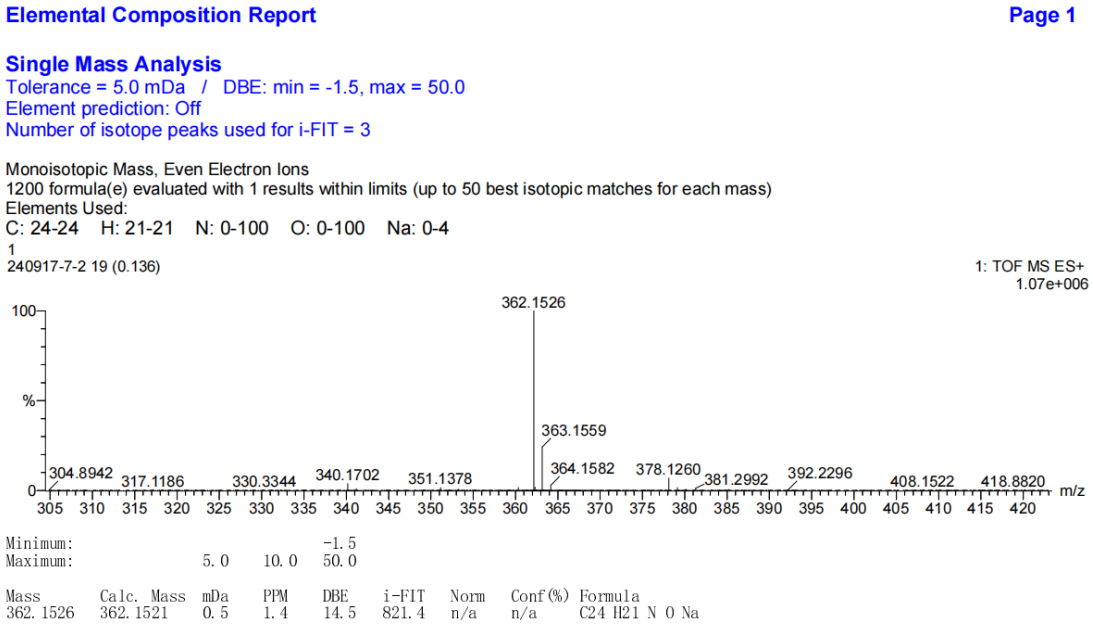

Figure S8. HRMS test of model compound **5**.

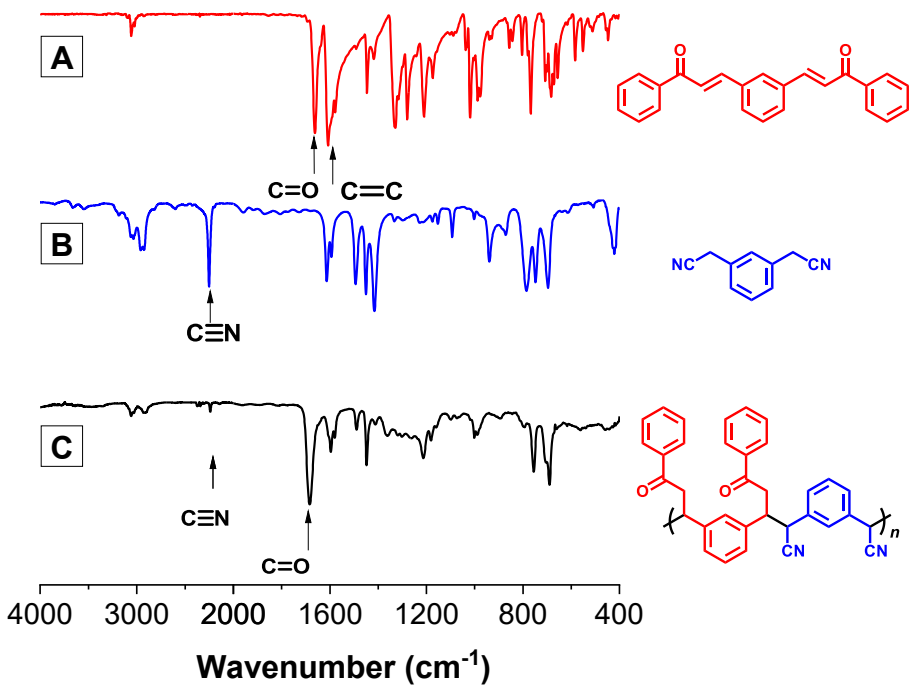

Figure S9. FT-IR spectra of **1a** (A), **2b** (B) and P**1a2b** (C).

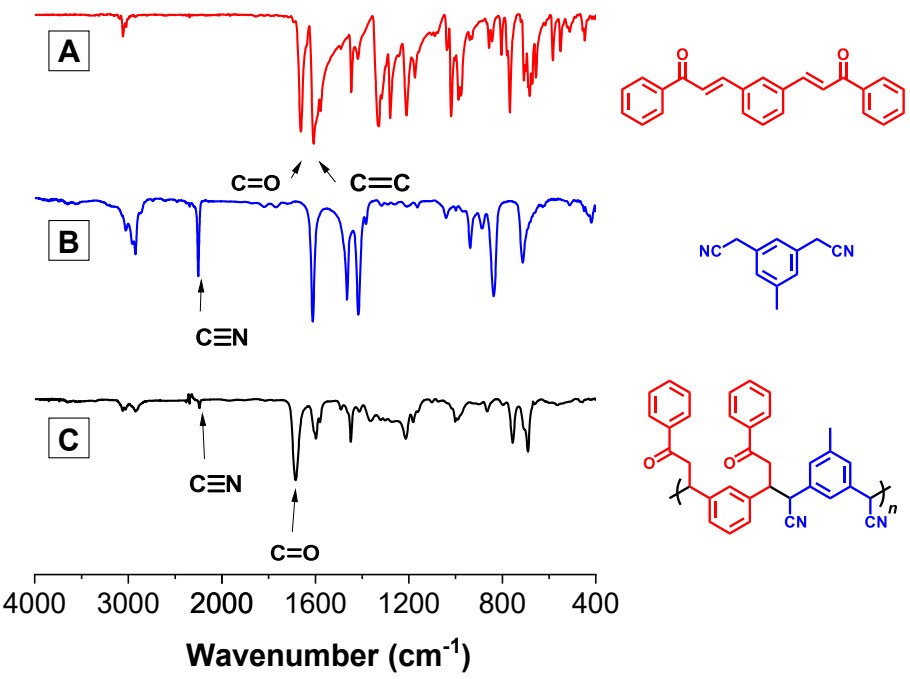

Figure S10. FT-IR spectra of **1a** (A), **2c** (B) and P**1a2c** (C).

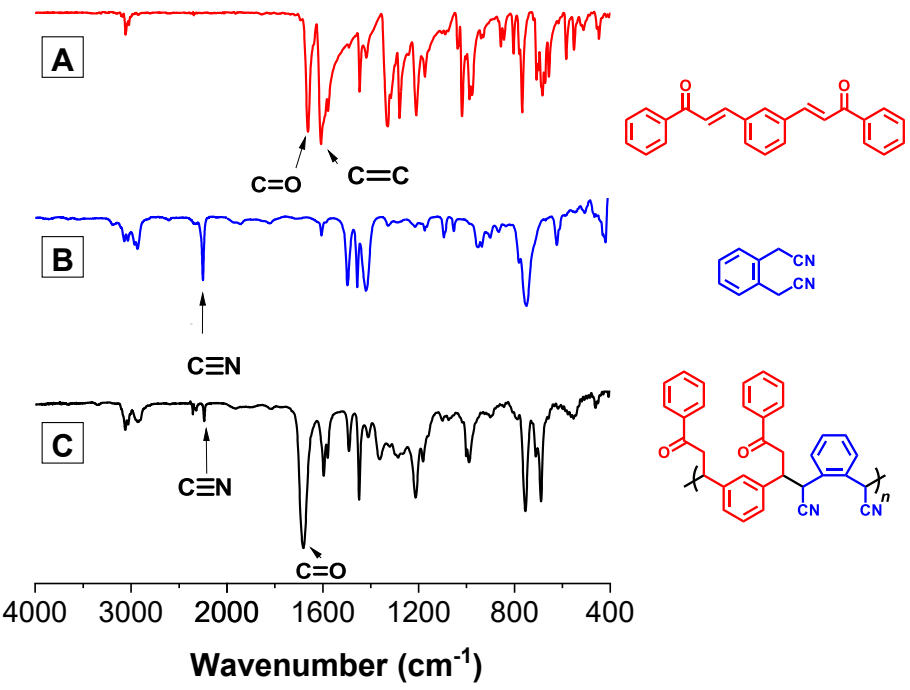

Figure S11. FT-IR spectra of **1a** (A), **2d** (B) and P**1a2d** (C).

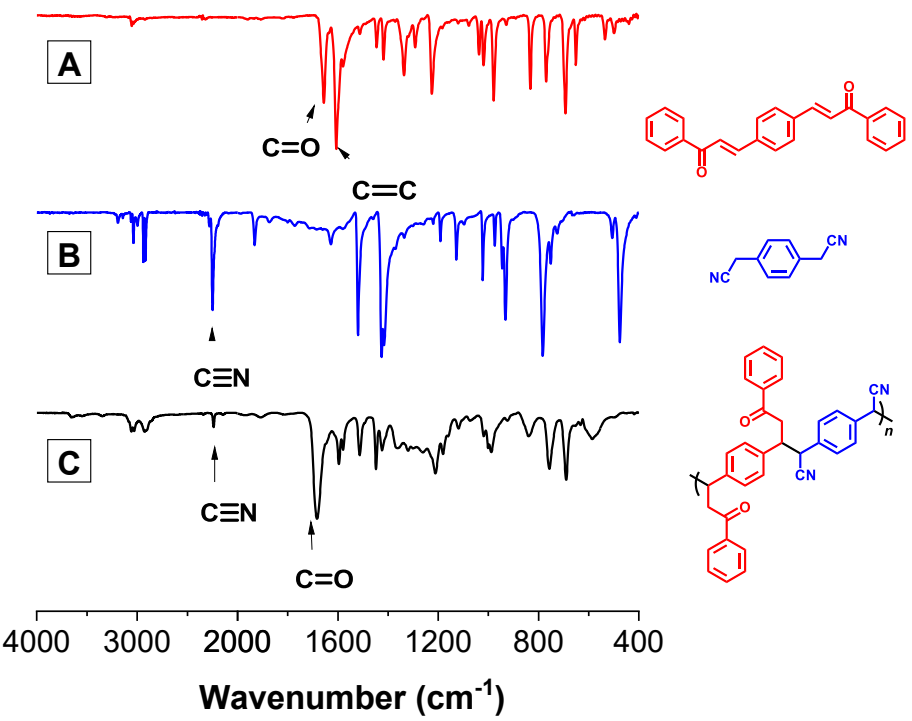

Figure S12. FT-IR spectra of **1b** (A), **2a** (B) and P**1b2a** (C).

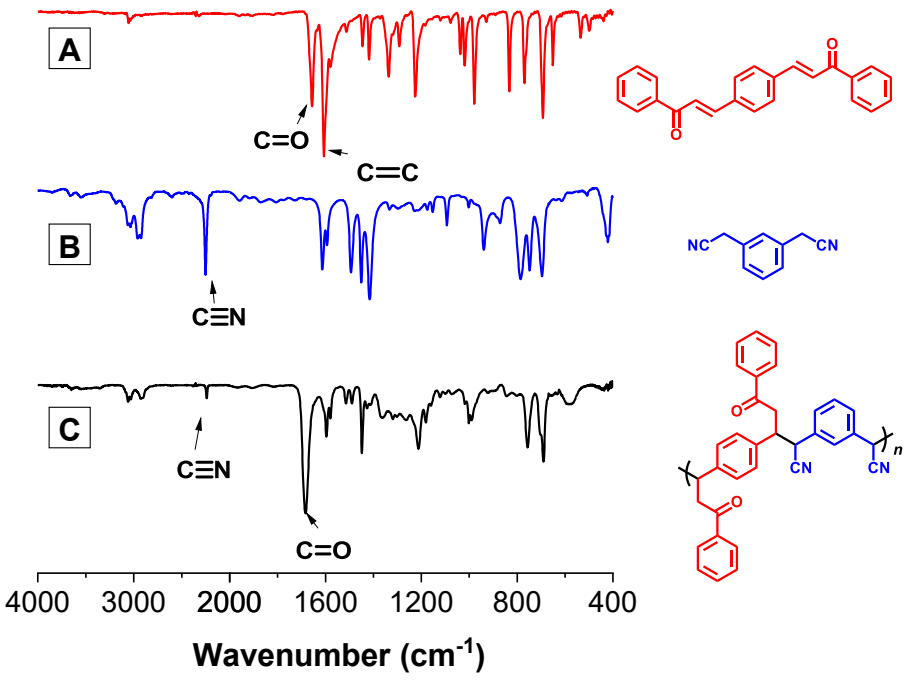

Figure S13. FT-IR spectra of **1b** (A), **2b** (B) and P**1b2b** (C).

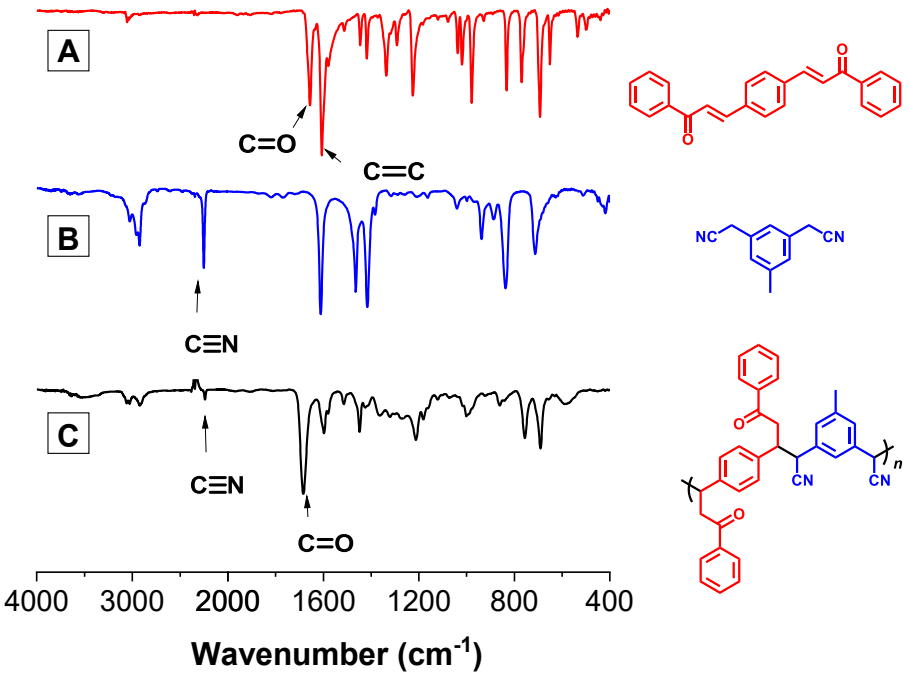

Figure S14. FT-IR spectra of **1b** (A), **2c** (B) and P**1b2c** (C).

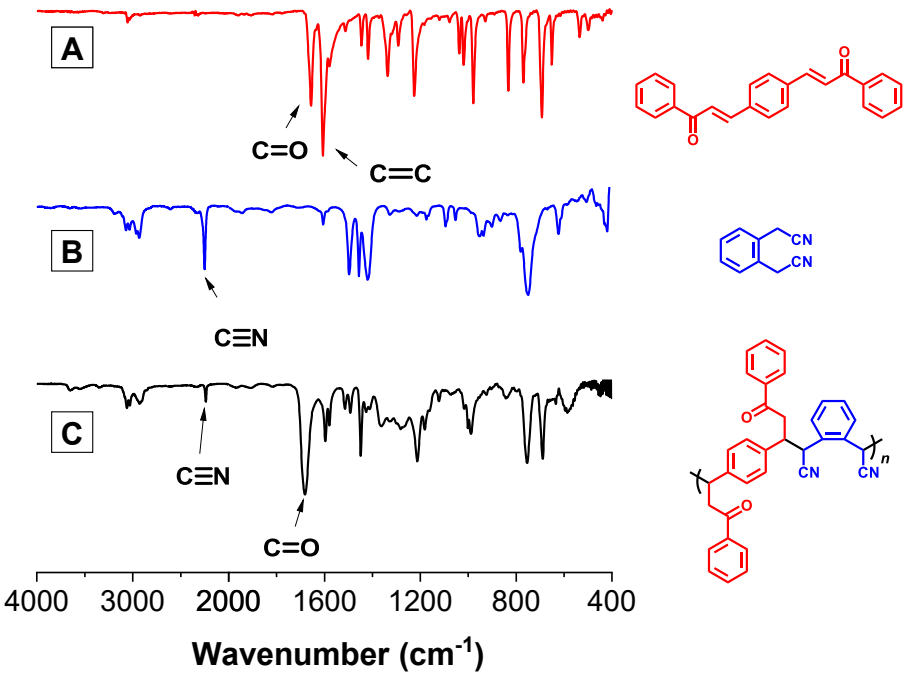

Figure S15. FT-IR spectra of **1b** (A), **2d** (B) and P**1b2d** (C).

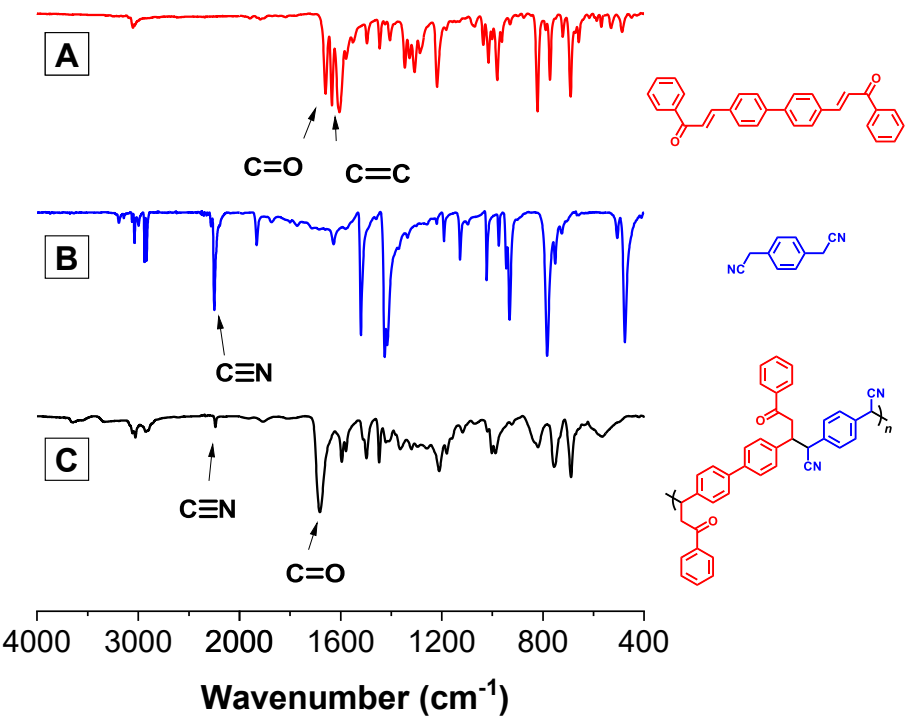

Figure S16. FT-IR spectra of **1c** (A), **2a** (B) and P**1c2a** (C).

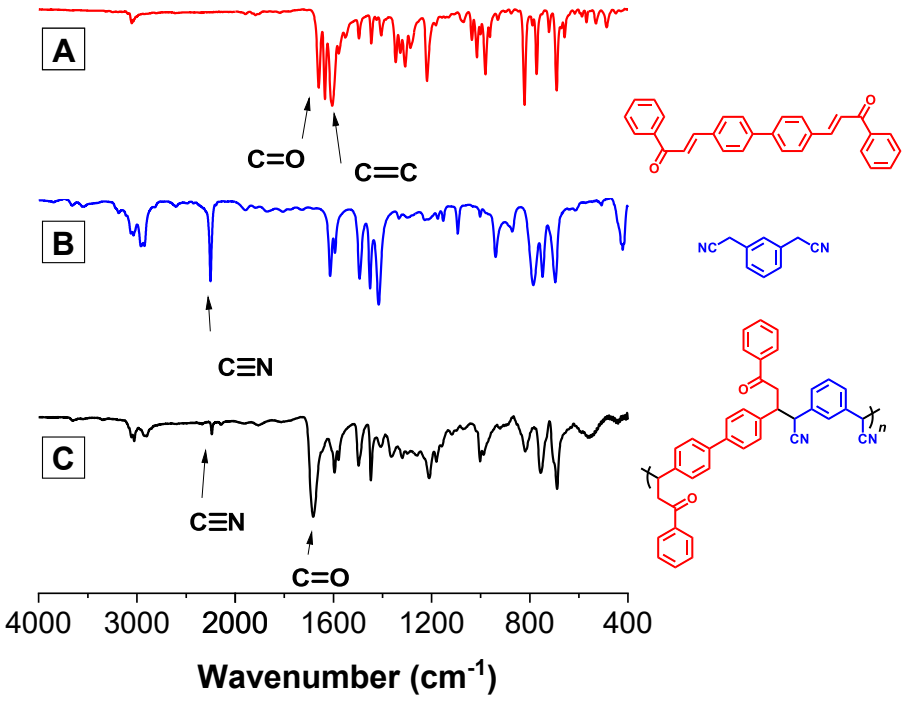

Figure S17. FT-IR spectra of **1c** (A), **2b** (B) and P**1c2b** (C).

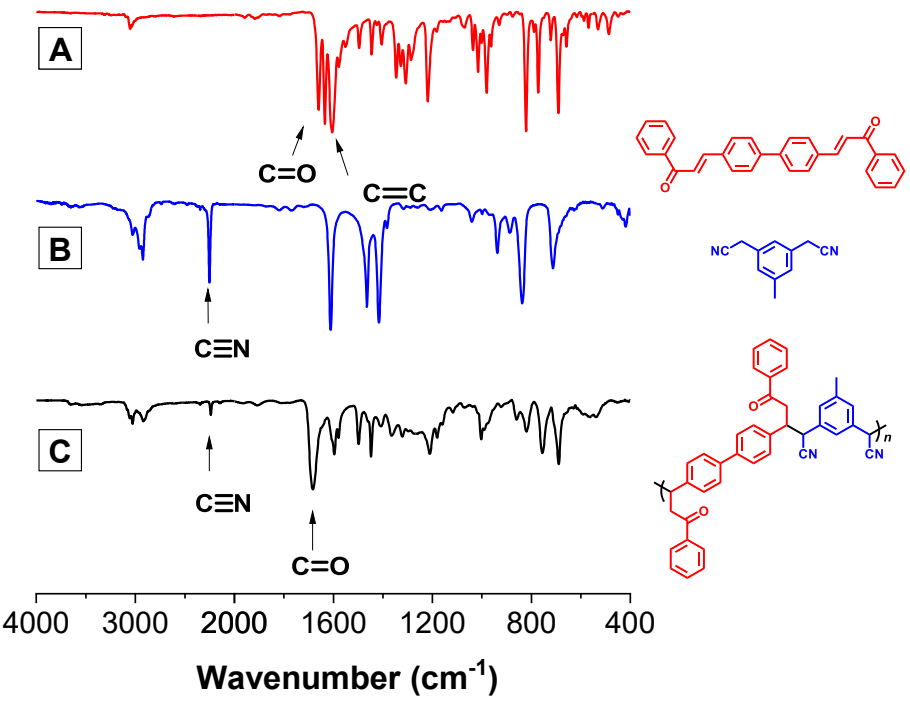

Figure S18. FT-IR spectra of **1c** (A), **2c** (B) and P**1c2c** (C).

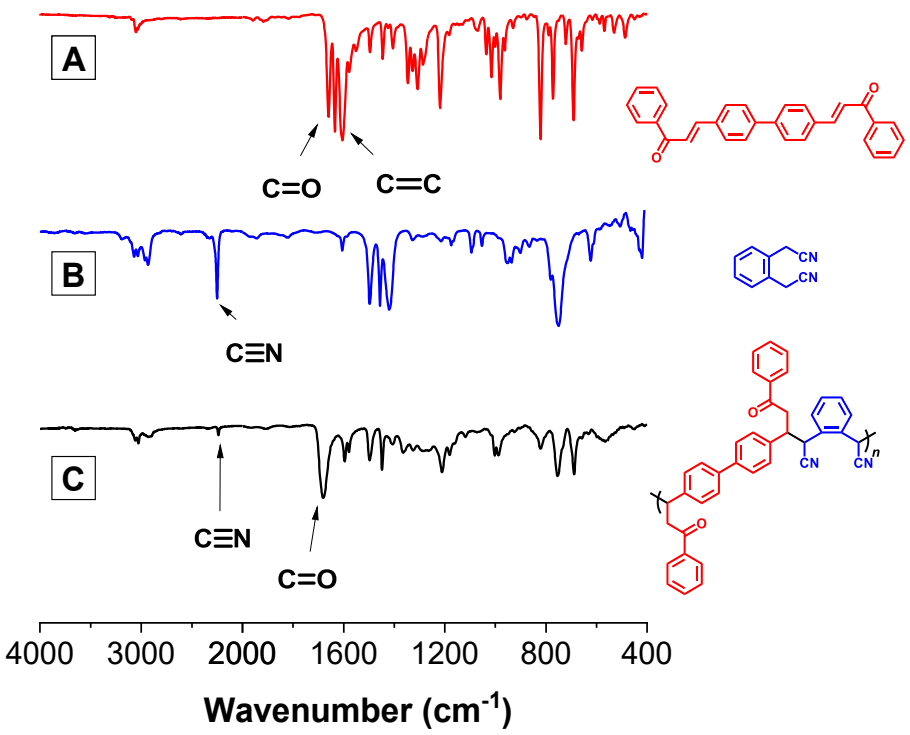

Figure S19. FT-IR spectra of **1c** (A), **2d** (B) and P**1c2d** (C).

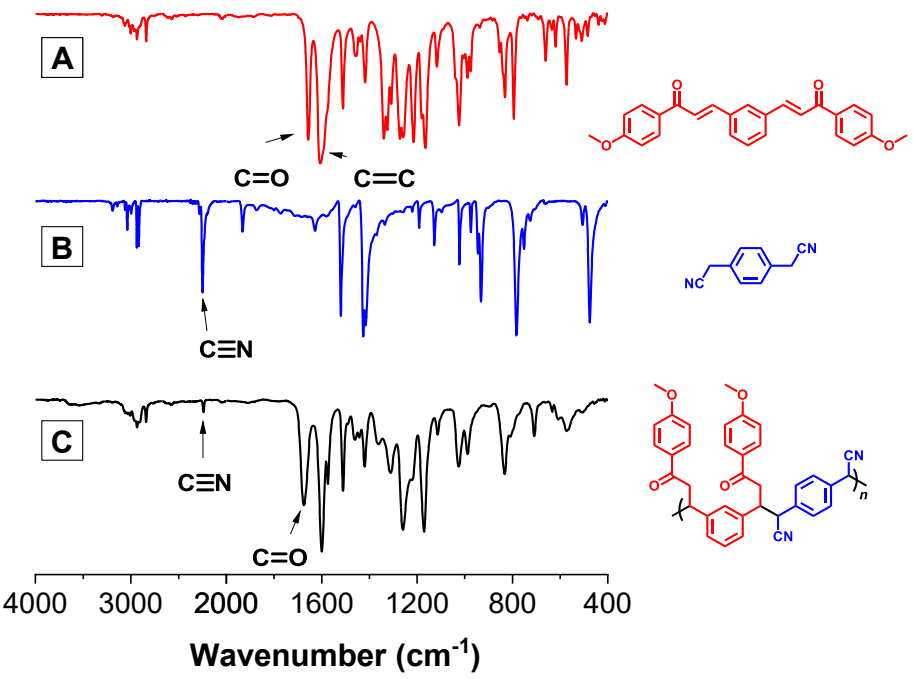

Figure S20. FT-IR spectra of **1d** (A), **2a** (B) and P**1d2a** (C).

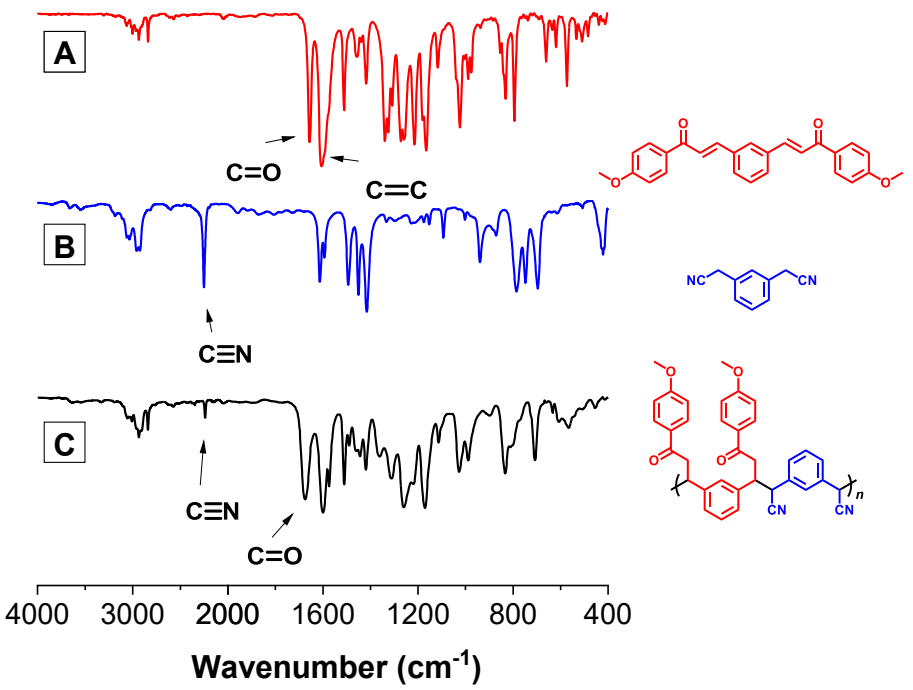

Figure S21. FT-IR spectra of **1d** (A), **2b** (B) and P**1d2b** (C).

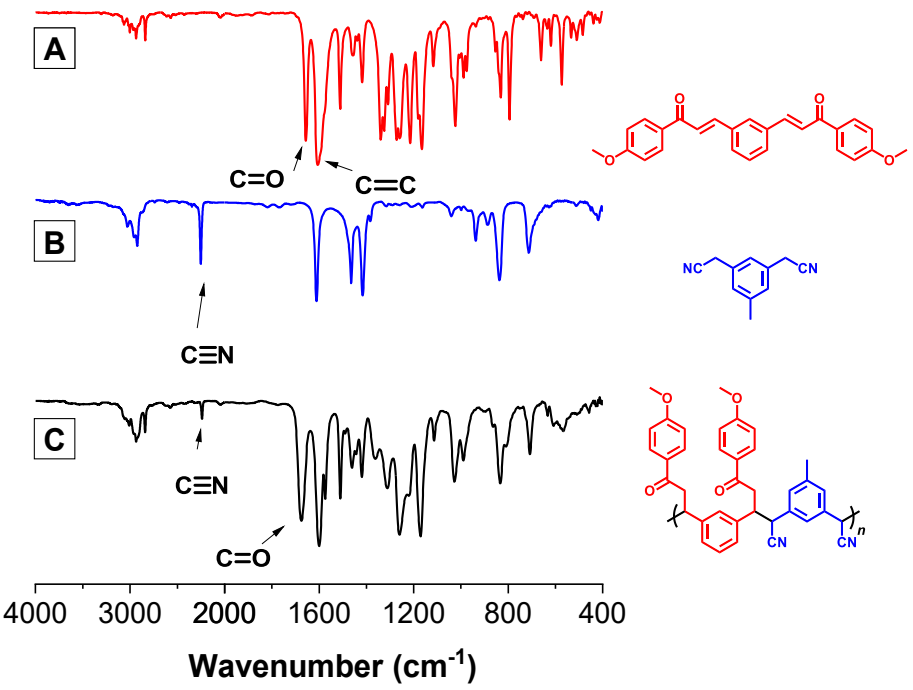

Figure S22. FT-IR spectra of **1d** (A), **2c** (B) and P**1d2c** (C).

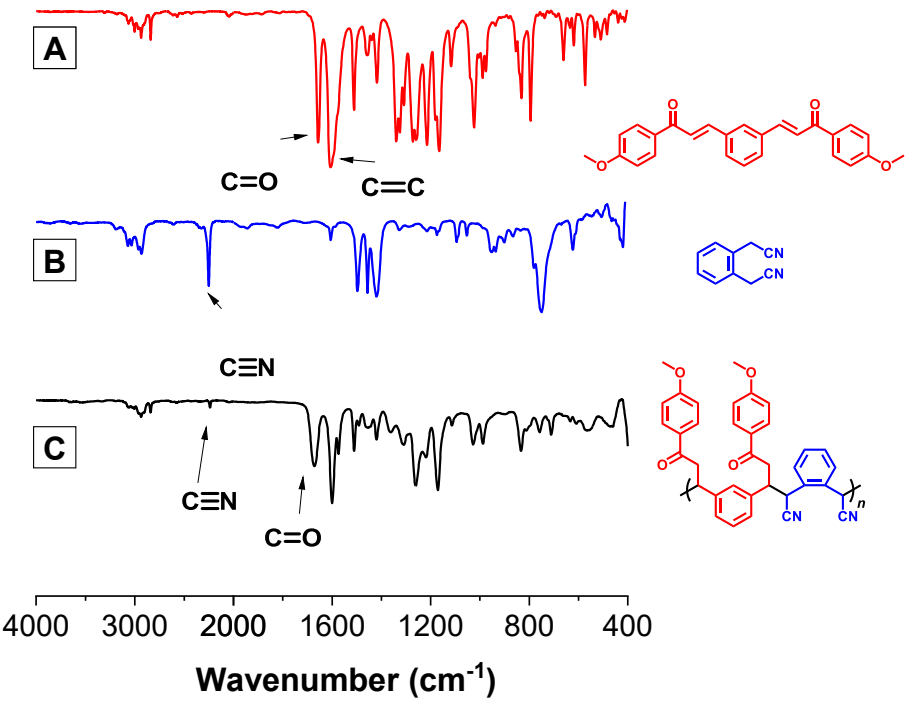

Figure S23. FT-IR spectra of **1d** (A), **2d** (B) and P**1d2d** (C).

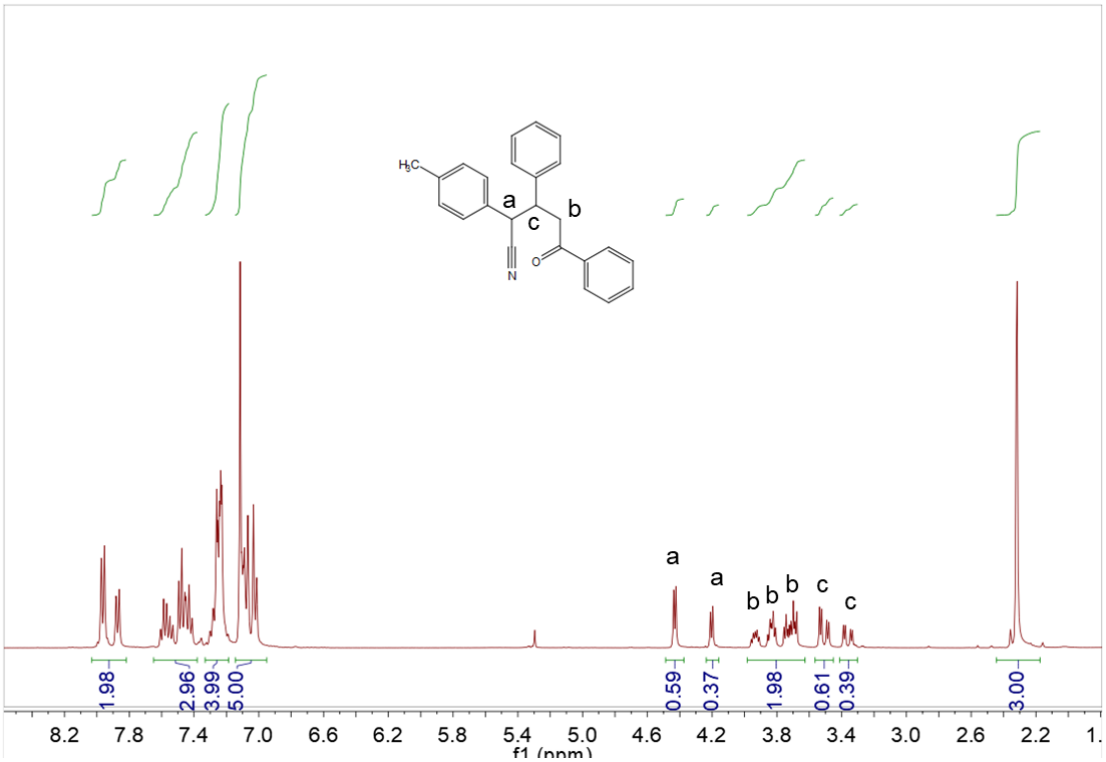

Figure S24. ^{1}H NMR spectra of model compound **5**.

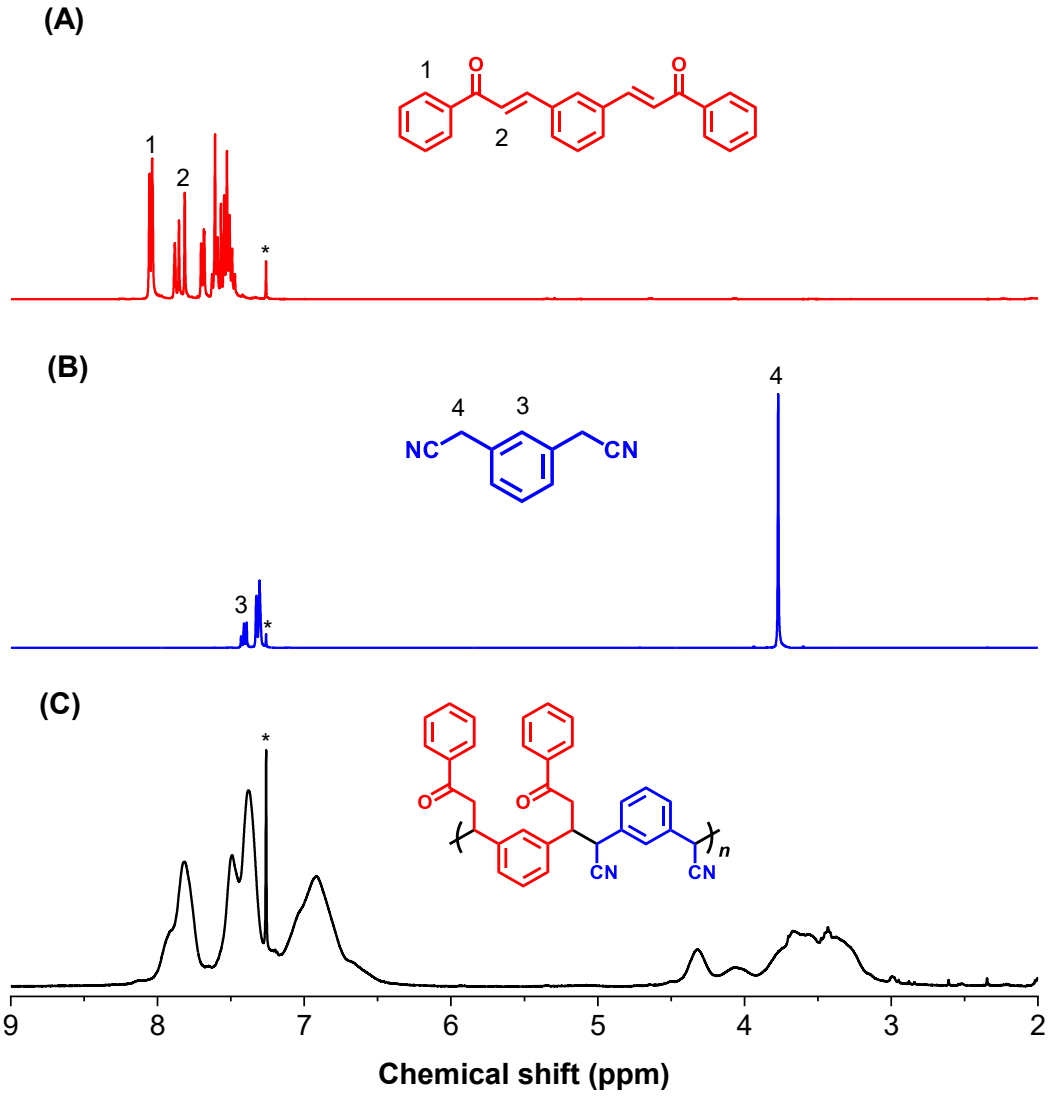

Figure S25. ^{1}H NMR spectra of **1a** (A), **2b** (B) and P**1a2b** (C) in $CDCl_3$. The solvent peaks are marked with asterisks.

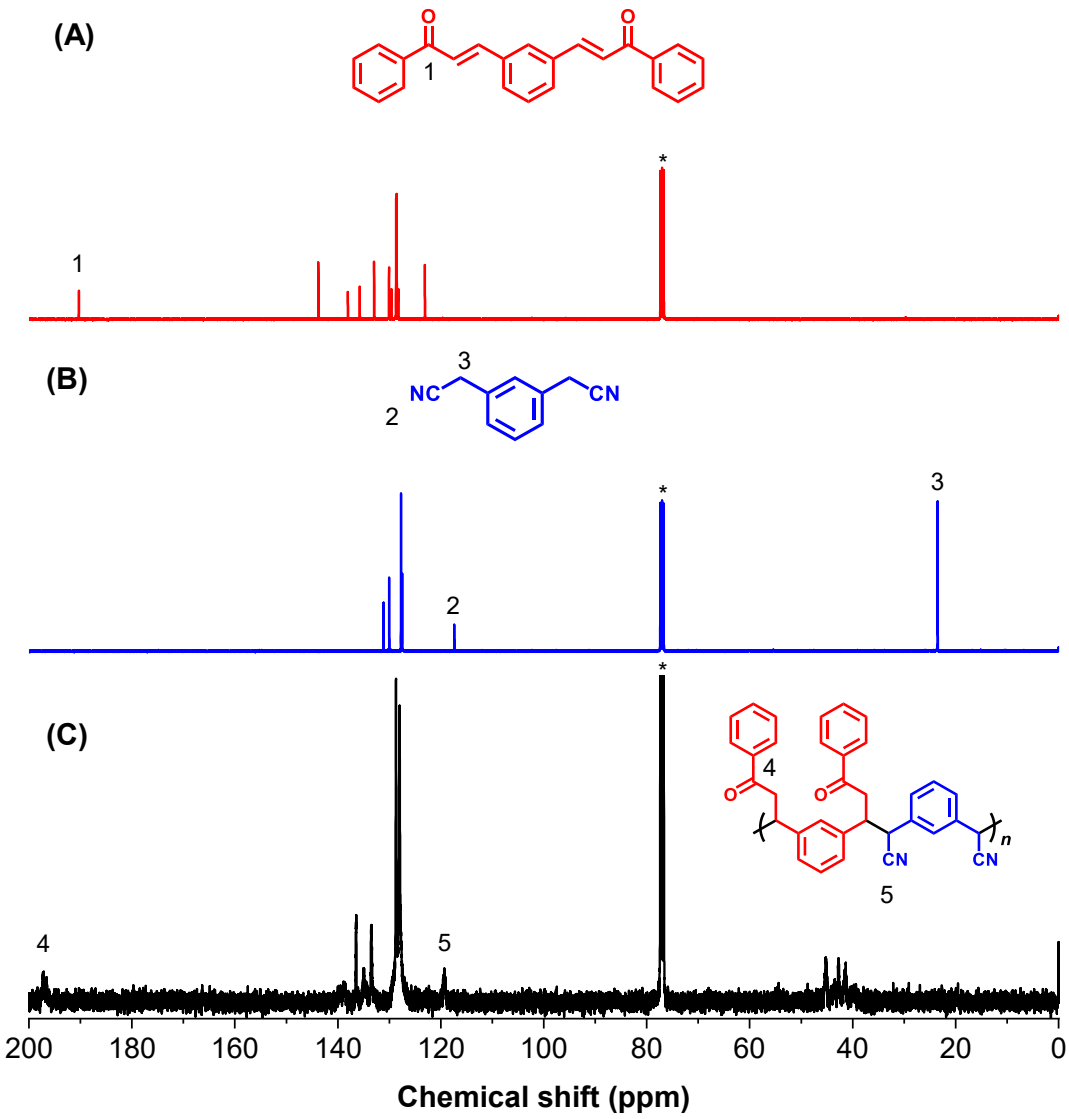

Figure S26. ^{13}C NMR spectra of **1a** (A), **2b** (B) and P**1a2b** (C) in $CDCl_3$. The solvent peaks are marked with asterisks.

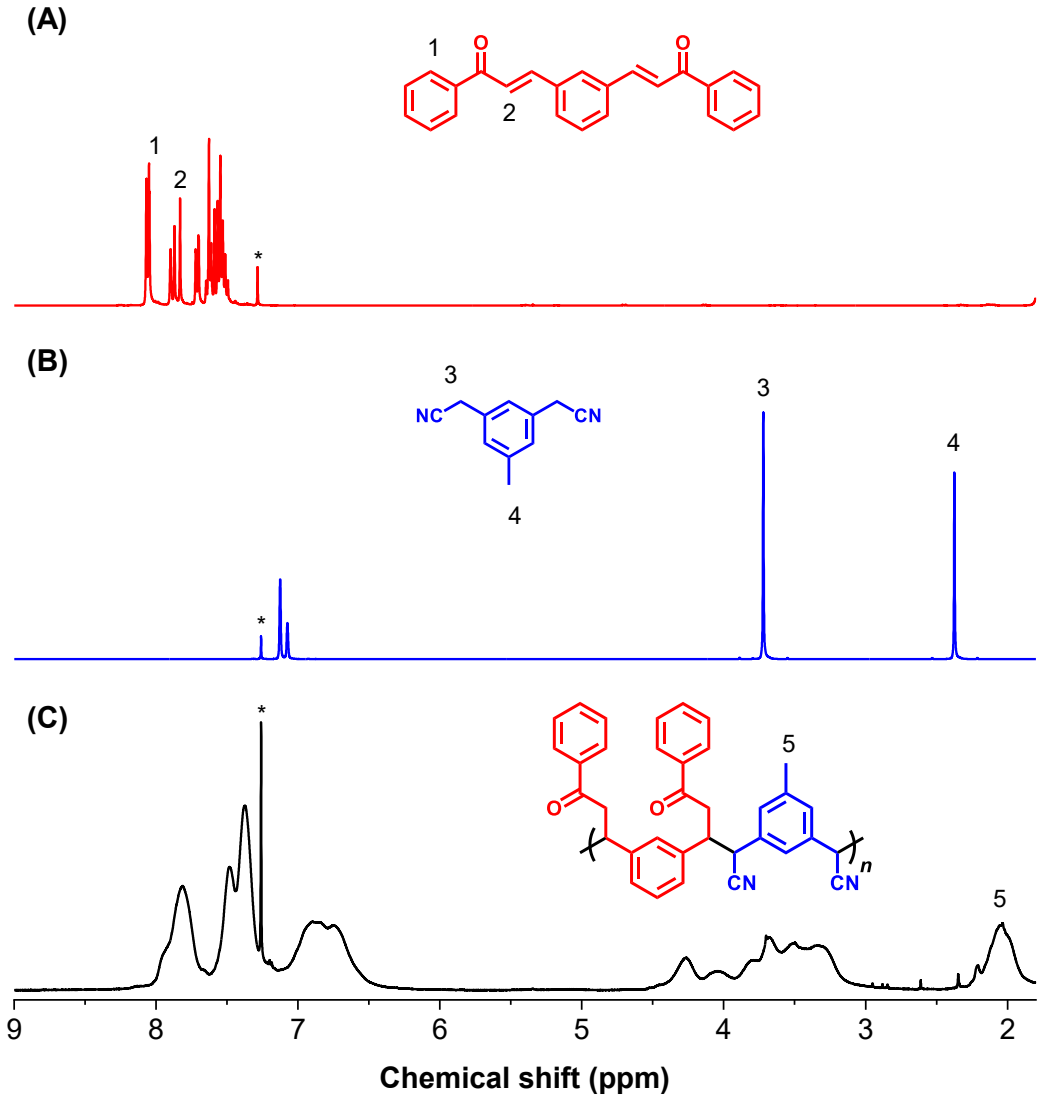

Figure S27. ^{1}H NMR spectra of **1a** (A), **2c** (B) and P**1a2c** (C) in $CDCl_3$. The solvent peaks are marked with asterisks.

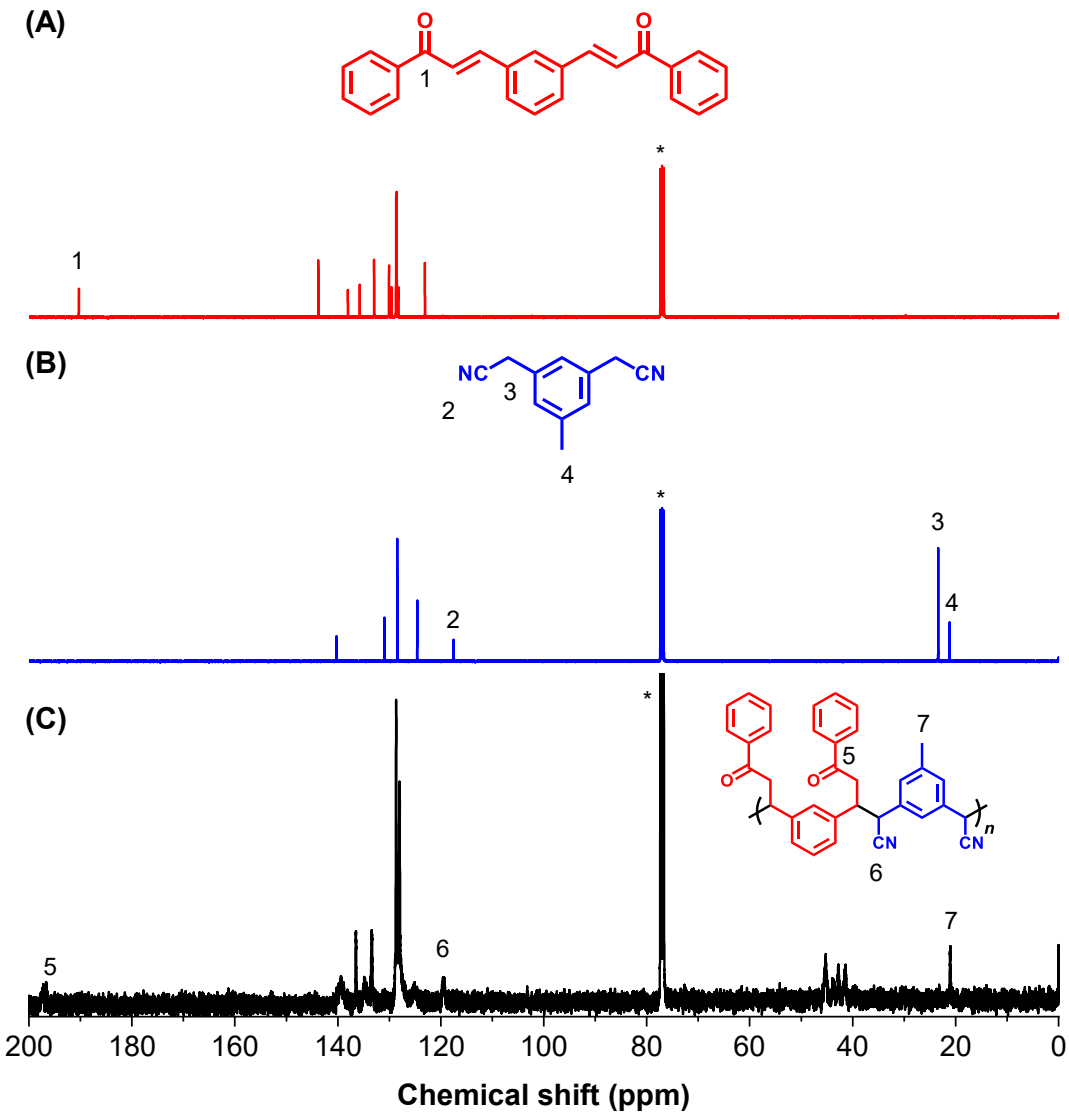

Figure S28. ^{13}C NMR spectra of **1a** (A), **2c** (B) and P**1a2c** (C) in $CDCl_3$. The solvent peaks are marked with asterisks.

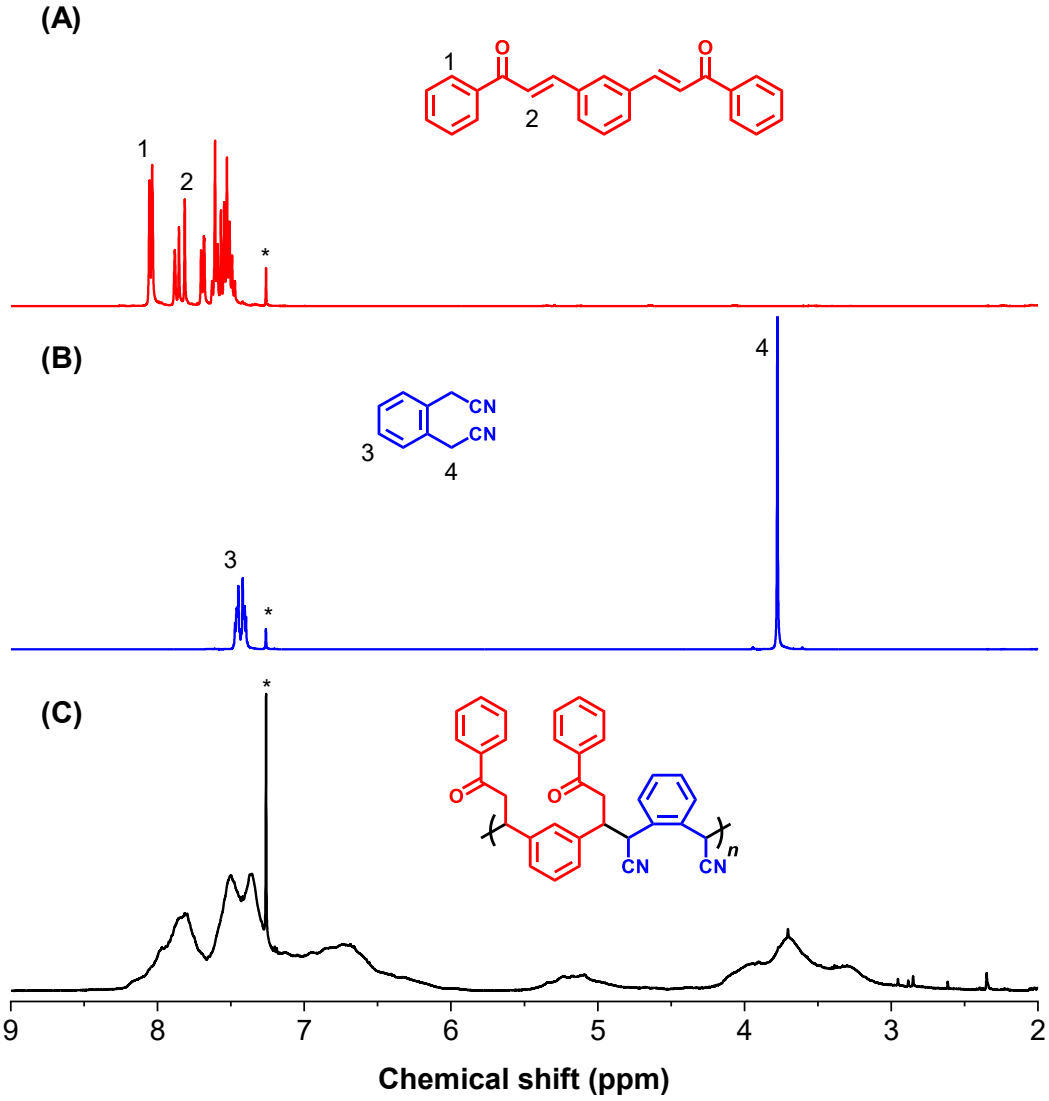

Figure S29. ^{1}H NMR spectra of **1a** (A), **2d** (B) and P**1a2d** (C) in $CDCl_3$. The solvent peaks are marked with asterisks.

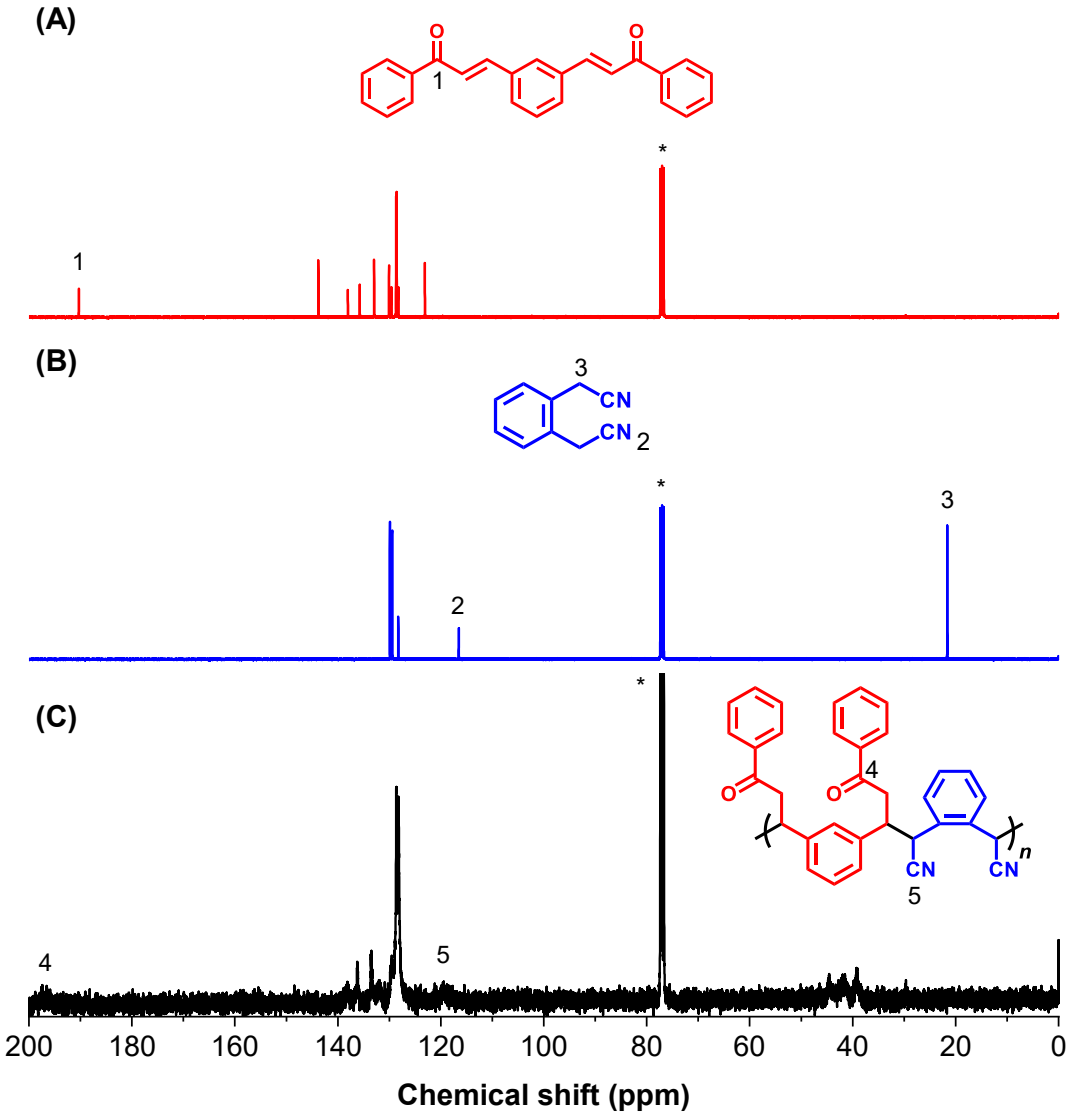

Figure S30. ^{13}C NMR spectra of **1a** (A), **2d** (B) and P**1a2d** (C) in $CDCl_3$. The solvent peaks are marked with asterisks.

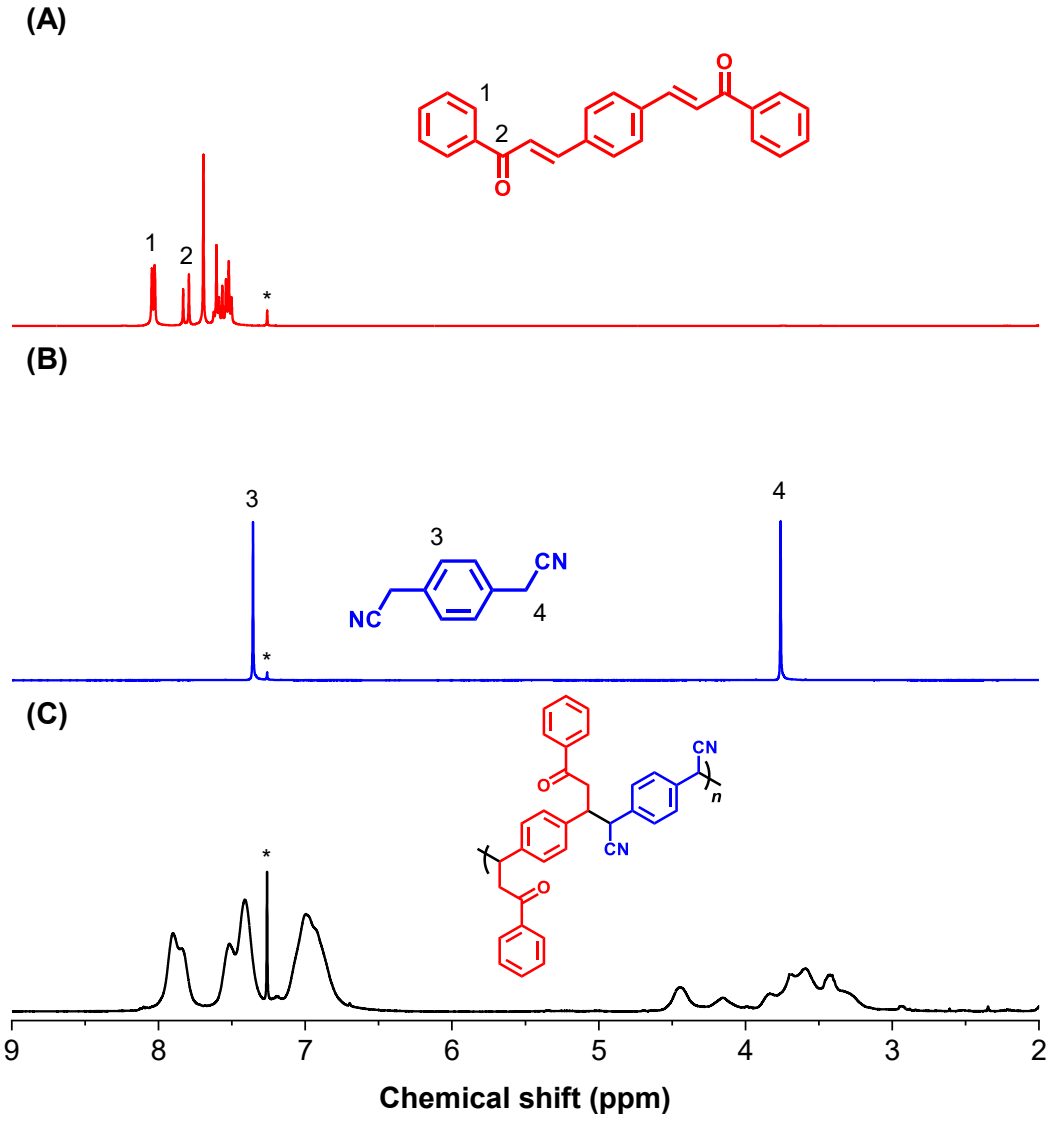

Figure S31. ^{1}H NMR spectra of **1b** (A), **2a** (B) and P**1b2a** (C) in $CDCl_3$. The solvent peaks are marked with asterisks.

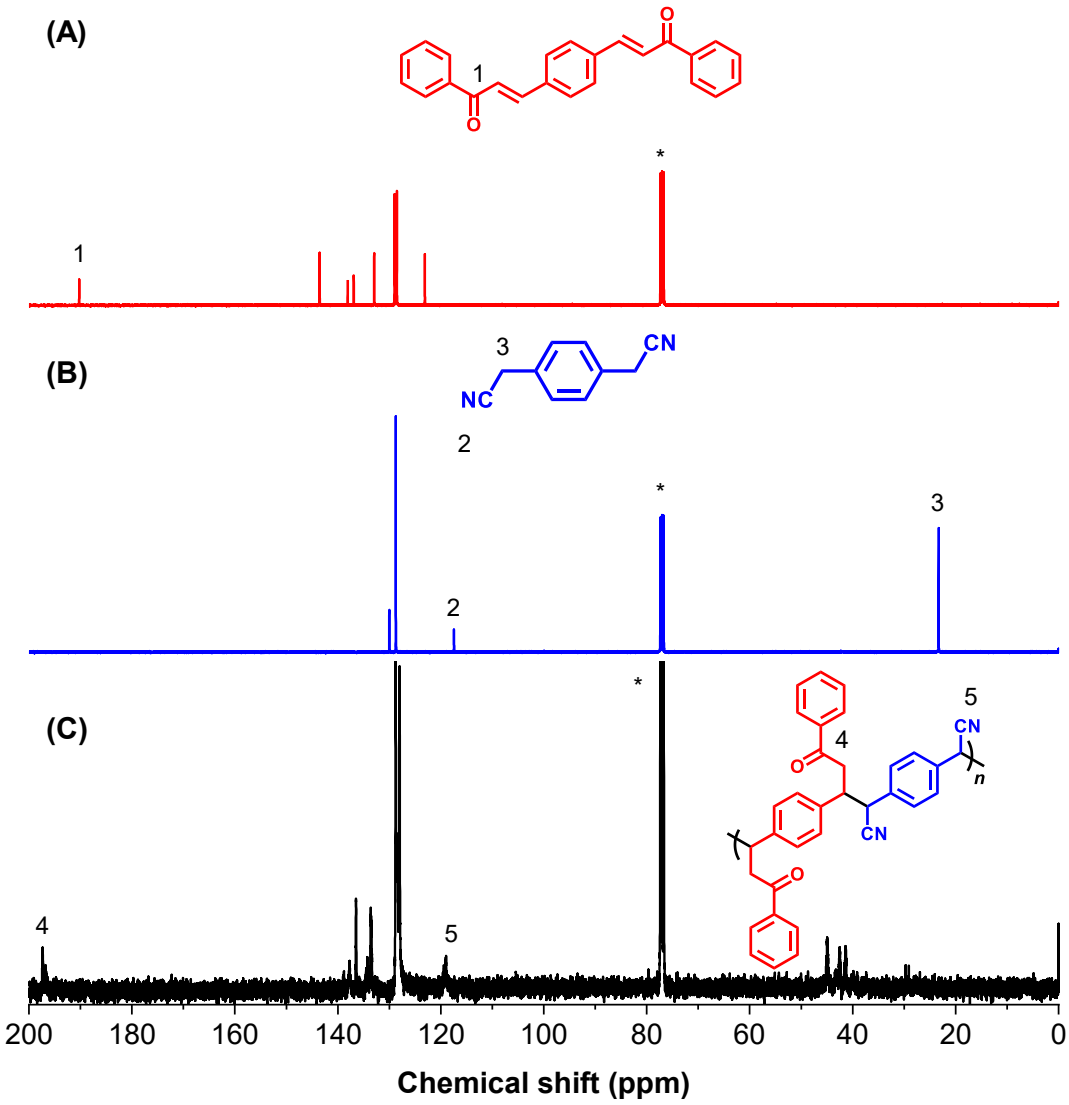

Figure S32. ^{13}C NMR spectra of **1b** (A), **2a** (B) and P**1b2a** (C) in $CDCl_3$. The solvent peaks are marked with asterisks.

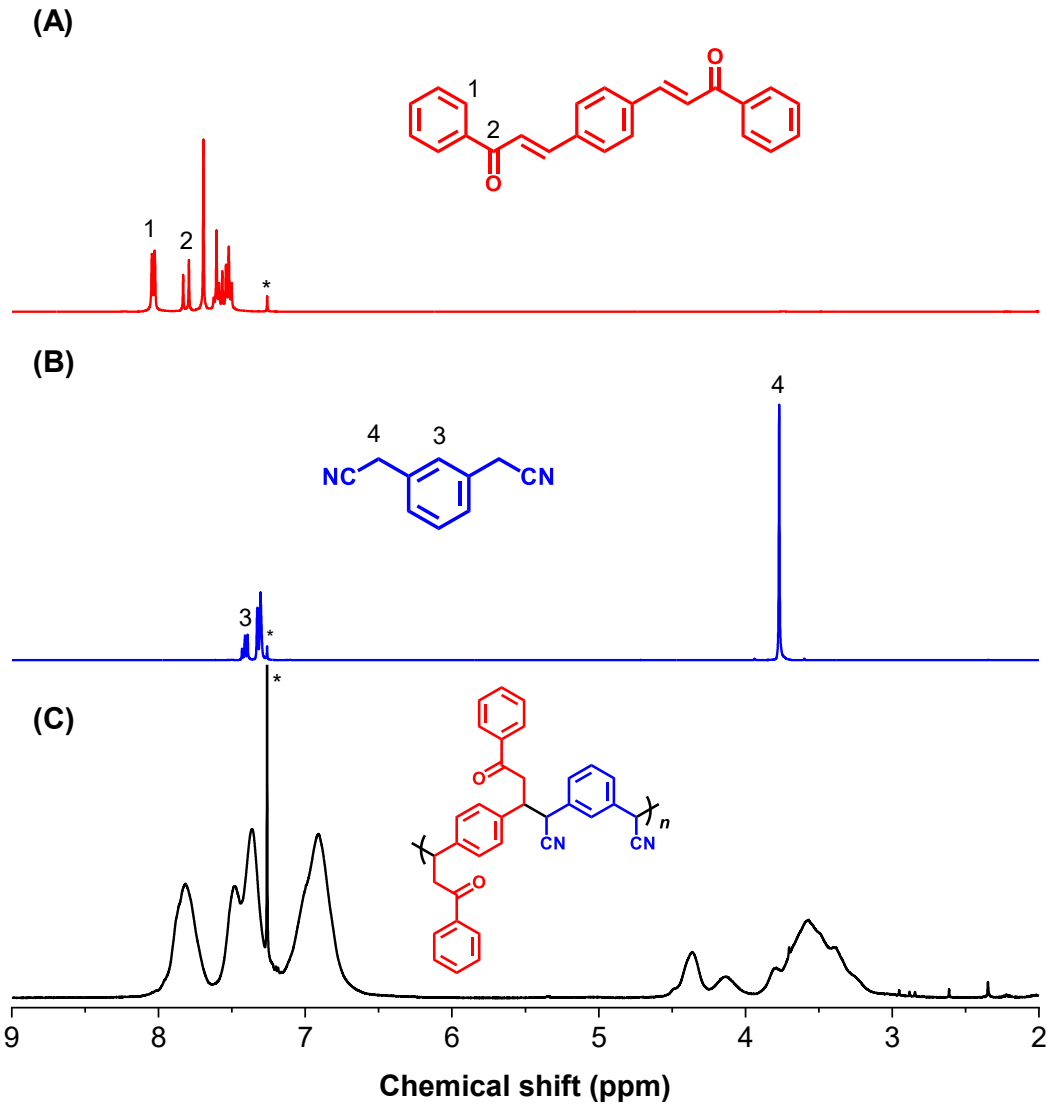

Figure S33. ^{1}H NMR spectra of **1b** (A), **2b** (B) and P**1b2b** (C) in $CDCl_3$. The solvent peaks are marked with asterisks.

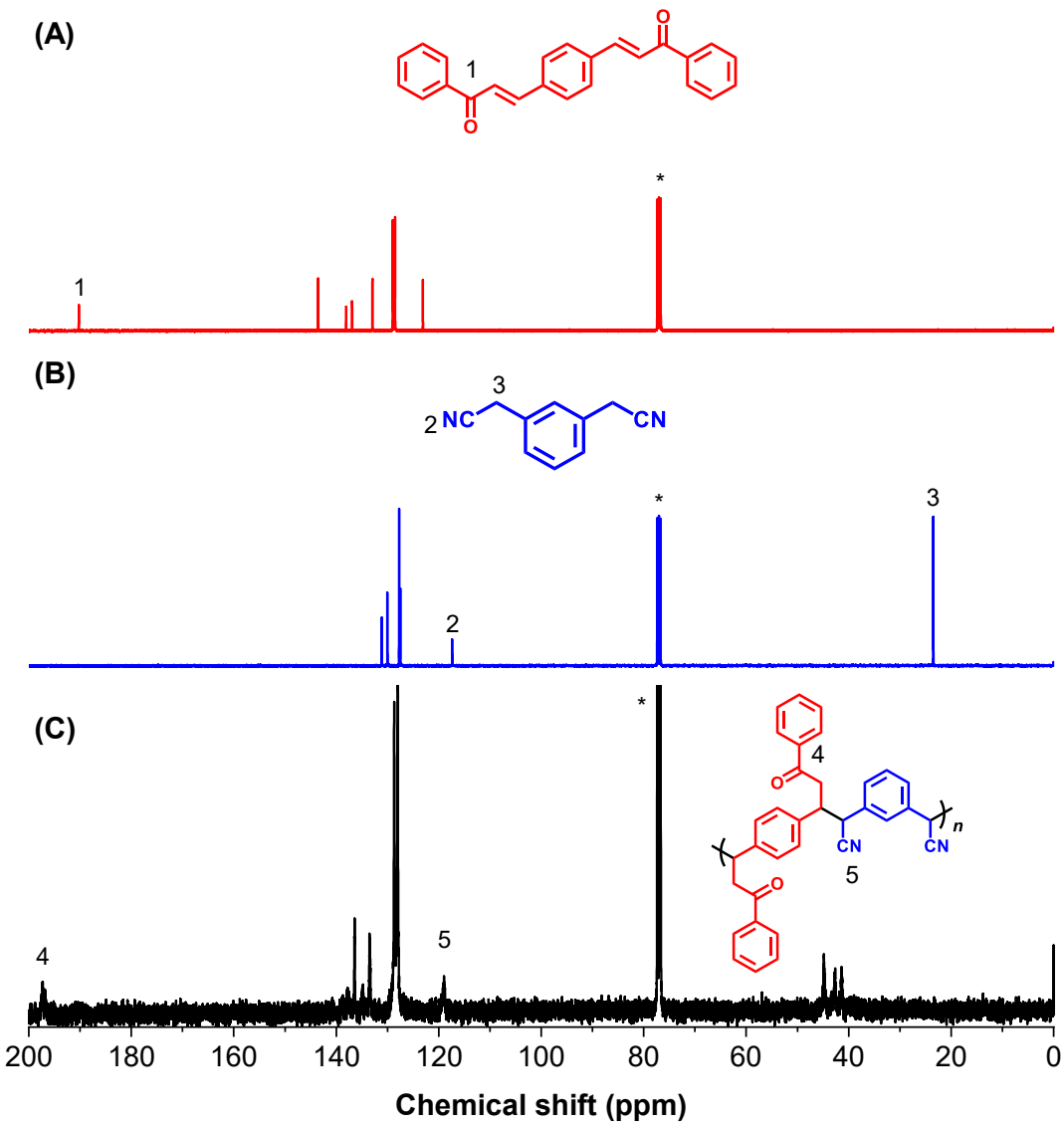

Figure S34. ^{13}C NMR spectra of **1b** (A), **2b** (B) and P**1b2b** (C) in $CDCl_3$. The solvent peaks are marked with asterisks.

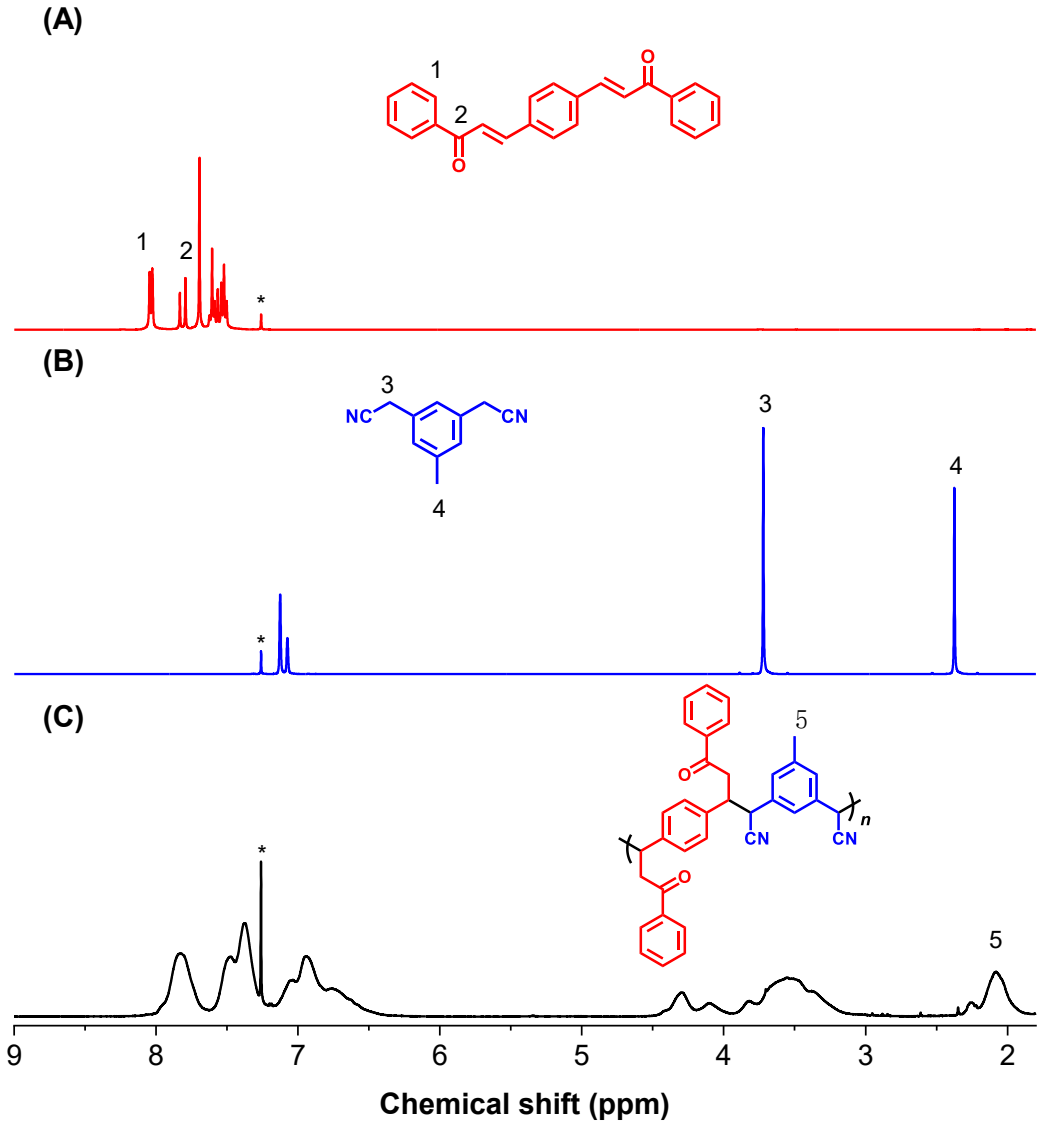

Figure S35. ^{1}H NMR spectra of **1b** (A), **2c** (B) and P**1b2c** (C) in $CDCl_3$. The solvent peaks are marked with asterisks.

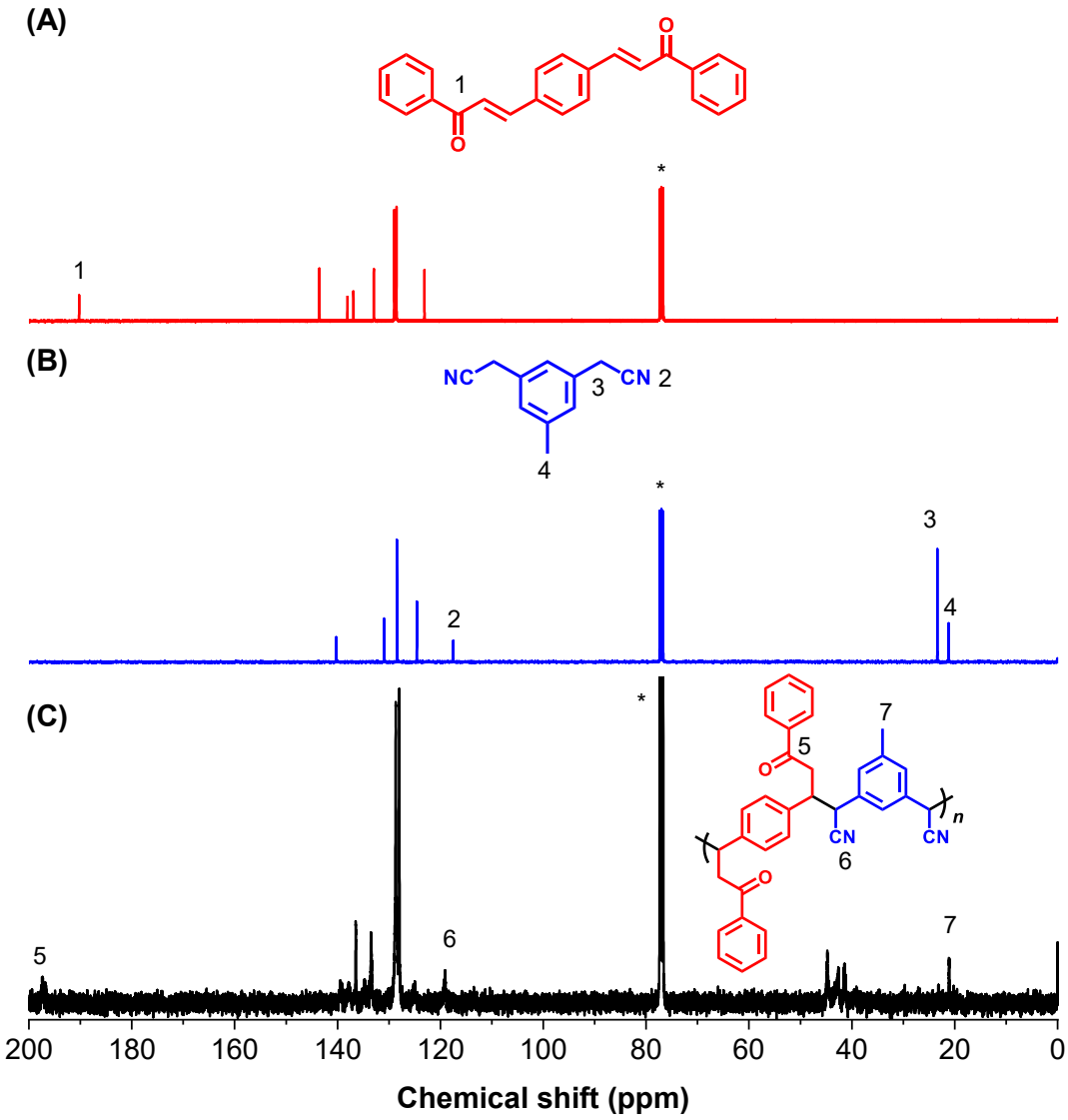

Figure S36. ^{13}C NMR spectra of **1b** (A), **2c** (B) and P**1b2c** (C) in $CDCl_3$. The solvent peaks are marked with asterisks.

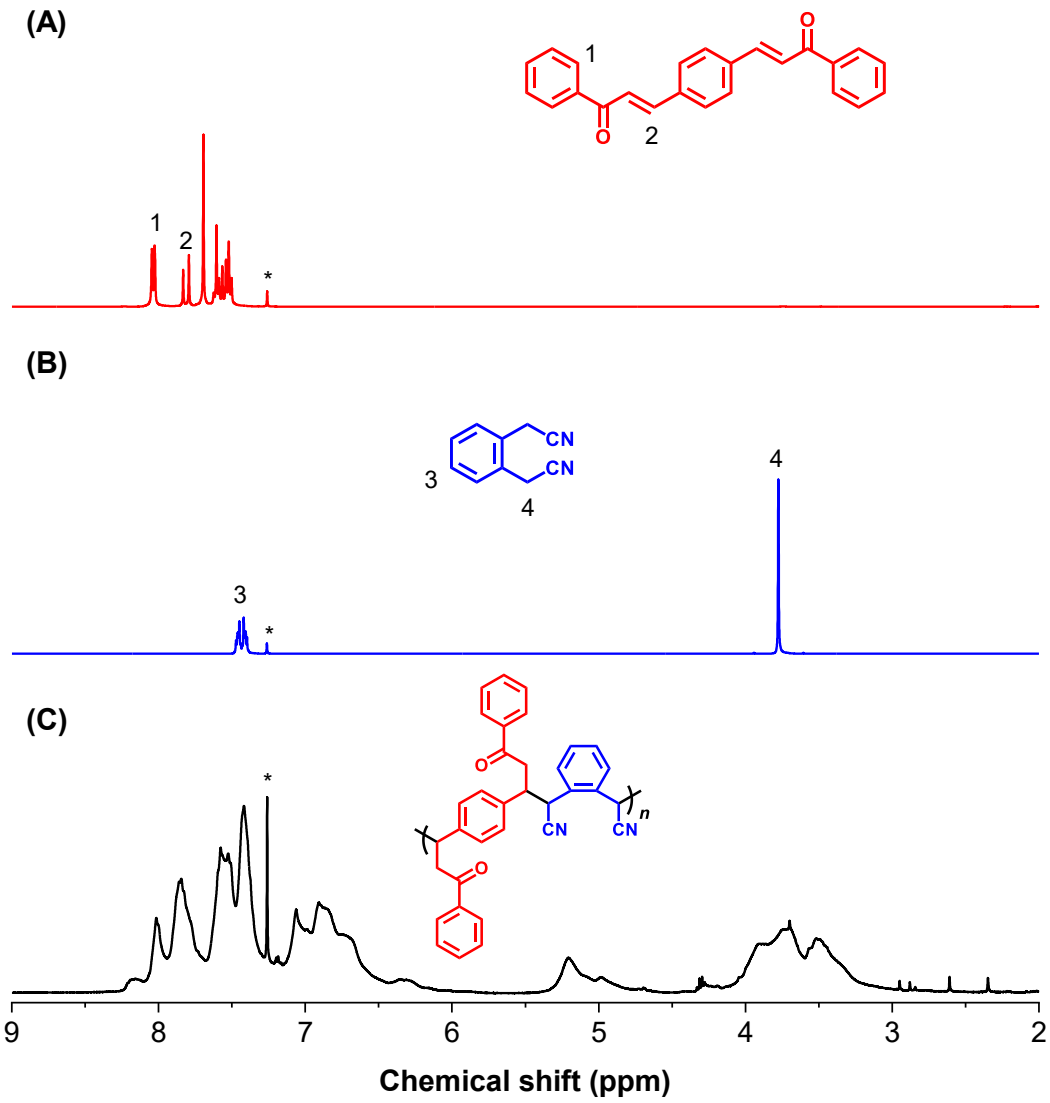

Figure S37. ^{1}H NMR spectra of **1b** (A), **2d** (B) and P**1b2d** (C) in $CDCl_3$. The solvent peaks are marked with asterisks.

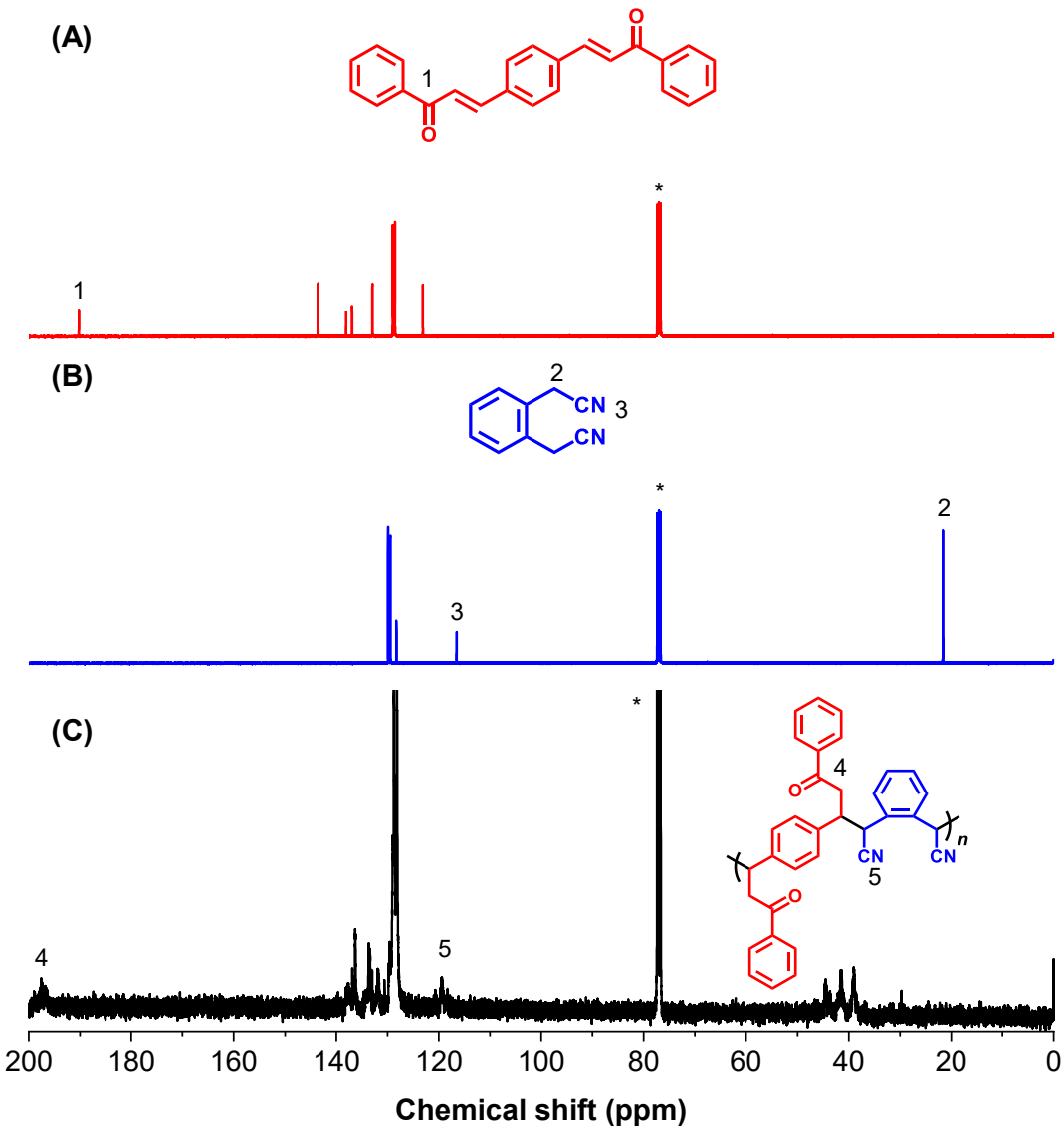

Figure S38. ^{13}C NMR spectra of **1b** (A), **2d** (B) and P**1b2d** (C) in $CDCl_3$. The solvent peaks are marked with asterisks.

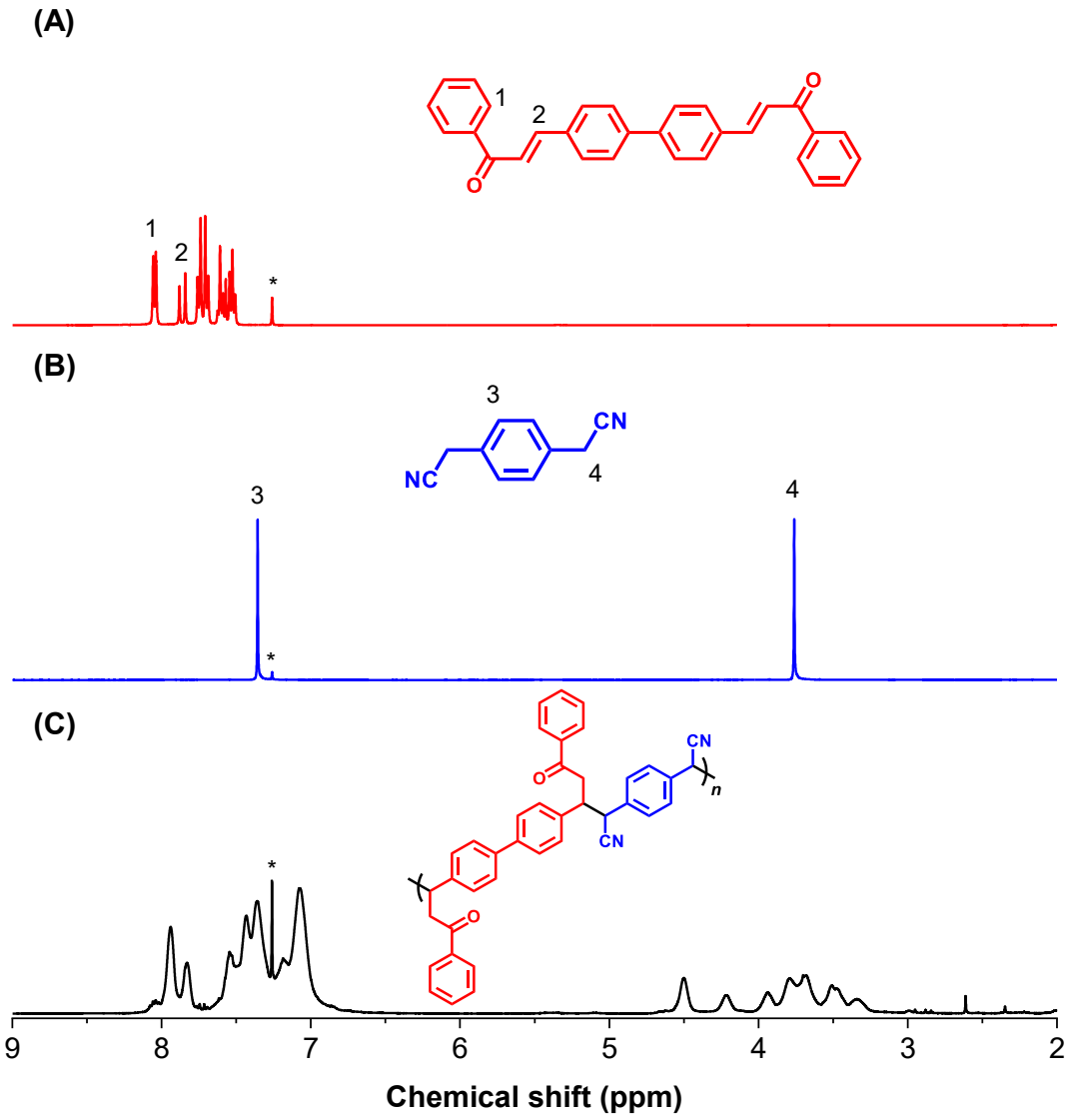

Figure S39. ^{1}H NMR spectra of **1c** (A), **2a** (B) and P**1c2a** (C) in $CDCl_3$. The solvent peaks are marked with asterisks.

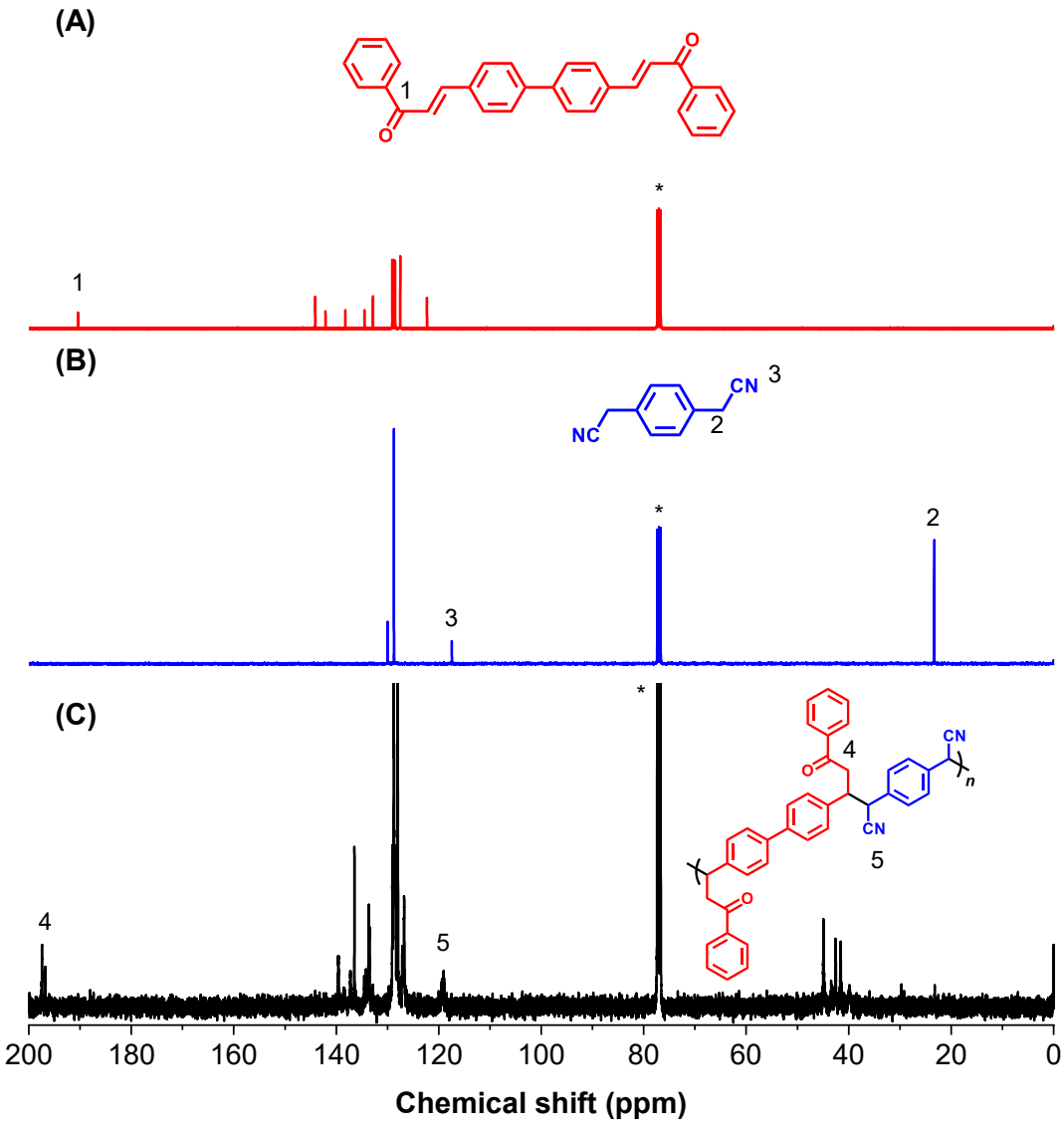

Figure S40. ^{13}C NMR spectra of **1c** (A), **2a** (B) and P**1c2a** (C) in $CDCl_3$. The solvent peaks are marked with asterisks.

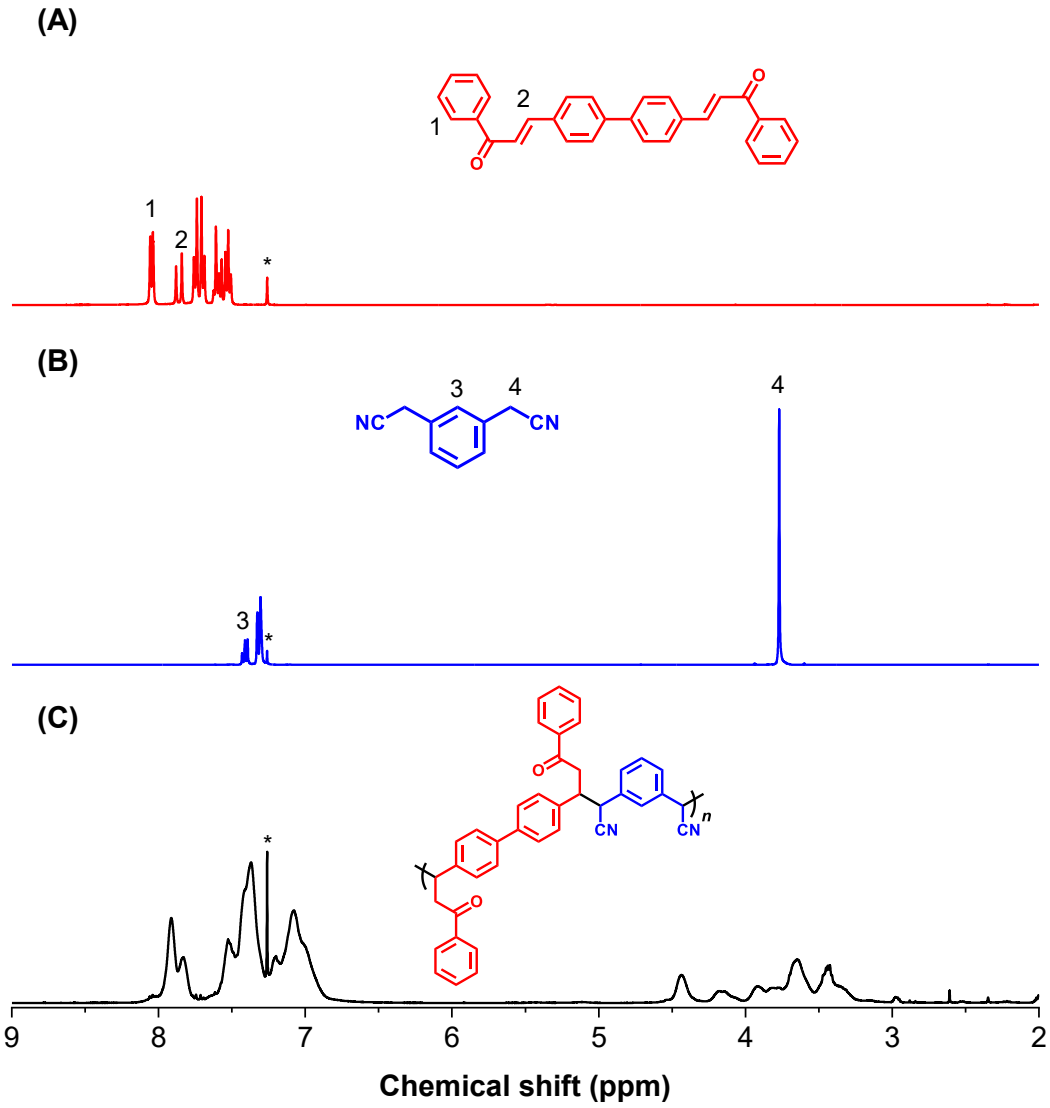

Figure S41. ^{1}H NMR spectra of **1c** (A), **2b** (B) and P**1c2b** (C) in $CDCl_3$. The solvent peaks are marked with asterisks.

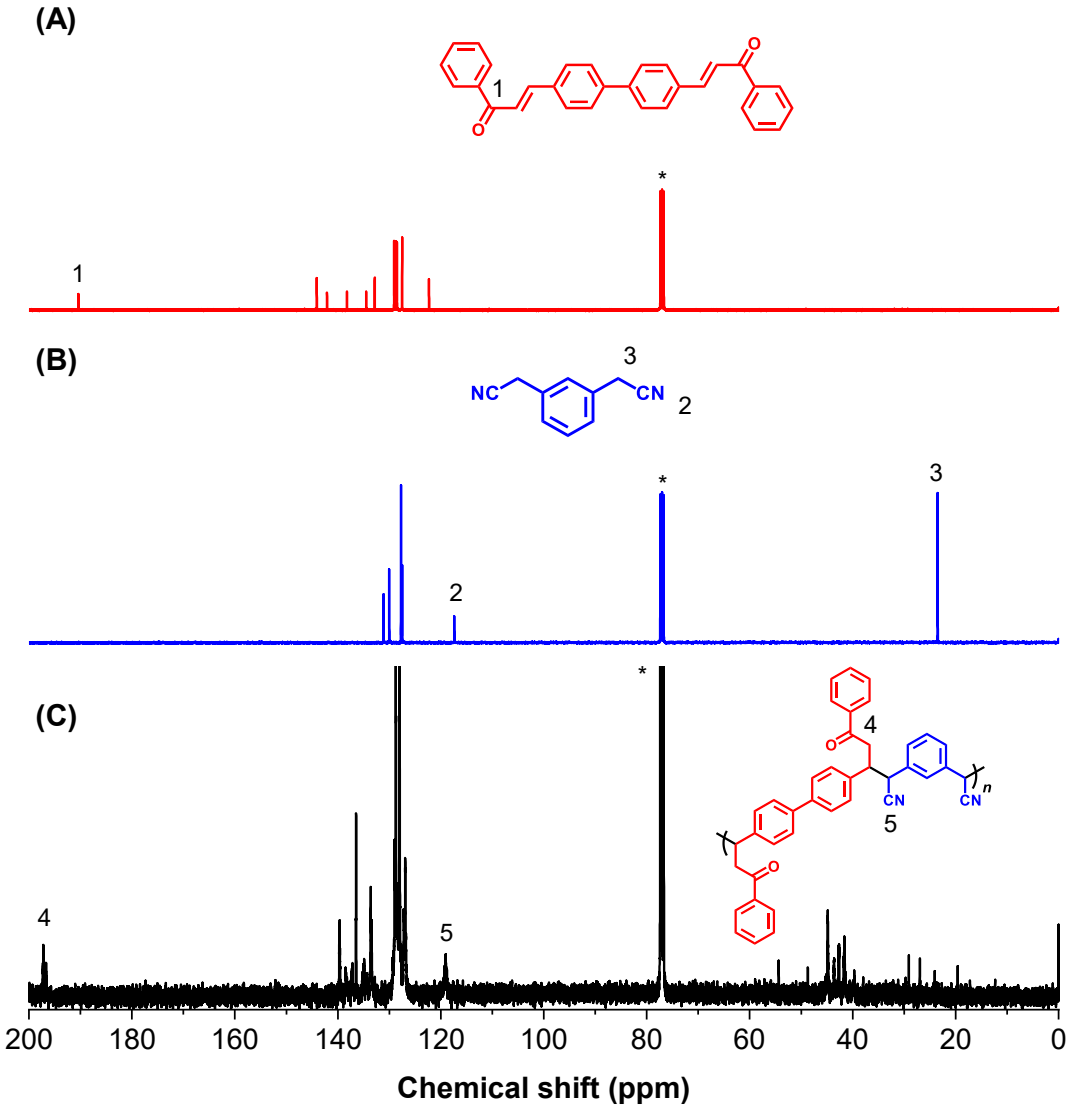

Figure S42. ^{13}C NMR spectra of **1c** (A), **2b** (B) and P**1c2b** (C) in $CDCl_3$. The solvent peaks are marked with asterisks.

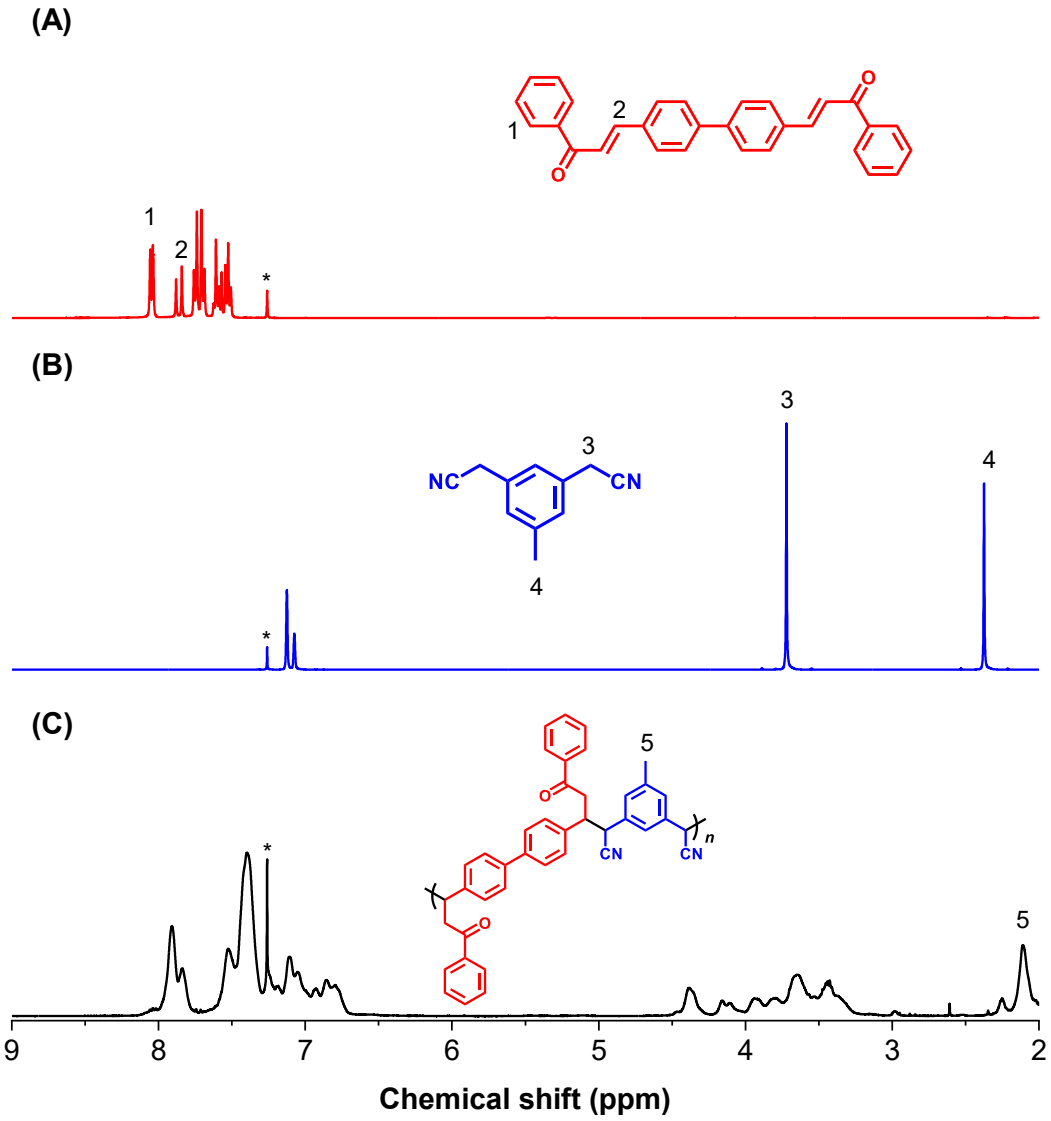

Figure S43. ^{1}H NMR spectra of **1c** (A), **2c** (B) and P**1c2c** (C) in $CDCl_3$. The solvent peaks are marked with asterisks.

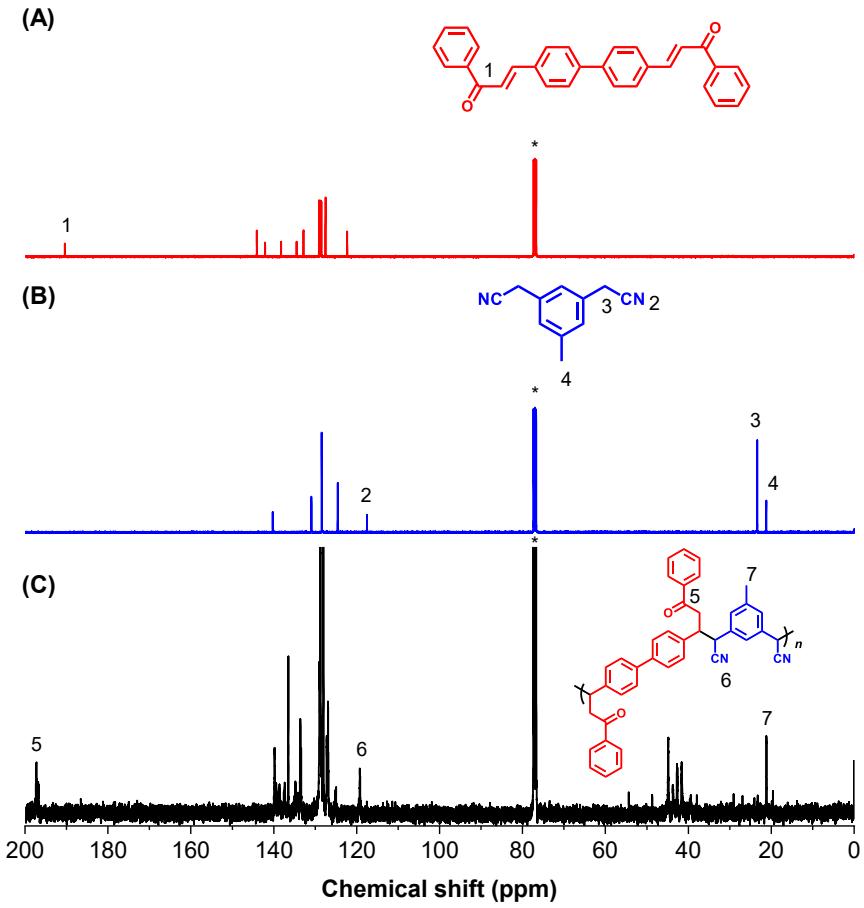

Figure S44. ^{13}C NMR spectra of **1c** (A), **2c** (B) and P**1c2c** (C) in $CDCl_3$. The solvent peaks are marked with asterisks.

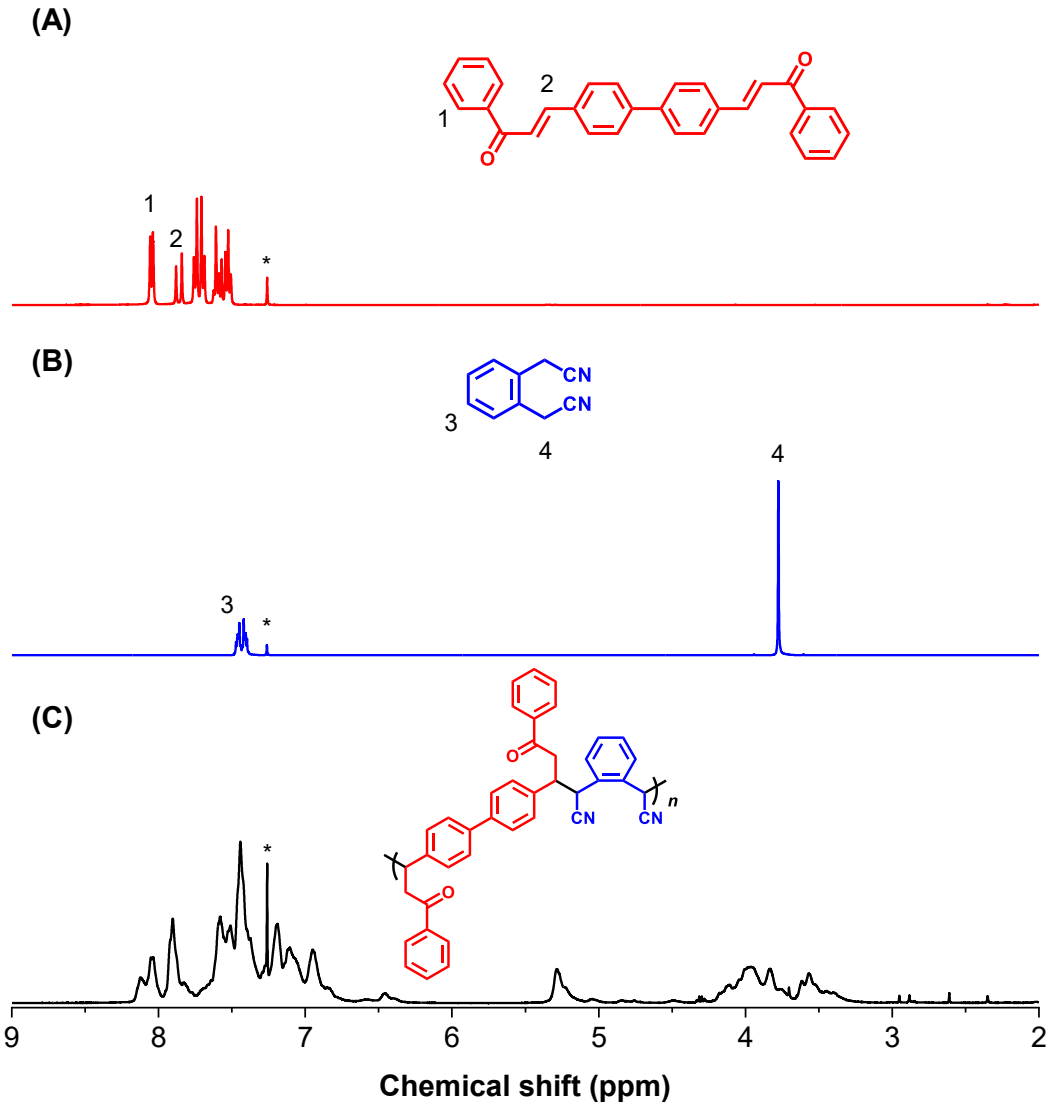

Figure S45. ^{1}H NMR spectra of **1c** (A), **2d** (B) and P**1c2d** (C) in $CDCl_3$. The solvent peaks are marked with asterisks.

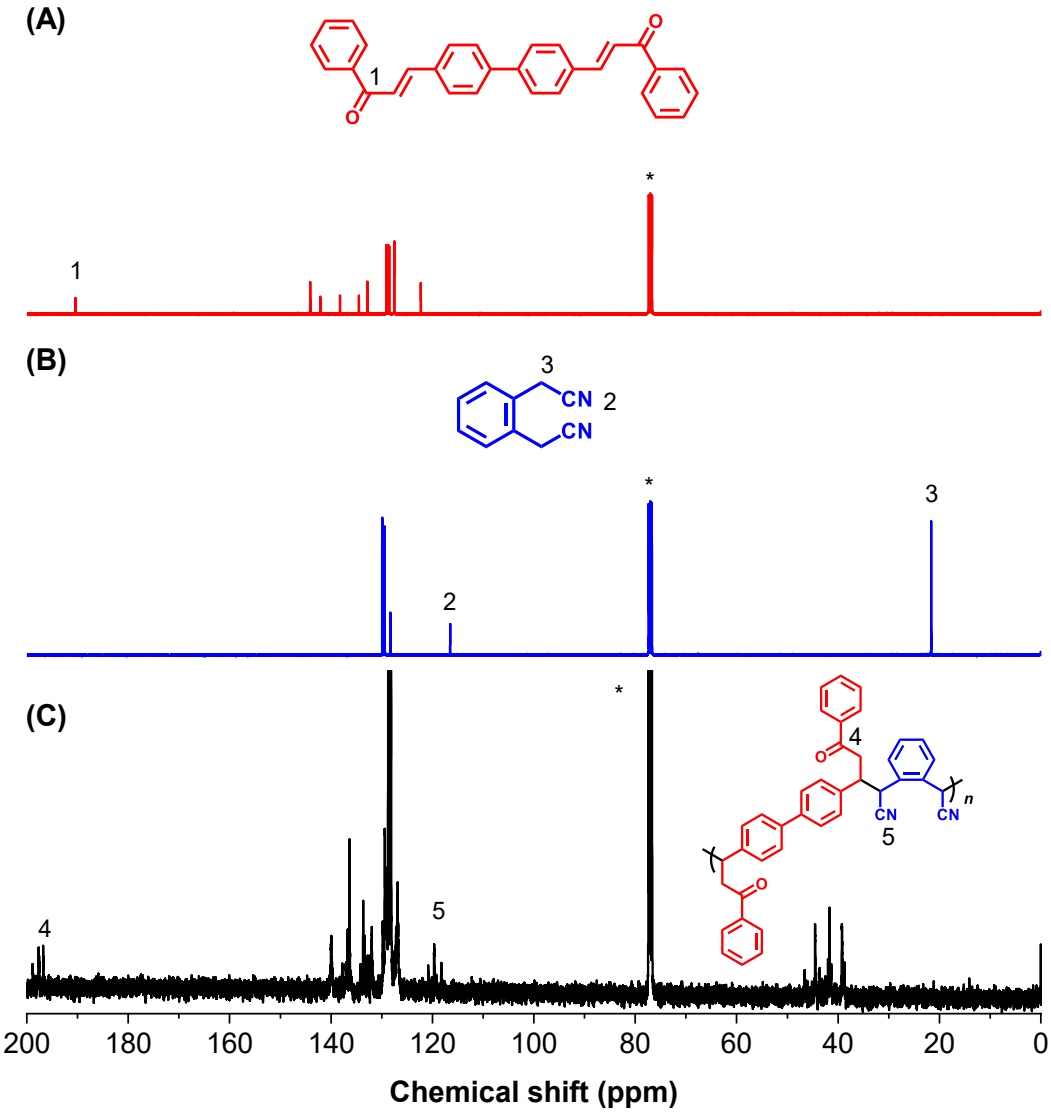

Figure S46. ^{13}C NMR spectra of **1c** (A), **2d** (B) and P**1c2d** (C) in $CDCl_3$. The solvent peaks are marked with asterisks.

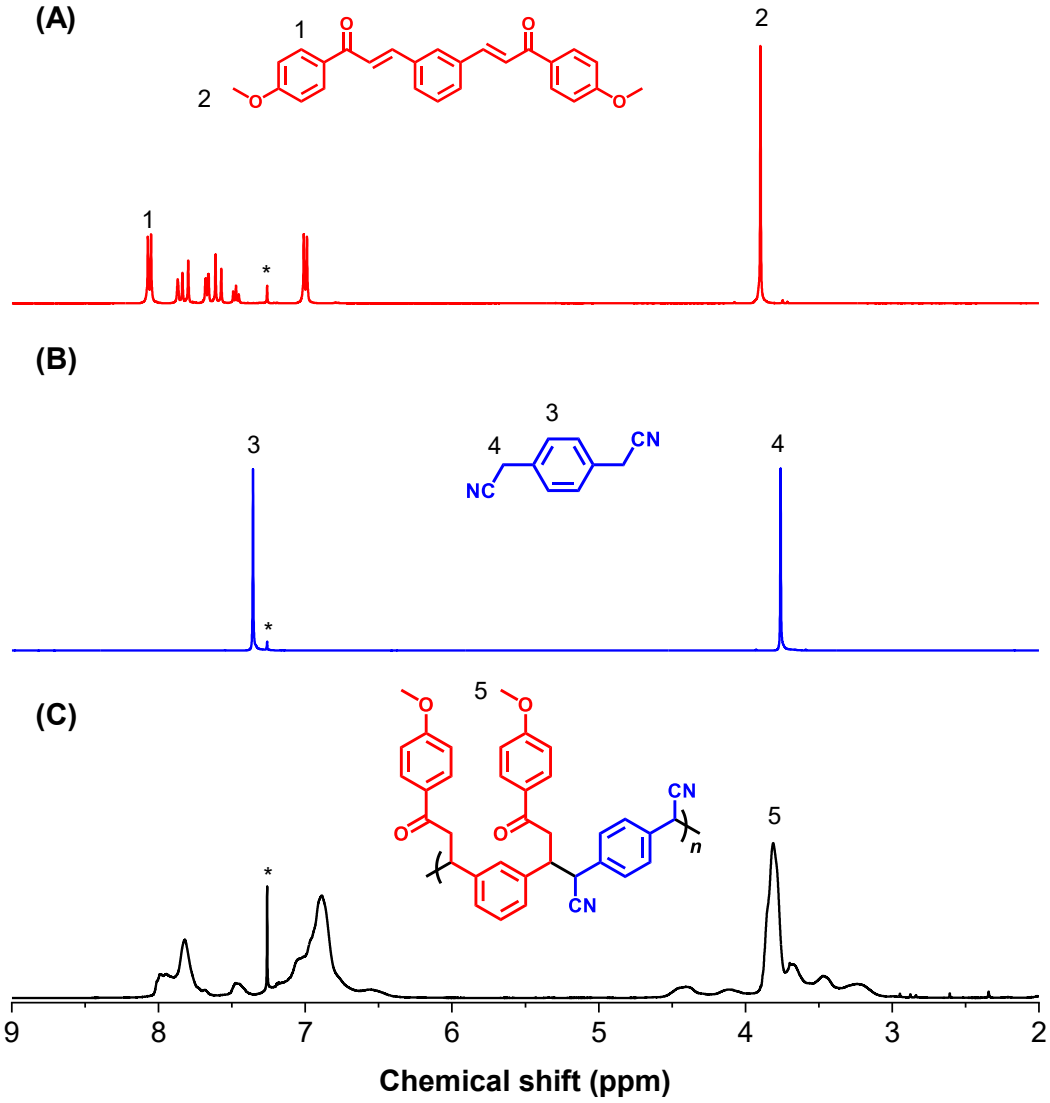

Figure S47. ^{1}H NMR spectra of **1d** (A), **2a** (B) and P**1d2a** (C) in $CDCl_3$. The solvent peaks are marked with asterisks.

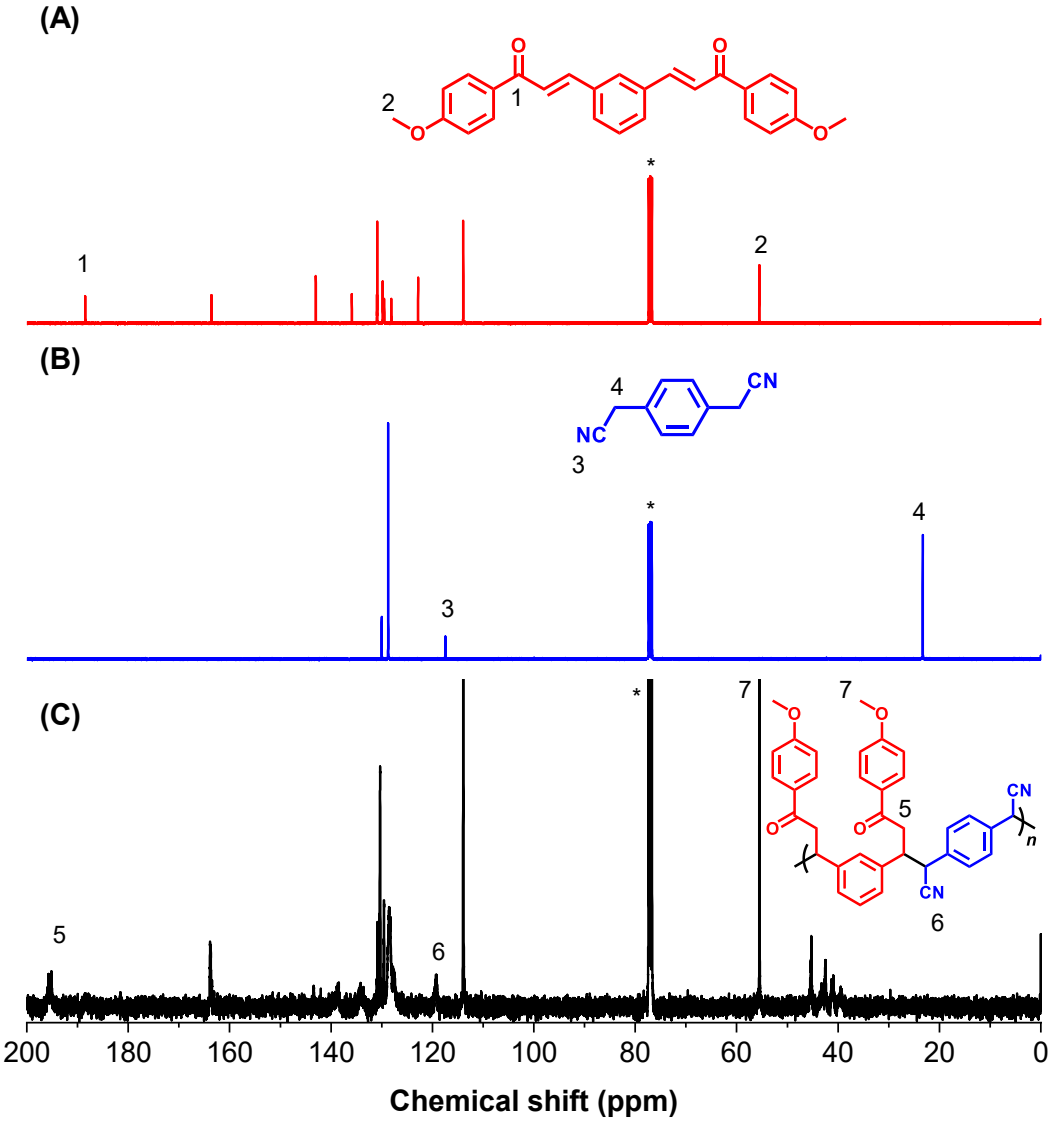

Figure S48. ^{13}C NMR spectra of **1d** (A), **2a** (B) and P**1d2a** (C) in $CDCl_3$. The solvent peaks are marked with asterisks.

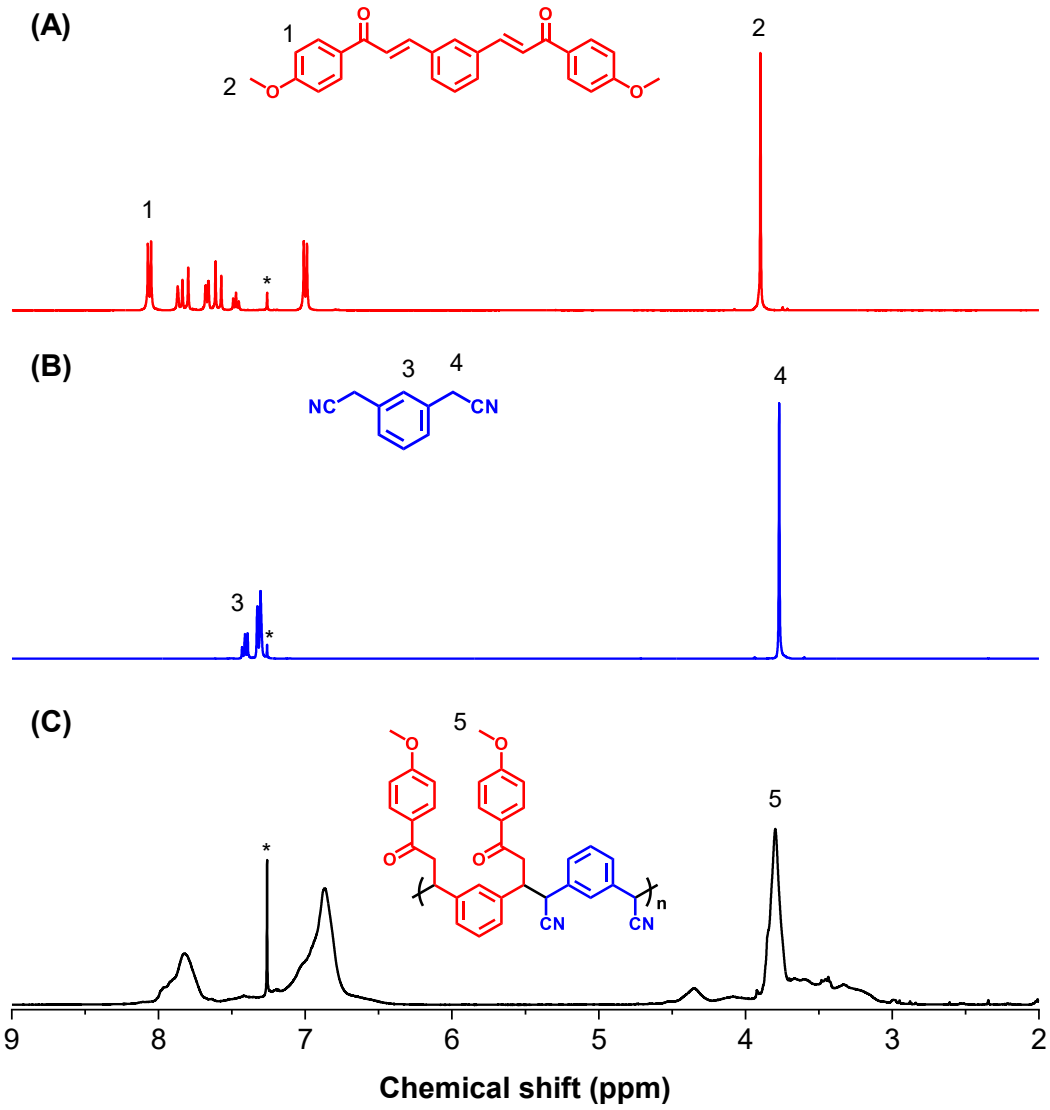

Figure S49. ^{1}H NMR spectra of **1d** (A), **2b** (B) and P**1d2b** (C) in $CDCl_3$. The solvent peaks are marked with asterisks.

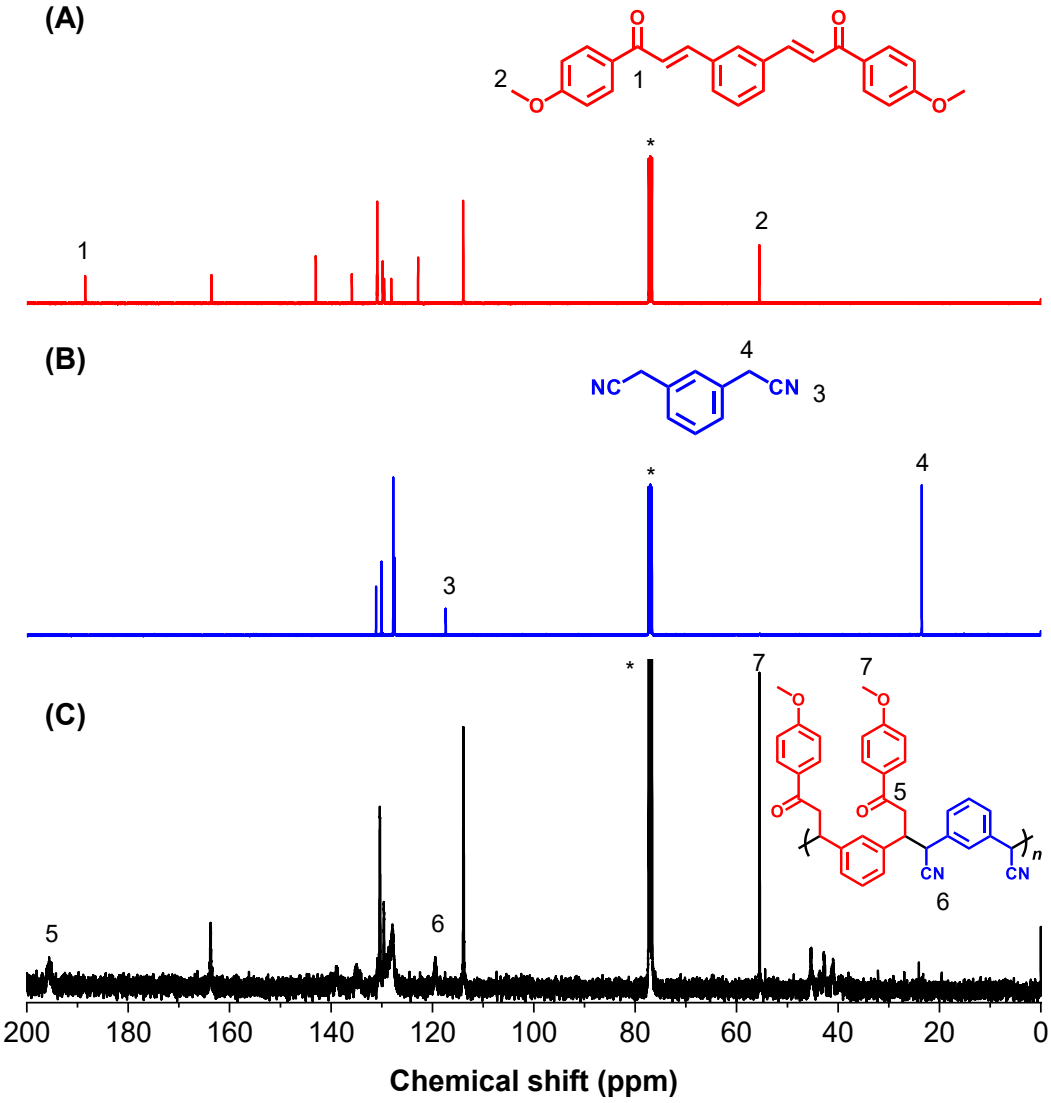

Figure S50. ^{13}C NMR spectra of **1d** (A), **2b** (B) and P**1d2b** (C) in $CDCl_3$. The solvent peaks are marked with asterisks.

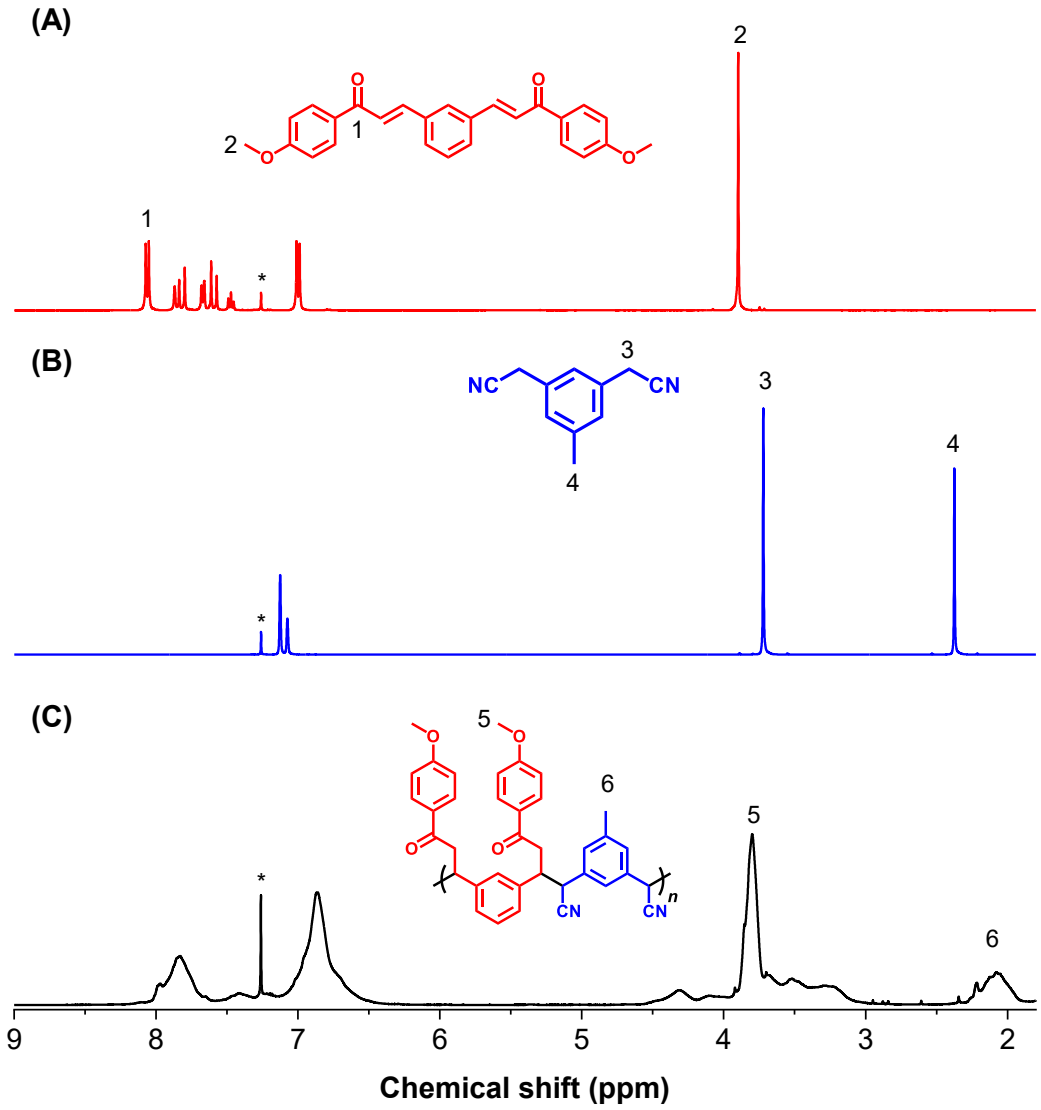

Figure S51. ^{1}H NMR spectra of **1d** (A), **2c** (B) and P**1d2c** (C) in $CDCl_3$. The solvent peaks are marked with asterisks.

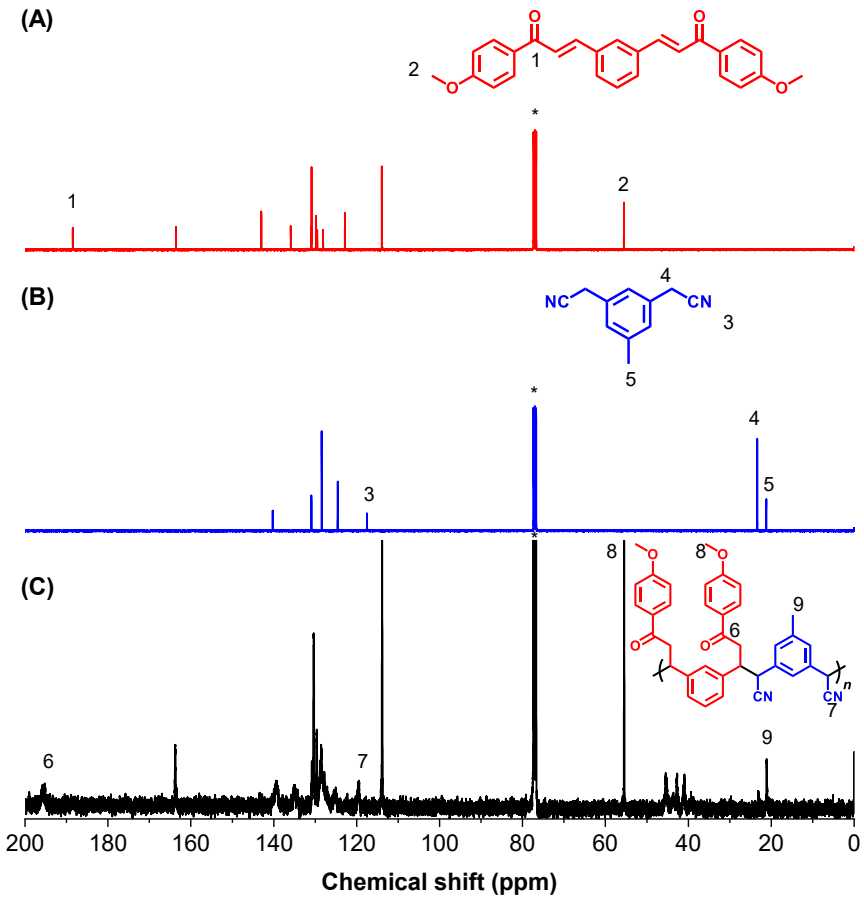

Figure S52. ^{13}C NMR spectra of **1d** (A), **2c** (B) and P**1d2c** (C) in $CDCl_3$. The solvent peaks are marked with asterisks.

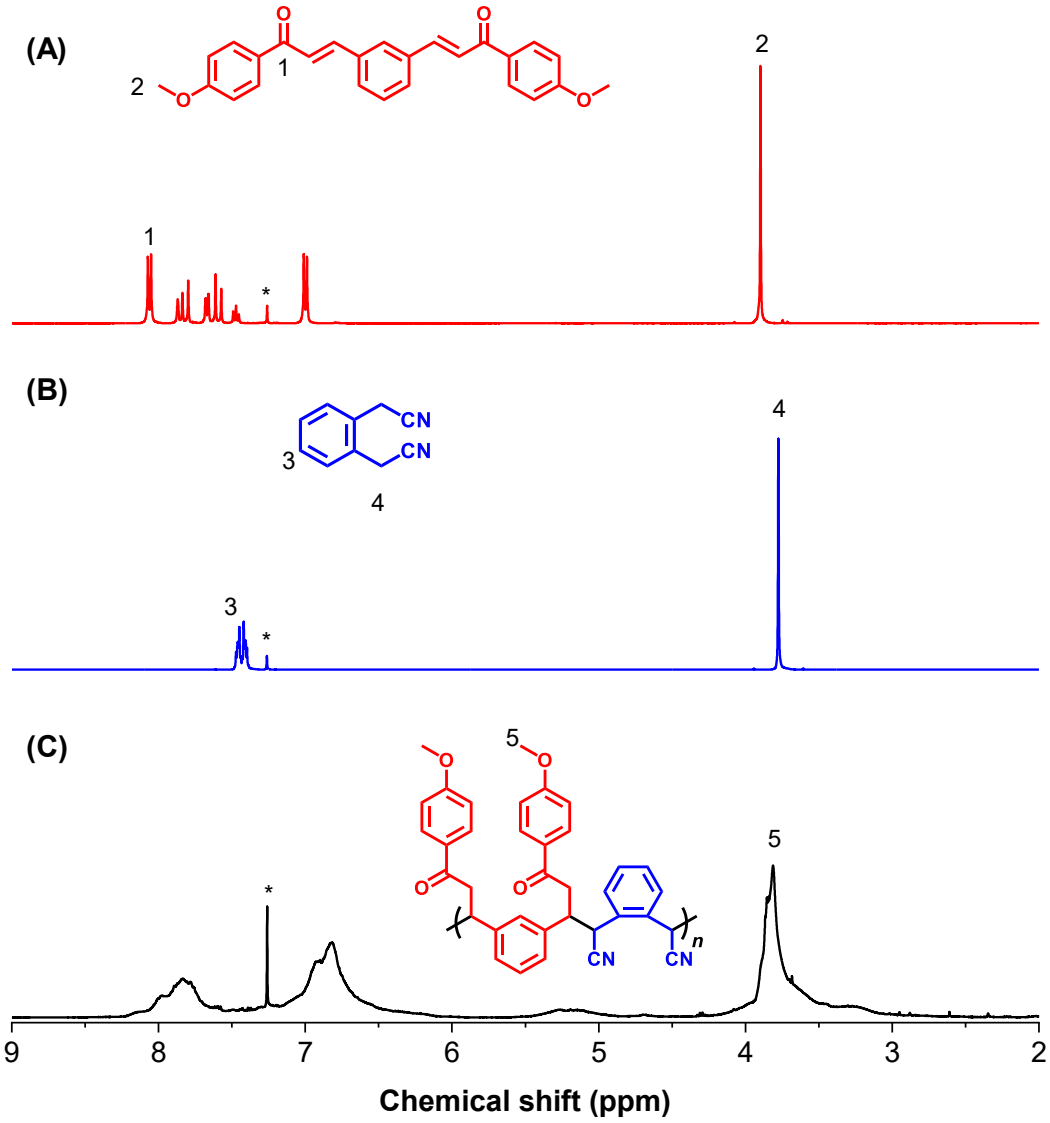

Figure S53. ^{1}H NMR spectra of **1d** (A), **2d** (B) and P**1d2d** (C) in $CDCl_3$. The solvent peaks are marked with asterisks.

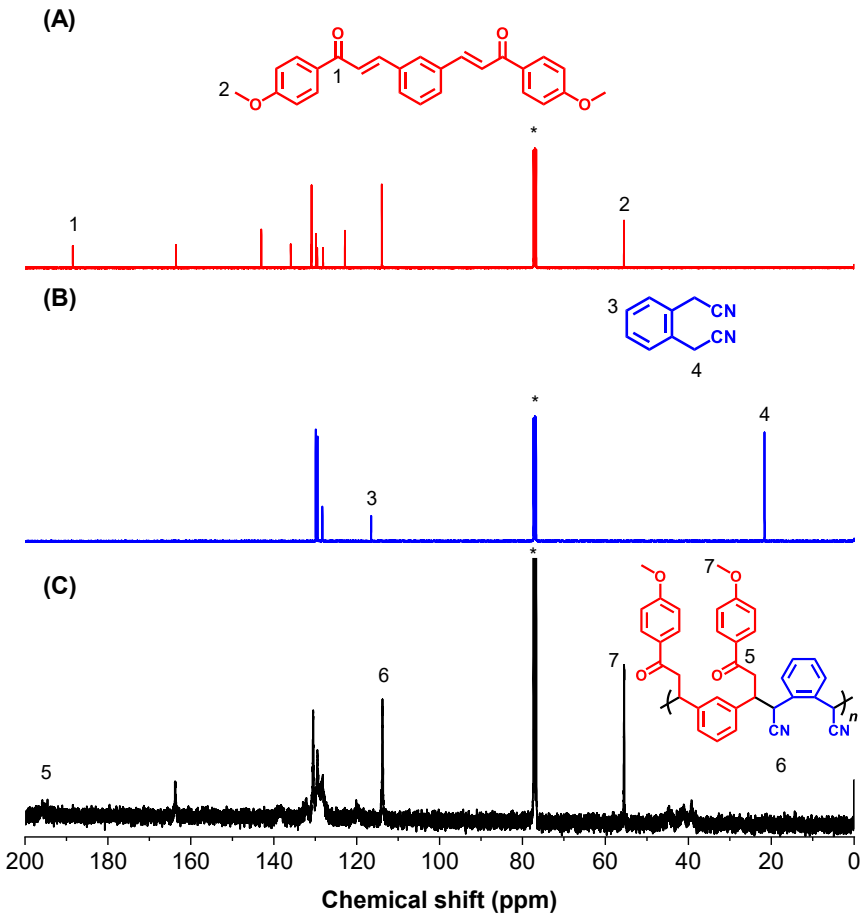

Figure S54. ^{13}C NMR spectra of **1d** (A), **2d** (B) and P**1d2d** (C) in $CDCl_3$. The solvent peaks are marked with asterisks.

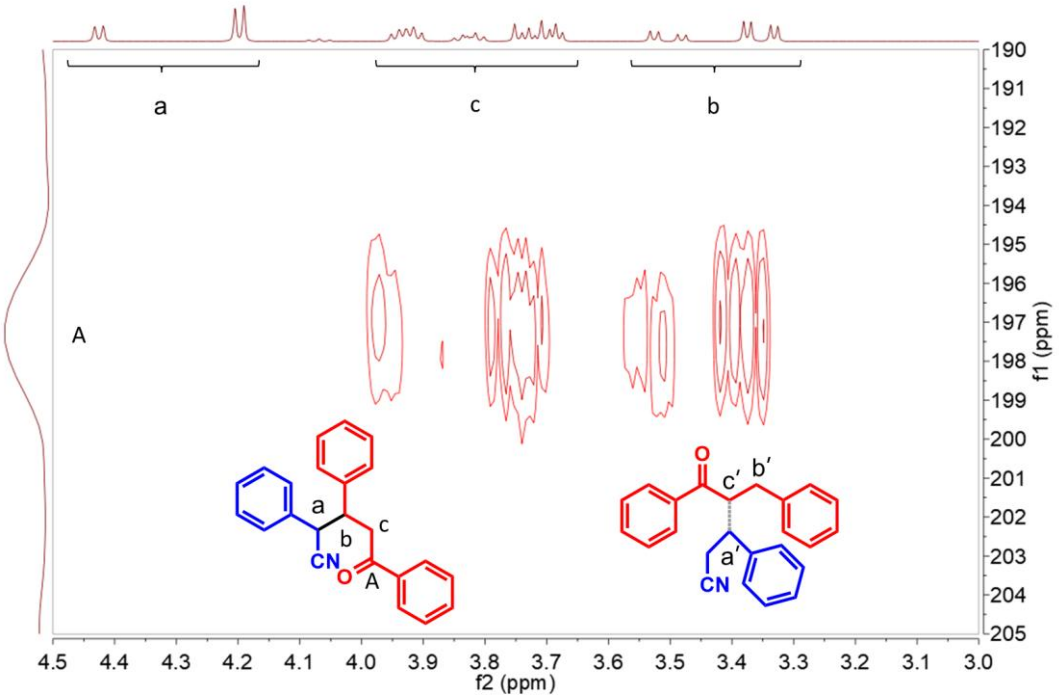

Figure S55. HMBC spectrum of model compound **5** in $CDCl_3$.

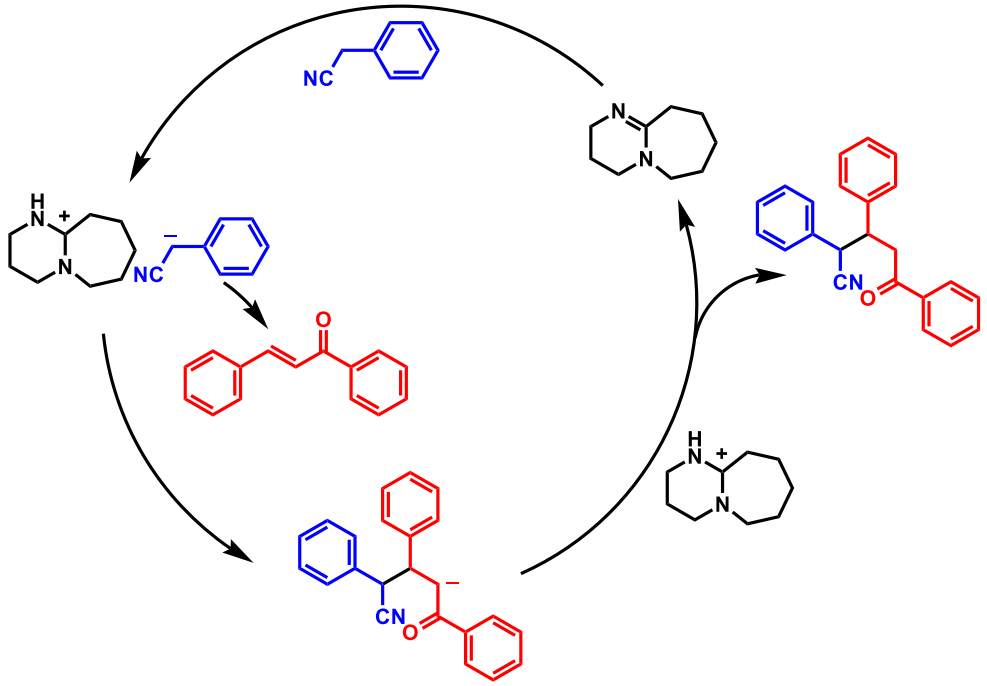

Figure S56. The probable mechanism of the C(sp^3)-H Michael polyaddition

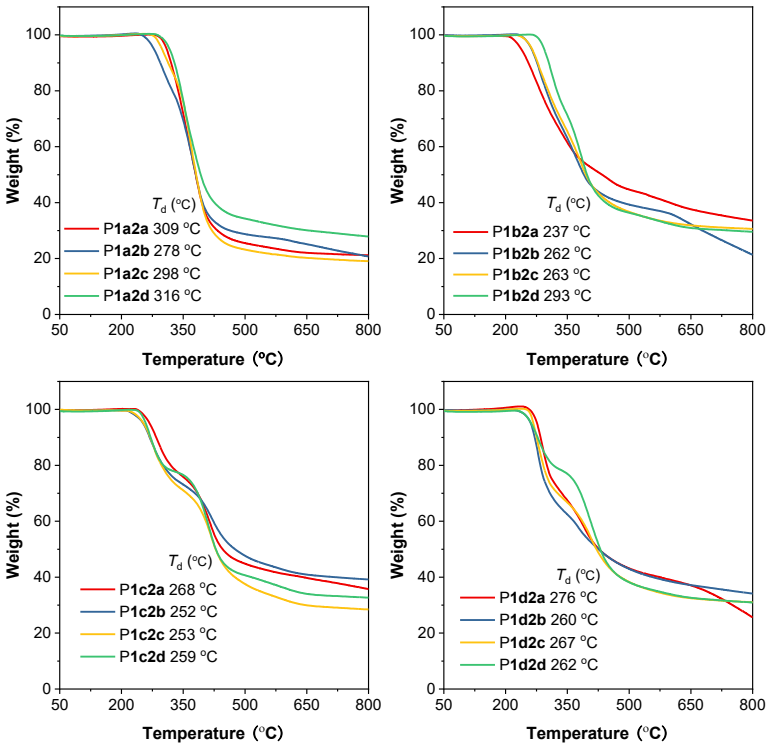

Figure S57. TGA curves of P**1a-1d/2a-2d**.

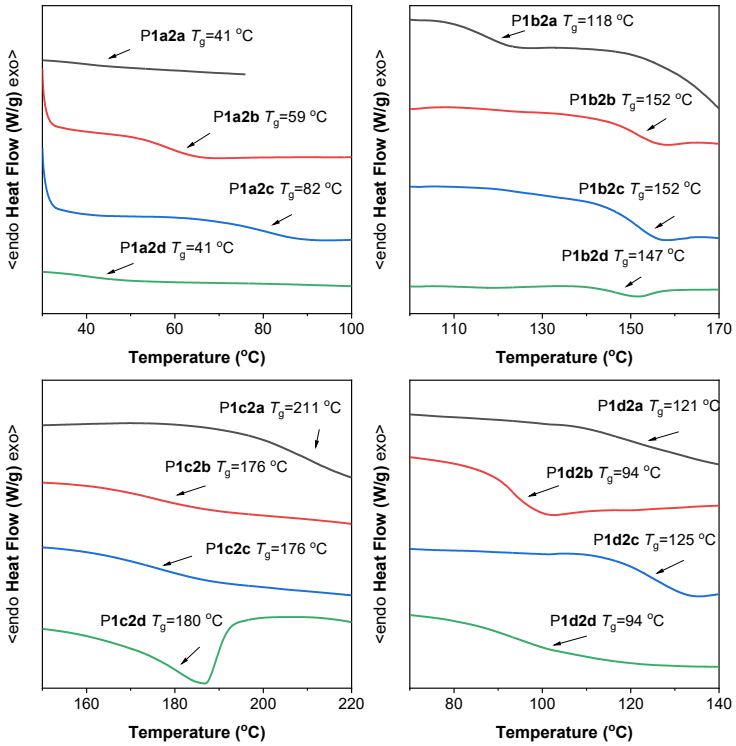

Figure S58. DSC curves of P**1a-1d/2a-2d**.

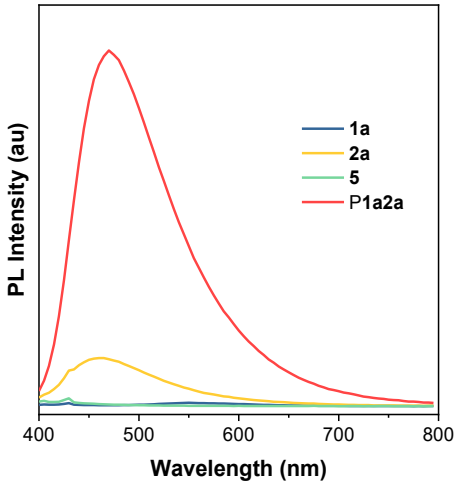

Figure S59. PL spectra of **1a**, **2a**, model compound **5**, and P**1a2a** in DMF (c = 1.0 × 10^{-3} M, λ_{ex} = 380 nm).

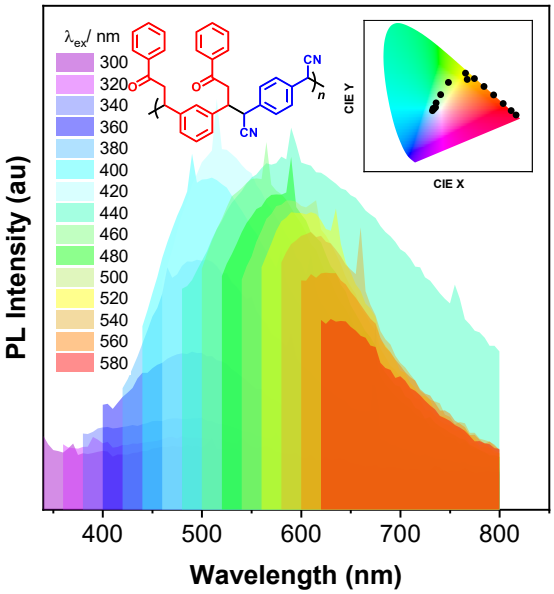

Figure S60. PL spectra of P**1a2a** in solid state with different excitation wavelengths. Inset: CIE coordination of P**1a2a** in solid state. (Excitation ranges: λ_{ex} = 300 − 580 nm).

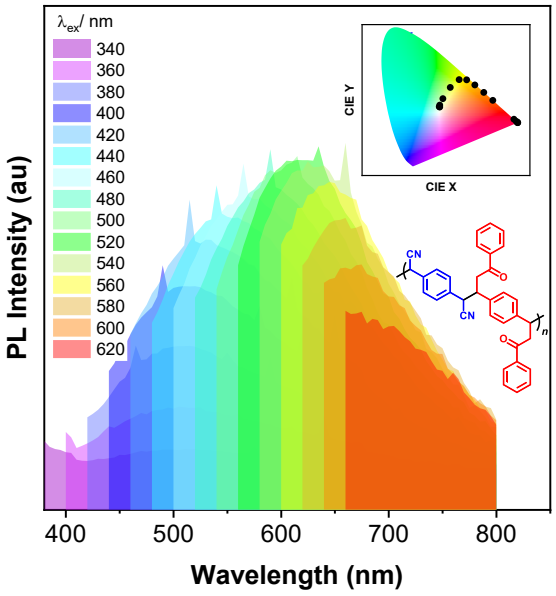

Figure S61. PL spectra of P**1b2a** in solid state with different excitation wavelengths. Inset: CIE coordination of P**1b2a** in solid state. (Excitation ranges: λ_{ex} = 340 − 620 nm).

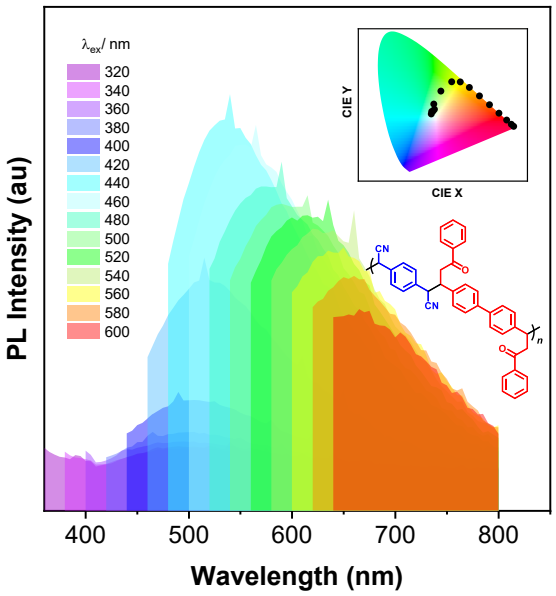

Figure S62. PL spectra of P**1c2a** in solid state with different excitation wavelengths. Inset: CIE coordination of P**1c2a** in solid state. (Excitation ranges: λ_{ex} = 320 − 600 nm).

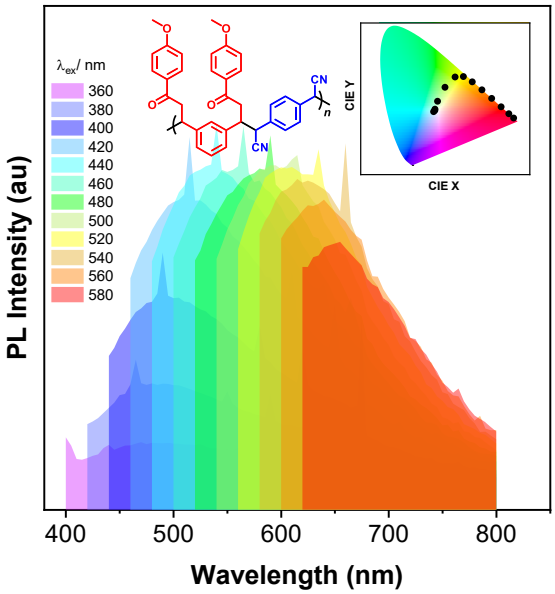

Figure S63. PL spectra of P**1d2a** in solid state with different excitation wavelengths. Inset: CIE coordination of P**1d2a** in solid state. (Excitation ranges: λ_{ex} = 360 − 580 nm).

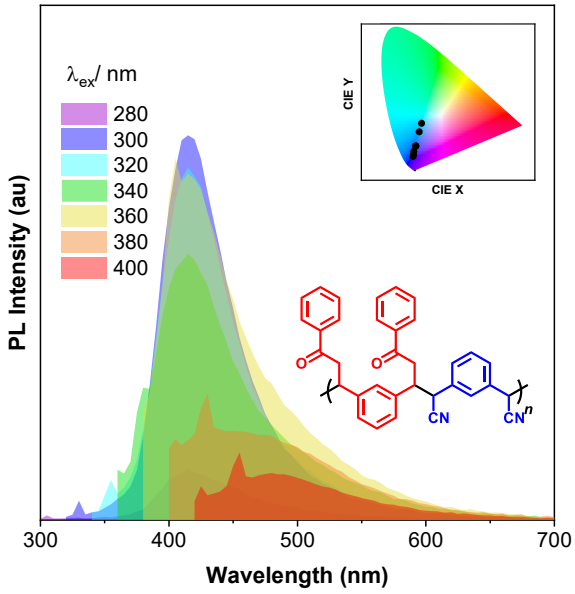

Figure S64. PL spectra of P**1a2b** in DMF (c = 1.0 × 10^{-3} M) with different excitation wavelengths. Inset: CIE coordination of P**1a2b** in DMF. (Excitation ranges: λ_{ex} = 280 − 400 nm).

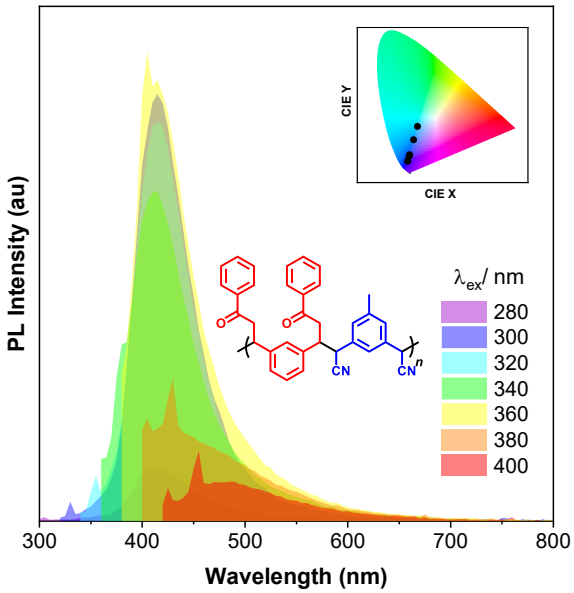

Figure S65. PL spectra of P**1a2c** in DMF (c = 1.0 × 10^{-3} M) with different excitation wavelengths. Inset: CIE coordination of P**1a2c** in DMF. (Excitation ranges: λ_{ex} = 280 − 400 nm).

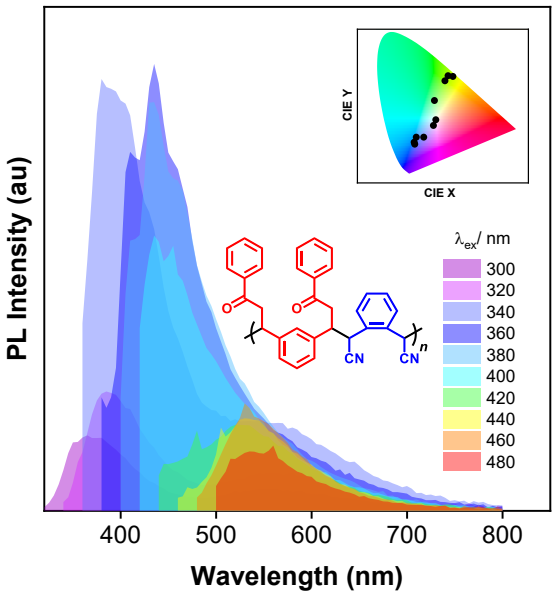

Figure S66. PL spectra of P**1a2d** in DMF (c = 1.0 × 10^{-3} M) with different excitation wavelengths. Inset: CIE coordination of P**1a2d** in DMF. (Excitation ranges: λ_{ex} = 300 − 480 nm).

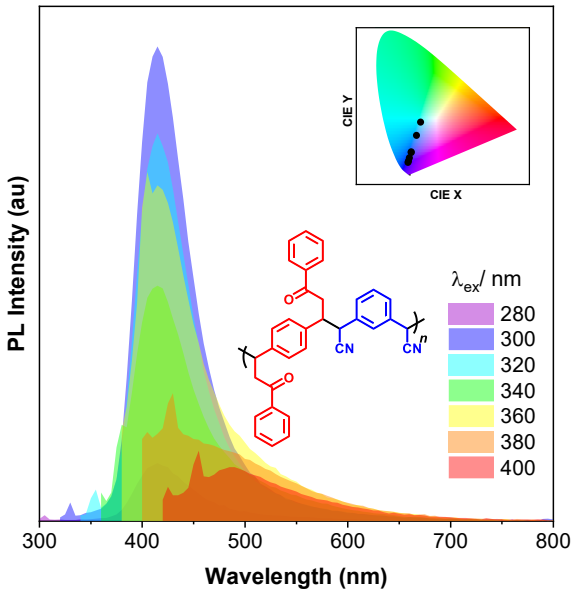

Figure S67. PL spectra of P**1b2b** in DMF (c = 1.0 × 10^{-3} M) with different excitation wavelengths. Inset: CIE coordination of P**1b2b** in DMF. (Excitation ranges: λ_{ex} = 280 − 400 nm).

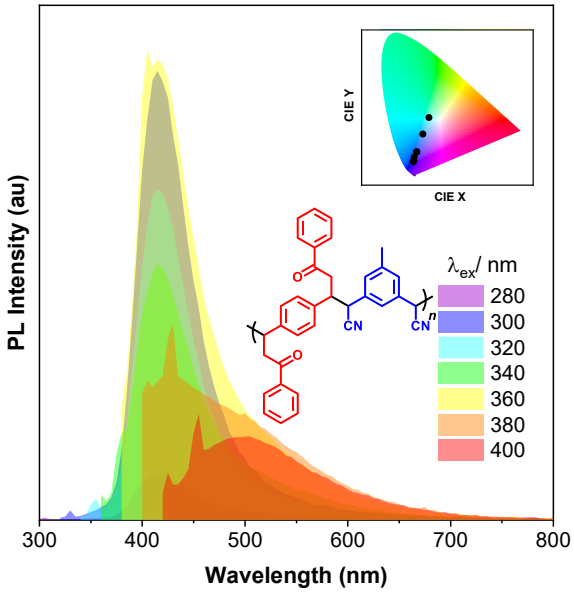

Figure S68. PL spectra of P**1b2c** in DMF (c = 1.0 × 10^{-3} M) with different excitation wavelengths. Inset: CIE coordination of P**1b2c** in DMF. (Excitation ranges: λ_{ex} = 280 − 400 nm).

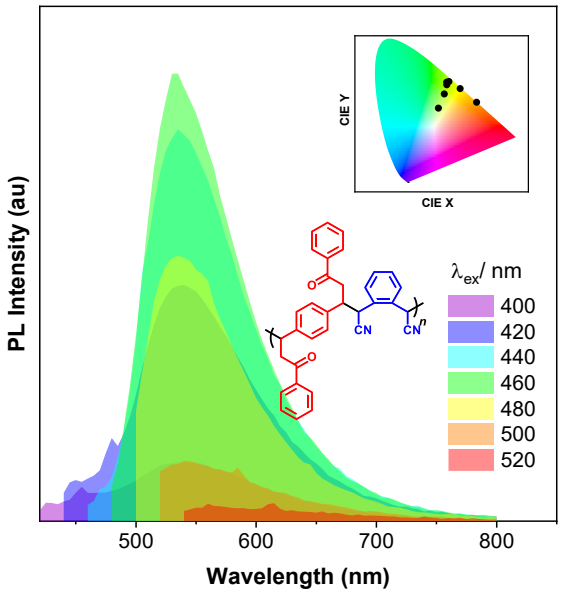

Figure S69. PL spectra of P**1b2d** in DMF (c = 1.0 × 10^{-3} M) with different excitation wavelengths. Inset: CIE coordination of P**1b2d** in DMF. (Excitation ranges: λ_{ex} = 400 − 520 nm).

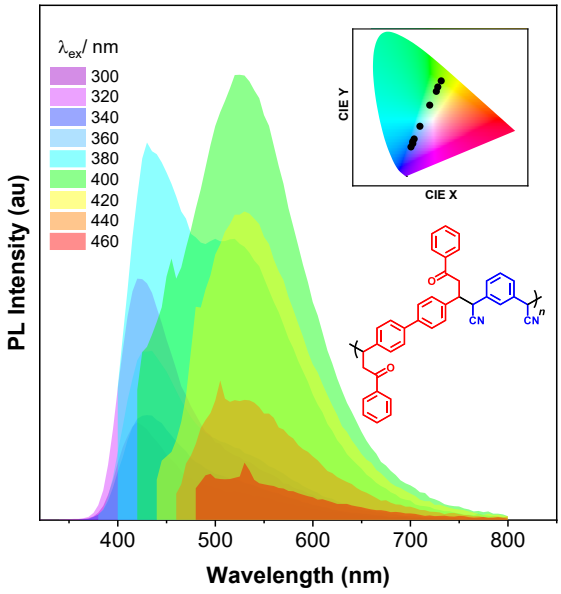

Figure S70. PL spectra of P**1c2b** in DMF (c = 1.0 × 10^{-3} M) with different excitation wavelengths. Inset: CIE coordination of P**1c2b** in DMF. (Excitation ranges: λ_{ex} = 300 − 460 nm).

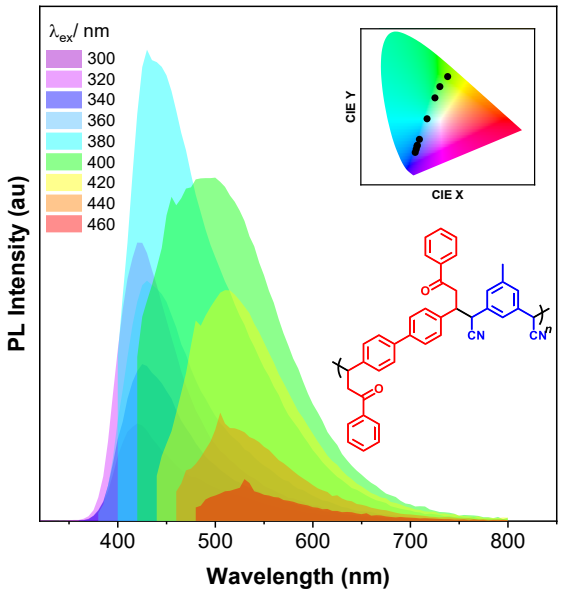

Figure S71. PL spectra of P**1c2c** in DMF (c = 1.0 × 10^{-3} M) with different excitation wavelengths. Inset: CIE coordination of P**1c2c** in DMF. (Excitation ranges: λ_{ex} = 300 − 460 nm).

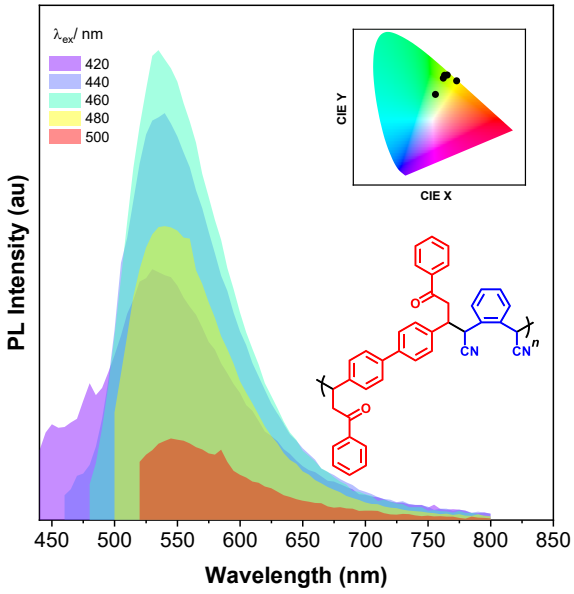

Figure S72. PL spectra of P**1c2d** in DMF (c = 1.0 × 10^{-3} M) with different excitation wavelengths. Inset: CIE coordination of P**1c2d** in DMF. (Excitation ranges: λ_{ex} = 420 − 500 nm).

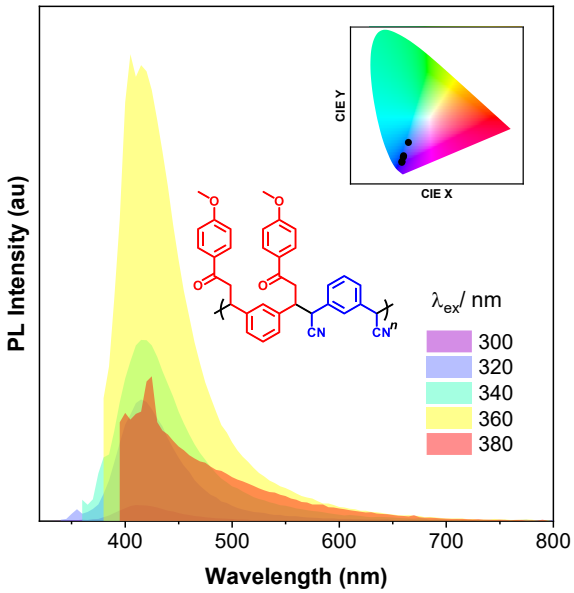

Figure S73. PL spectra of P**1d2b** in DMF (c = 1.0 × 10^{-3} M) with different excitation wavelengths. Inset: CIE coordination of P**1d2b** in DMF. (Excitation ranges: λ_{ex} = 300 − 380 nm).

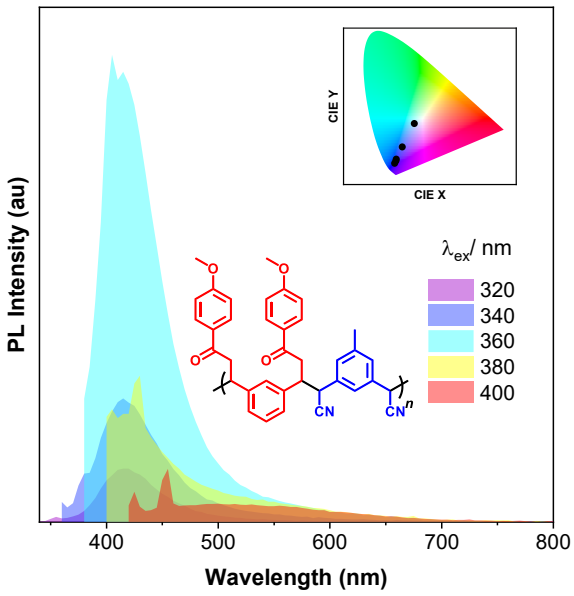

Figure S74. PL spectra of P**1d2c** in DMF (c = 1.0 × 10^{-3} M) with different excitation wavelengths. Inset: CIE coordination of P**1d2c** in DMF. (Excitation ranges: λ_{ex} = 320 − 400 nm).

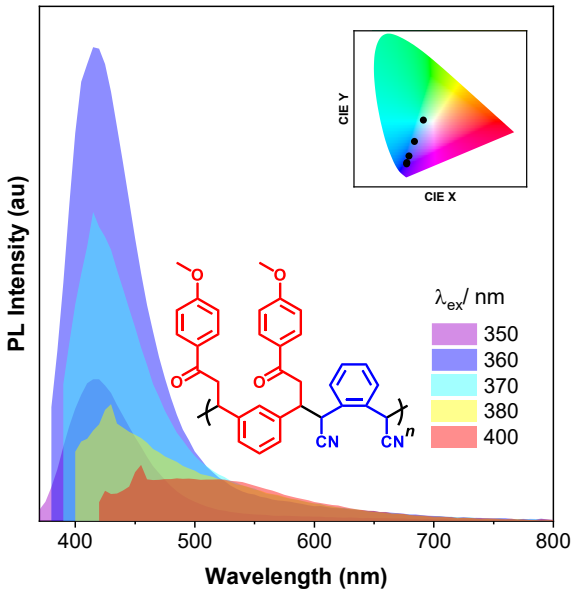

Figure S75. PL spectra of P**1d2d** in DMF (c = 1.0 × 10^{-3} M) with different excitation wavelengths. Inset: CIE coordination of P**1d2d** in DMF. (Excitation ranges: λ_{ex} = 350 − 400 nm).

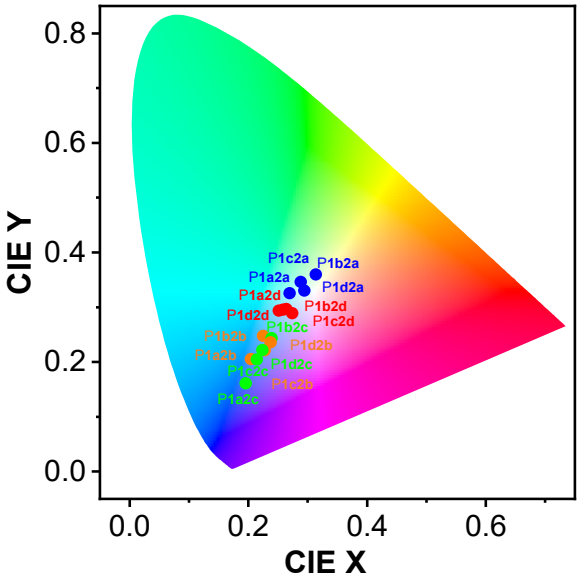

Figure S76. CIE coordination of power P**1a2a-1d2d** (λ_{ex} = 360 nm). Blue mark P**1a2a-d**; Orange mark P**1b2a-d**; Green mark P**1c2a-d**; Red mark P**1d2a-d**.

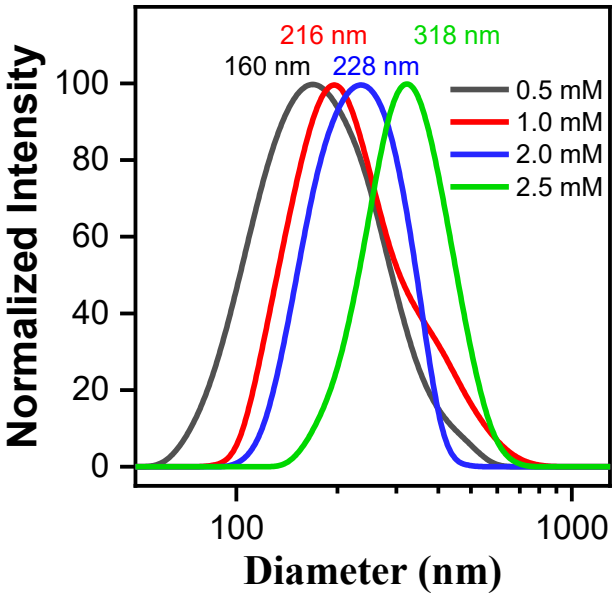

Figure S77. DLS data of P**1a2a** under different concentration.

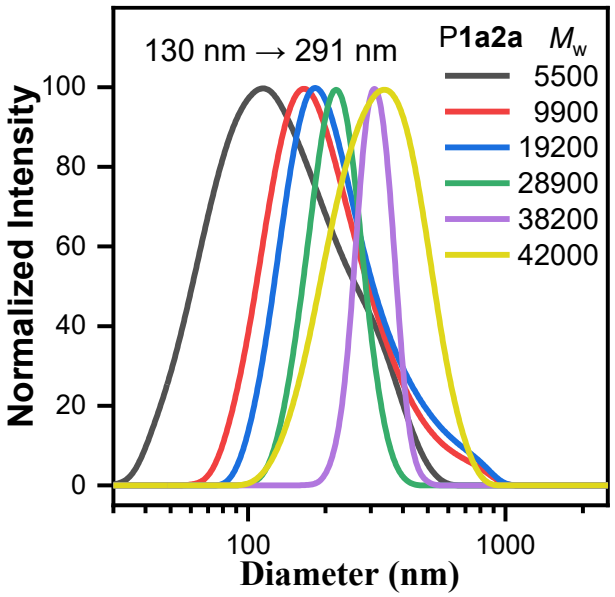

Figure S78. DLS data of P**1a2a** (1.0×10^{-3} M in DMF) under different molecular weights.

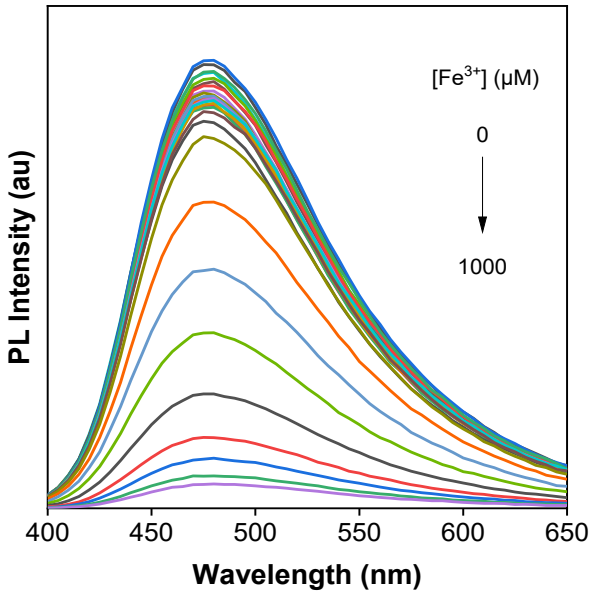

Figure S79. PL spectra of the P**1a2a** (1.0×10^{-3} M in DMF) probe with different concentration of Fe^{3+} (λ_{ex} = 365 nm).

References

1. L. Tian, Molclus program, Version 1.9.9.9, http://www.keinsci.com/research /molclus.html (accessed February19 2022).
2. C. Bannwarth, E. Caldeweyher, S. Ehlert, A. Hansen, P. Pracht, J. Seibert, S. Spicher and S. Grimme, *WIREs Computational Molecular Science*, 2021, **11**, e1493.
3. P. Pracht, E. Caldeweyher, S. Ehlert and S. Grimme, *ChemRxiv*, 2019, DOI: 10.26434/chemrxiv.8326202.v1.
4. Frisch, M.; Trucks, G. W.; Schlegel, H. B.; Scuseria, G. E.; Robb, M. A.; Cheeseman, J. R.; Scalmani, G.; Barone, V.; Mennucci, B.; Petersson, G.; Others, Gaussian 09, revision A. 03. In Gaussian, Inc., Wallingford CT: 2016.
5. (a) P. J. Stephens, F. J. Devlin, C. F. Chabalowski and M. J. Frisch, *J. Phys. Chem.*, 1994, **98**, 11623-11627.
6. S. Grimme, J. Antony, S. Ehrlich and H. Krieg, *J. Chem. Phys.*, 2010, **132**, 154104.
7. S. Grimme, S. Ehrlich and L. Goerigk, *J. Comput. Chem.*, 2011, **32**, 1456-1465.
8. P. C. Hariharan and J. A. Pople, *Theor. Chim. Acta*, 1973, **28**, 213-222.
9. W. J. Hehre, R. Ditchfield and J. A. Pople, *J. Chem. Phys.*, 1972, **56**, 2257-2261.
10. Y. Zhao and D. G. Truhlar, *Theor. Chem. Acc.*, 2008, **120**, 215-241.
11. F. Weigend and R. Ahlrichs, *Phys. Chem. Chem. Phys.*, 2005, **7**, 3297-3305.
12. T. Lu and Q. Chen, *J. Comput. Chem.*, 2022, **43**, 539-555.
13. T. Lu and F. Chen, *J. Comput. Chem.*, 2012, **33**, 580-592.
14. W. Humphrey, A. Dalke and K. Schulten, *J. Mol. Graphics*, 1996, **14**, 33-38.